Chemical equilibria and intrinsic kinetics of reactions in molten nitrate salt

Von der Fakultät 4 – Energie-, Verfahrens- und Biotechnik der Universität Stuttgart zur Erlangung der Würde einer Doktor-Ingenieurin (Dr.-Ing.) genehmigte Abhandlung

Vorgelegt von

Veronika Anna Sötz
aus Regensburg

Hauptberichter:	Prof. Dr. André Thess
Mitberichter:	Prof. Dr. Hubert Motschmann
Prüfungsvorsitzender:	Prof. Dr. Siegfried Schmauder
Tag der mündlichen Prüfung:	29.10.2020

Institut für Gebäudeenergetik, Thermotechnik und Energiespeicherung
der Universität Stuttgart

2021

Eigenständigkeitserklärung

Ich erkläre, dass ich abgesehen von den ausdrücklich bezeichneten Hilfsmitteln die Dissertation selbständig verfasst habe.

Köln, den _____ _____

Veronika Sötz

Acknowledgements

I would like to thank the following people who have enabled, accompanied and encouraged the research leading to this thesis.

Prof. André Thess (University of Stuttgart), for his precious advice regarding the focus of this thesis, and the persistent encouragement to improve the quality of my scientific presentations and communications.

Prof. Hubert Motschmann (University of Regensburg), who sharpened my mind for physical chemistry during the master's program, and kindly agreed to be the co-referee of this thesis.

Dr. Thomas Bauer, for supervising this thesis, and guiding me through the entire process from the first ideas to experiments and the generation of results to publications.

All colleagues from the group 'Thermal Systems for Fluids', for the great teamwork; Dr. Alexander Bonk and Freerk Klasing, for scientific discussions; Ulrike Kröner, Markus Braun, Jochen Forstner and Andrea Hanke, for great technical expertise.

Kai Risthaus, Dr. Marc Linder and many others, who spared their time, and listened to the demanding parts of this thesis, which helped a lot to organize my thoughts.

Dr. Christian Odenthal and Dr. Inga Bürger, for their support regarding software and modeling questions.

The 'Kölner' colleagues from the Institute of Engineering Thermodynamics, especially Andreas Kohzer, for the positive atmosphere that is a great source of motivation.

My parents Beate and Hubert, and my sister Mirjam, who never got tired of asking about the progress of this thesis, although the topic partly remained mystical for them.

Table of contents

Abstract

The nitrate salt mixture Solar Salt is applied as heat storage material in large-scale energy storage systems that are essential components of concentrating solar power plants to enable dispatchable electricity production. The maximum storage temperature does not exceed 565 °C in existing systems, but is intended to increase in the future to improve the efficiency and the capacity of the storage technology. However, chemical reactions in the molten Solar Salt intensify and accelerate with increasing temperature, leading to thermal instability of the storage material, and to decomposition products including corrosive ions and toxic gases. The decomposition process must be understood to maintain material stability at increased temperatures. In this thesis, the reactions that form the relevant decomposition products are experimentally investigated and mathematically described. The reaction of nitrate ions to nitrite ions constitutes the first step of the decomposition process, and the chemical equilibrium is described in two temperature regimes (450-550 and 560-630 °C). The intrinsic kinetics of the nitrite formation are investigated up to 550 °C by thermogravimetric analysis, and a differential rate law for both forward and reverse reaction kinetics is derived. In a second step, the nitrite ions are considered to decompose to oxide ions. Uniquely, this thesis presents experiments that prove chemical equilibrium including oxide ions in Solar Salt. Adding nitrous gases to a synthetic air purge stabilizes the oxide content, which is demonstrated at 600 and 620 °C. These results are particularly valuable, because oxide ions have shown to aggravate steel corrosion in Solar Salt, and thereby reduce the lifetime of the storage system. The intrinsic kinetics of the oxide formation are investigated in air atmosphere up to 630 °C. A mathematical kinetics description is developed, and the parameters are obtained by fitting the experimental results. Overall, the decomposition reactions form a consistent network, characterized by chemical equilibria and intrinsic kinetics of two reactions. The results can improve molten salt heat storage technology by providing Solar Salt stability predictions at existing and higher operation temperatures.

Kurzzusammenfassung in deutscher Sprache

Titel:

Chemische Gleichgewichte und die intrinsische Reaktionskinetik in einer Nitratsalzschmelze

Die Nitratsalzmischung „Solarsalz“ wird als Wärmespeichermedium in großtechnischen Speichersystemen eingesetzt, die wesentliche Bestandteile von konzentrierenden Solarkraftwerken sind, um die Stromproduktion der Nachfrage anzupassen. Die Speichertemperatur beträgt in bestehenden Systemen maximal 565 °C, soll aber zukünftig ansteigen, um den Wirkungsgrad bei der Verstromung und die Speicherkapazität zu erhöhen. Chemische Reaktionen in Flüssigsalz werden jedoch durch steigende Temperaturen beschleunigt und verstärkt, was zu thermischer Instabilität des Speichermaterials führt und wodurch vermehrt Zersetzungsprodukte einschließlich korrosiver Ionen und toxischer Gase entstehen. Ein grundlegendes Verständnis des Zersetzungsprozesses ist notwendig, um die Materialien bei erhöhten Temperaturen stabil zu halten. In dieser Dissertation sind Reaktionen, die relevanten Zersetzungsprodukte bilden, experimentell untersucht und mathematisch beschrieben. Die Reaktion von Nitrationen zu Nitritionen stellt den ersten Schritt des Zersetzungsprozesses dar und das zugehörige chemische Gleichgewicht ist in zwei Temperaturbereichen (450-550 und 560-630 °C) bestimmt. Die intrinsische Kinetik der Nitritbildung ist bis 550 °C durch thermogravimetrische Analyse untersucht. Das differentielle Zeitgesetz enthält die Kinetik der Hin- als auch der Rückreaktion. Die Zersetzung von Nitritionen weiter zu Oxidionen wird als zweiter Schritt betrachtet. Erstmalig zeigt diese Arbeit Experimente, die ein chemisches Gleichgewicht mit Beteiligung von Oxidionen in Solarsalz belegen. Der Zusatz nitroser Gase zum Spülgas (synthetische Luft) stabilisiert den Oxidgehalt, was bei 600 und 620 °C nachgewiesen ist. Diese Ergebnisse sind besonders wertvoll, da Oxidionen Stahlkorrosion in Solarsalz verstärken. Die intrinsische Kinetik der Oxidbildung ist in Luftatmosphäre bis 630 °C untersucht und mathematisch ausgedrückt. Die Kinetikparameter sind durch Fit der experimentellen Ergebnisse ermittelt. Insgesamt bilden die Zersetzungsreaktionen ein konsistentes Netzwerk, das durch chemische Gleichgewichte und die intrinsische Kinetik zweier Reaktionen beschrieben ist. Die Ergebnisse tragen zur Entwicklung der Flüssigsalz-Wärmespeichertechnologie durch Vorhersage der Solarsalzstabilität bei bestehenden und höheren Betriebstemperaturen bei.

$A_{(R)}$	Pre-exponential factor in the Arrhenius equation of reaction (R)	$varying$
c_p	Heat capacity of the storage material	$J \cdot kg^{-1} \cdot K^{-1}$
c_i	Molar concentration of species i	$mol \cdot m^{-3}$
$c_{i,eq}$	Molar concentration of species i at chemical equilibrium	$mol \cdot m^{-3}$
$E_{a,(R)}$	Activation energy of reaction (R)	$kJ \cdot mol^{-1} \cdot K^{-1}$
G_i	Gibbs free energy of formation of species i	$kJ \cdot mol^{-1}$
$G_{p,T}$	Gibbs free energy at constant pressure and temperature	$kJ \cdot mol^{-1}$
$\Delta_{(R)}G$	Gibbs free energy of reaction (R)	$kJ \cdot mol^{-1}$
H_i	Enthalpy of formation of species i	$kJ \cdot mol^{-1}$
$\Delta_{(R)}H$	Enthalpy of reaction (R)	$kJ \cdot mol^{-1}$
$K_{(R)}$	Equilibrium constant of reaction (R)	1
$k_{f,(R)}$	Forward reaction rate constant of reaction (R)	$varying$
$k_{r,(R)}$	Reverse reaction rate constant of reaction (R)	$varying$
m	Mass of storage material	kg
n_i	Amount of substance of species i	mol
p_i	Partial pressure of gas i	bar
p_0	Reference pressure, 1 bar	bar
Q_s	Capacity of the heat storage system	J
R	Ideal gas constant, $8.314\ J \cdot mol^{-1} \cdot K^{-1}$	$J \cdot mol^{-1} \cdot K^{-1}$
$r_{(R)}$	Reaction rate of reaction (R)	$mol \cdot m^{-3} \cdot s^{-1}$
S_i	Entropy of formation of species i	$J \cdot mol^{-1} \cdot K^{-1}$
$\Delta_{(R)}S$	Entropy of reaction (R)	$J \cdot mol^{-1} \cdot K^{-1}$
s	Slope of a linear fit curve	$varying$
t	Time	s, h
ΔT	Operating temperature range of the storage system	K
T^0	Heat sink temperature	K
T_h	Maximum storage temperature	$°C, K$
T	Temperature	$°C, K$
V	Volume	m^3
x_i	Molar ratio of i relative to the total amount of substance	$mol \cdot mol^{-1}$
$x_{i,eq}$	Molar ratio of i relative to the total amount of substance at chemical equilibrium	$mol \cdot mol^{-1}$
y_0	Y-intercept of a linear fit curve	$varying$
η	Efficiency of the conversion heat-to-power	1
μ_i	Chemical potential of i	$J \cdot mol^{-1}$
μ_i^*	Chemical potential of I at a reference state	$J \cdot mol^{-1}$
ν_i	Stoichiometric coefficient of i	1
ξ	Progress of a physical-chemical process (reaction, phase change)	mol
ρ	Density of Solar Salt	$kg \cdot m^{-3}$

(N)	Nitrite forming reaction, defined at page 6
(O)	Oxide forming reaction, defined at page 6
(C)	Carbonate forming reaction, defined at page 7
(G)	Gas phase reaction of nitrous gases, defined at page 7

CSP	Concentrating solar power
TES	Thermal energy storage
HTF	Heat transfer fluid
IC	Ion chromatography
TGA	Thermogravimetric analysis

A^-	Deprotonated form of acid HA
B^-	Base, proton acceptor
CO_2	Carbon dioxide
Cl^-	Chloride ion
CO_3^{2-}	Carbonate ion
HA	Acid, protonated molecule A
HB	Protonated form of base B^-
HCl	Hydrochloric acid
H_2CO_3	Carbonic acid
H_2O	Water
HCO_3^-	Hydrogen carbonate ion
H^+	Hydrogen cation, proton
K_2CO_3	Potassium carbonate
KNO_3	Potassium nitrate
KNO_2	Potassium nitrite
K_2O	Potassium oxide
K^+	Potassium cation
Na_2CO_3	Sodium carbonate
$NaNO_3$	Sodium nitrate
$NaNO_2$	Sodium nitrite
Na_2O	Sodium oxide
Na^+	Sodium cation
N_2	Nitrogen
NO	Nitrogen monoxide
NO_2	Nitrogen dioxide
N_2O	Dinitrogen oxide
$'N_2O_3'$	Mixture of gases with stoichiometric ratio nitrogen:oxygen 2:3
NO_3^-	Nitrate anion, nitrate ion
NO_2^-	Nitrite anion, nitrite ion
O_2	Oxygen
O^{2-}	Oxide ion
OH^-	Hydroxide ion

1 Introduction

Two critical chemical reactions that occur during thermal decomposition of molten nitrate salts are focused on in this thesis. The formation of nitrite ions and oxide ions is investigated experimentally, and model descriptions regarding the intrinsic kinetics and the thermodynamic equilibria are developed for both reactions. The results demonstrate the time dependence of the decomposition progress, and the feasibility of salt stabilization by meeting the requirements of chemical equilibria. The examined material Solar Salt is applied in thermal energy storage, and the motivation for the presented physical-chemical study is based on actual technological developments, which is expounded in this first introductory section.

A reliable and adequate energy supply is mandatory for almost all aspects of modern life. Persistence and progress of industry and economy, social life, health care, traffic, information technology and much else requires various types of energy. The energy demand is fluctuating in the rhythm of day and night, heat and cold, weekend, workdays, and holidays. In the past, the overwhelming part of energy demand in Germany was covered by fossil energy sources (coal, oil, gas), and nuclear energy. They allow energy generation whenever it is needed, independent from other restrictions. Some plants are designed for constant supply, and therefore appropriate for the base load of the electrical grid. Others can be used for temporary demand peaks. For reasons of climate protection, carbon neutrality and ecology, the fossil energy sources are gradually complemented and replaced by renewable energy sources, e.g. sun and wind. Both depend on weather conditions which fluctuate over time. Thus, they are per se not suitable for base load energy supply, and for adjusting the energy production to the demand peaks. Briefly spoken, the coexistence of fluctuating demand and fluctuating generation of energy requires storage technologies for the times of dispatch. The storage systems need to be charged with excess energy, and they provide energy later on. [1-4]

Different types of energy (e.g. thermal, electrical, or mechanical energy) generally can be converted into each other. The classification of energy storage in figure 1.1 is based on the different types of energy. For thermal energy storage (TES), temperature differences or gradients are required to heat up (or to cool down) a material, or to induce a phase change of a material. TES can be a cost-efficient energy storage technology because of the use of low-price materials, and because of its scalability. Liquid storage materials are favorable due to their pumpability. [5,6]

The material Solar Salt (a mixture of 60 wt.% sodium nitrate and 40 wt.% potassium nitrate) is investigated in this thesis. Compared to alternatively possible materials, it can be used in a broad operation temperature range (low melting temperature and high thermal stability); it is nontoxic, and

has a high density, high heat capacity, low viscosity, low vapor pressure and a competitive price. Hence, Solar Salt is already applied in large-scale storage systems connected to concentrating solar power plants (see section 1.1). [7-12]

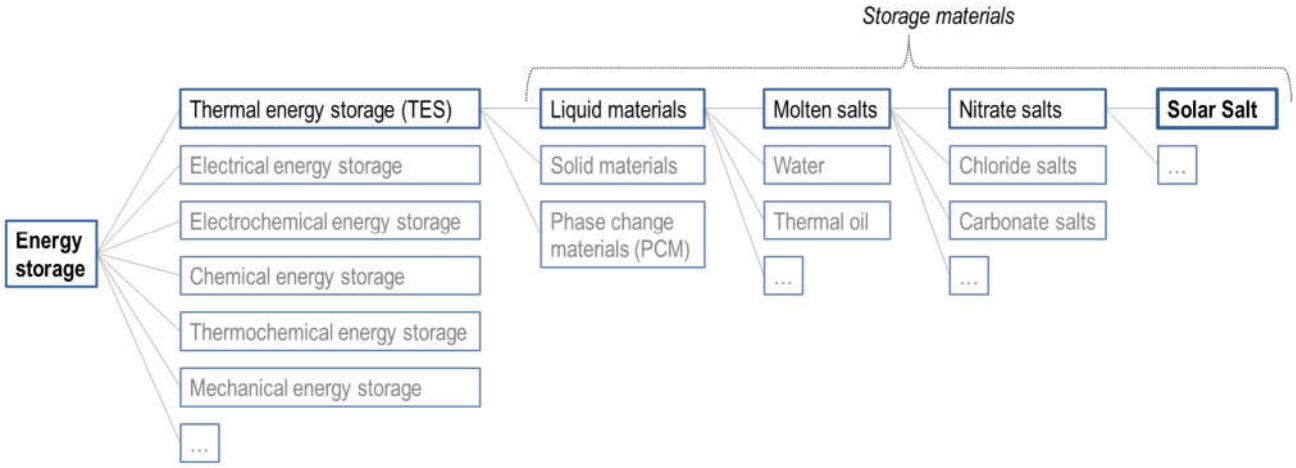

Figure 1.1: Types of energy storage, structured with a focus on the storage material. Solar Salt which is the storage material considered in this thesis belongs to the category of thermal energy storage in liquids. It is a nitrate salt mixture used in its liquid state.

1.1 State-of-the-art technology

Solar Salt is a widely used material to transfer and store thermal energy in concentrating solar power (CSP) plants. A general set-up of a CSP plant comprises mirrors that concentrate the sunlight. The light is absorbed and transformed to heat (thermal energy), and the heat is used to generate electrical power in a steam turbine. The two common types of CSP plants differ in the type of mirror and absorber arrangement, as well as in the arising absorber temperatures. Most CSP plants currently in operation belong to the parabolic trough type. Their linear parabolic mirrors and the absorber tubes in the focal point are sketched in Figure 1.2(a). Thermal oil which is mainly used as heat transfer fluid (HTF) flows through the absorber tubes reaches temperatures up to 400 °C. A currently expanding sector of CSP plants are of the solar power tower type. A field of almost planar reflectors (called heliostats) concentrates the sunlight on a central receiver (see figure 1.2(b)), where the temperatures are notably higher than in the parabolic trough plants. Therefore, steam or molten salts are chosen as HTF instead of thermal oil for thermal stability reasons. At the time of writing, practically all large-scale tower installations utilize molten salt as HTF and storage medium due to a lack of affordable storage solutions for steam as HTF. The higher temperatures enhance the efficiency of the power generation, and the storage capacity (see section 1.2), which are advantages of the power tower technology. [8,9,13,14]

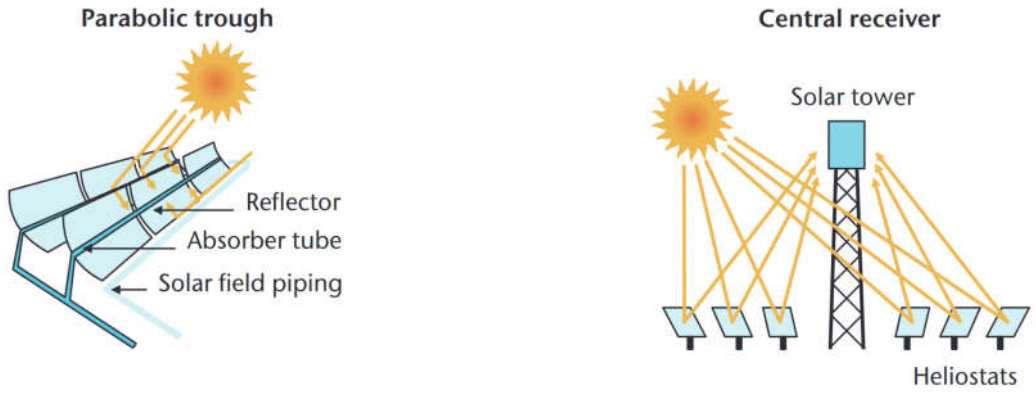

Figure 1.2: Two major types of reflector and absorber arrangements in CSP plants. The figures are taken from the reference [8].

Integration of TES into CSP plants enables operation of the steam turbine also during the night or in cloudy weather. If thermal oil is used as HTF, the heat is transferred to molten salt, which is termed indirect storage (e.g. in the CSP plants Noor II, Morocco and Andasol, Spain). If Solar Salt is applied as HTF, it can be stored directly in insulated tanks (e.g. in the CSP plants Archimede, Italy and Delingha, China). [15] The integration of a direct storage unit into a solar power tower plant is sketched in figure 1.3. The two tanks are located in between the receiver tower and the steam generator of the power block, and serve as a reservoir for hot and cold molten salt. To conclude, integration of Solar Salt TES to CSP is commercially available. It adds the benefit of continuous power generation and flexibility to the CSP technology, which are unique features among the renewable energy plants. [8,9,16]

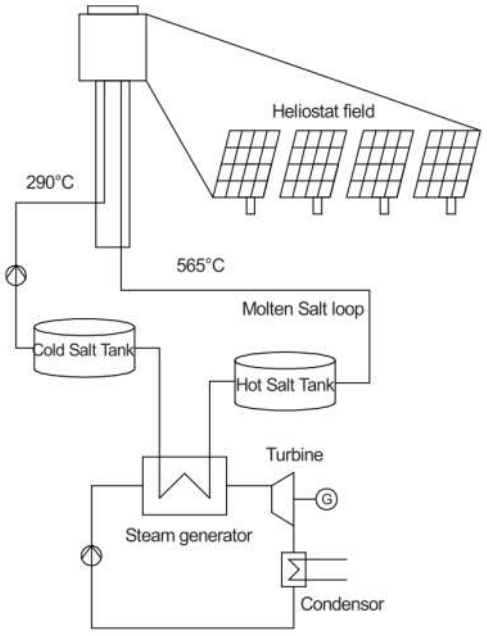

Figure 1.3: Integration of molten Salt TES in a central receiver CSP plant. The molten salt is used as both heat transfer fluid and storage medium in a so-called direct storage system. The figure is taken from the reference [16].

1.2 Motivation

The existing large-scale Solar Salt TES systems demonstrate the technical feasibility, and the industrial interest for this type of energy storage. Further cost reduction is intended to promote renewable energy generation, and to keep Solar Salt TES competitive compared to other energy storage options. Cost reductions can be achieved in several ways. First, the lifetime of the storage system, in particular of the storage material, can increase. Increased lifetime enables longer operation of the storage system at similar capital costs. Second, broadening the operation temperature range reduces the amount of storage material at constant storage capacity. Equation (1) describes the amount of heat that can be stored Q_s when a material with mass m and heat capacity c_p is heated (or cooled) to a temperature difference of ΔT. For Solar Salt, the lower operating temperature is restricted by the melting point. In this case, smaller tank volumes are sufficient to store a certain amount of heat when the upper storage temperature increases, which is sketched in figure 1.4. Since the storage material is one of the major cost factors, reducing the amount of material has a significant effect. [6] Third, the temperatures can increases to enhance the efficiency of the conversion heat-to-power. This correlation is shown in equation (2), with η being the Carnot efficiency, and T_h and T^0 being the maximum storage temperature and the heat sink temperature, respectively. Advanced and efficient steam turbines require temperatures above the actual state-of-the-art temperature of Solar Salt (about 565 °C). [9,13,17]

$$Q_s = m \cdot c_p \cdot \Delta T \tag{1}$$

$$\eta = 1 - T^0/T_h \tag{2}$$

Regarding the Solar Salt, lifetime and temperature increase are limited by material degradation and decomposition processes. Long-term laboratory tests and pilot plants reveal corrosion of steel components that are in contact with the molten salt, evolution of toxic gases, pressure increase and the formation of solid phases or precipitates. Thermal decomposition of the nitrate salt mixture becomes faster and stronger with increasing temperature. [18-23]

The resulting dilemma is summarized in figure 1.4. Further development of CSP plants and the Solar Salt TES technology by increasing the upper temperature is intended. This increase positively affects the storage capacity (or the material expense, respectively) and the power cycle efficiency. However, higher temperatures entail material degradation related to thermal decomposition, which are addressed in this thesis.

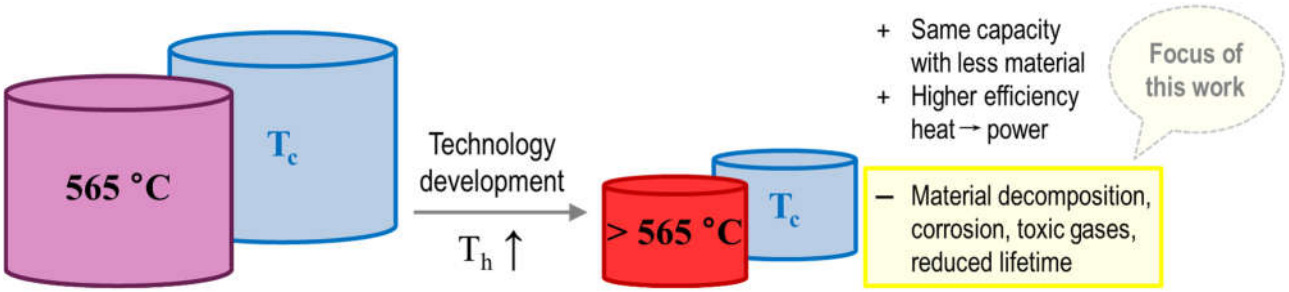

Figure 1.4: Development of Solar Salt TES towards higher temperatures. An upper storage temperature above the state-of-the-art limit of 565 °C is beneficial with regard to the material expense and the conversion efficiency, but also challenging in terms of material stability.

One conceivable solution is to expand the thermal stability of Solar Salt towards higher temperatures. Generally, measures that stabilize the molten salt at higher temperatures are equally appropriate to prolong the lifetime of Solar Salt in state-of-the-art systems. For the success of this approach, knowledge about the thermal decomposition of Solar Salt is absolutely necessary. This thesis focusses on a detailed understanding of the decompositions process, the network of chemical reactions, the participating ions and gases, chemical equilibria and reaction kinetics. The resulting descriptions are intended to contribute to the prediction of optimum conditions for material stability, such as specific operating strategies or adjustment of the atmosphere. Finally, this work aims to help establish highly efficient, sustainable and economic Solar Salt TES systems.

1.3 State-of-knowledge on nitrate salt chemistry

This section provides an overview of material data, qualitative observations in previous laboratory tests, and the reaction chemistry according to literature. Most reviewed studies refer to Solar Salt, which is a mixture of sodium nitrate ($NaNO_3$) and potassium nitrate (KNO_3). Besides, it is sometimes reasonable to include investigations of the single salts, of similar nitrate salts or nitrate salt mixtures. The emphasis is on the data and findings that are relevant for the investigations of this thesis. In this section, the literature is reviewed on a more general level. The **papers I, II and III** (see appendix) provide detailed insights with regard to the particular research topics.

Solar salt is composed of 60 wt.% (64 mol%) sodium nitrate and 40 wt.% (36 mol%) potassium nitrate. The eutectic composition is found to be the equimolar mixture [24]. The density ρ is described by equation (3), which is based on the data of the references [25,26].

$$\rho = 2268.9\ kg \cdot m^{-3} - 0.6395\ kg \cdot m^{-3} \cdot K^{-3} \cdot T \qquad (3)$$

1.3 State-of-knowledge on nitrate salt chemistry

The application of Solar Salt in TES systems requires compatibility of the molten salt and steel. Therefore, corrosion is addressed in many studies. The literature reveals that corrosion intensifies with increasing temperatures [20,21,27,28], by impurities in the molten salt [29-31], and with salt aging [18,32]. Corrosion mechanisms are postulated by some authors [22,33], but not definitely proven. Molten nitrate salts are known to spread intensely on many surfaces, e.g. metals or ceramics. In small-scale experiments, a significant amount of the salt sample can creep out of the crucible or distribute over the entire set-up.

Evolution of gases from the molten nitrate salt is observed. Early studies report gas bubbles, or measured the volume of the emerging gas [34]. Development of gas analysis methods allowed the identification of the gas types and ratios. Oxygen gas (O_2) is found most frequently, followed by nitrogen monoxide (NO) and nitrogen dioxide (NO_2), nitrogen (N_2) and dinitrogen oxide (N_2O). [35-38] Linking the gas species with chemical reactions is reviewed in the following paragraphs.

Undecomposed molten Solar Salt contains sodium cations (Na^+) and potassium cations (K^+), and nitrate anions (NO_3^-). For molten salt decomposition, the anion chemistry dominates. Hence, the discussion focuses on anion reactions. The most frequently reported thermal decomposition reaction of nitrate salts is the formation of nitrite ions and oxygen gas according to reaction (N). [39-43] In oxygen containing atmospheres, the reaction obtains chemical equilibrium. The nitrite ion concentration at chemical equilibrium increases with increasing temperature and decreasing oxygen partial pressure. Thermodynamic data of the reaction equilibrium of reaction (N) are published for the Solar Salt mixture [42], for a similar mixture of sodium nitrate and potassium nitrate [39], and for the single salts [40,41,44]. This data enables the calculation of the nitrate and nitrite ion content depending on the temperature and oxygen partial pressure. The reaction kinetics are investigated for the single salts [40,41,45], and for an equimolar mixture of $NaNO_3$ and KNO_3 [39,46]. A comprehensive description of the reversible reaction kinetics in Solar Salt is missing. A detailed review of the literature of reaction (N) can be found in **paper I**.

$$NO_3^- \rightleftharpoons NO_2^- + 0.5\ O_2 \qquad \text{(N)}$$

Above 500 °C, the formation of oxide ions (O^{2-}) is reported. It is accompanied by the evolution of gases. Nitrous gases (e.g. NO and NO_2), oxygen and nitrogen are mentioned in different publications, e.g. via reactions (4) and (5). The stoichiometry of the evolving gases remains uncertain in the literature. Therefore, it is reasonable to condense the varying proposed reaction equations to reaction (O), which substitutes the particular reaction gases with $'N_2O_3'$. $'N_2O_3'$ serves as a placeholder for any mixture of gases with a stoichiometric ratio 3:2 of nitrogen to oxygen. In the literature, the oxide

forming reactions are expected to be reversible, although evidence for the reversibility and for chemical equilibrium is lacking. Nitrate ions are discussed less frequently as reactants than nitrite ions. Several studies assume that the reaction kinetics are first order with respect to nitrite ions.[32,35-37,47-53]

$$2\,NO_2^- \rightleftharpoons O^{2-} + NO_2 + NO \tag{4}$$

$$2\,NO_2^- \rightleftharpoons O^{2-} + N_2 + 1.5\,O_2 \tag{5}$$

$$2\,NO_2^- \rightleftharpoons O^{2-} + 'N_2O_3' \tag{O}$$

The carbonate ion (CO_3^{2-}) formation according to reaction (C) is mentioned in several publications. Some studies exclude the formation of carbonates by avoiding sources of carbon (e.g. by using CO_2-free purge gas or atmospheres). [19,20,23,42,54,55]

$$O^{2-} + CO_2 \rightleftharpoons CO_3^{2-} \tag{C}$$

In the gas phase, the oxidation of NO to NO_2 via reaction (G) is reported. [53] Thermodynamic data for equilibrium predictions are available [44]. The ratios of NO and NO_2 at 0.2 bar oxygen pressure are shown in figure 1.5. The kinetics of this reaction are reviewed by Tsukahara. [56] Only the original publications of Tipper et al., Ashmore et al. and Olbregts et al. [57-59] match the temperature range that is relevant for Solar Salt.

$$NO + 0.5\,O_2 \rightleftharpoons NO_2 \tag{G}$$

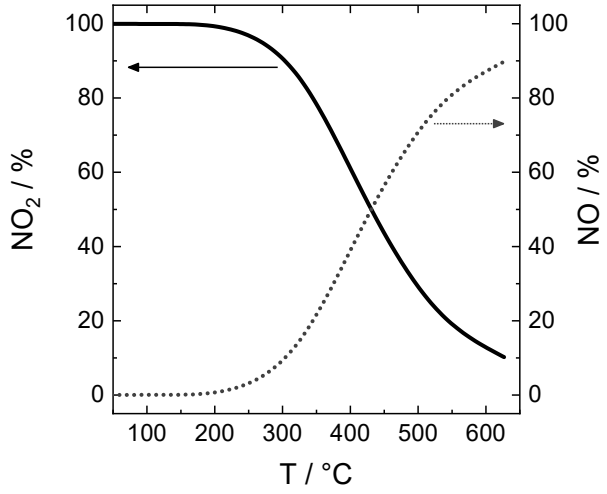

Figure 1.5: Gas phase equilibrium of reaction (G) at 0.2 bar O_2 calculated with listed thermodynamic data [44]. The equilibrium ratio of nitrogen monoxide and nitrogen dioxide depends on the temperature. A similar diagram is published in the reference [60].

In brief, the nitrite forming reaction (N) is well accepted, and to a certain extent quantitatively described in the literature. The oxide formation in nitrate salts is discussed qualitatively, and many reaction equations are proposed. The research topics of this thesis connect to the literature. Literature gaps and the resulting research questions are deduced in the following section 1.4.

1.4 Aims and scope of research

This thesis presents experiments and theoretical considerations that focus on thermal decomposition reactions of molten Solar Salt. The aim is to identify and experimentally prove the reactions, to quantify them, and to develop a model description in terms of mathematical equations.

According to previous studies, mainly nitrite ions and oxide ions are formed in molten Solar Salt. The nitrite ion formation (reaction (N)) is first observed when the molten salt temperature rises. It is considered as a starting reaction that provides a basis for further decomposition processes. Therefore, accurate knowledge about the nitrite ion forming reaction is necessary for the description of the entire thermal decomposition. The thermodynamic data of reaction (N) in Solar Salt is only published in one reference [42]. Confirming the existing thermodynamic results, also in comparison to single salt data, and providing a broader data basis is the first objective in **paper I**. The kinetics of reaction (N) are not described for Solar Salt in the literature, and their description for a similar salt mixture is only valid for the particular experimental conditions in the reference [39]. A reliable description of the intrinsic kinetics for the forward and reverse reaction (N), which is in agreement with the chemical equilibrium, is intended in the second part of **paper I**. Both reaction kinetics and thermodynamics are expected to include the influence of the temperature, and of the oxygen pressure in the connected gas atmosphere.

High concentrations of alkali oxide ions are related to intense corrosion of steel, which is in contact with molten Solar Salt. Additionally, oxide ions can further react to chromium oxide ions, which would lead to toxicity and disposal issues. Hence, scientific findings on the oxide ion formation are crucial to avoid these reactions, and to maintain material quality in molten salt systems. The literature presents various reaction equations that include oxide ion formation, but none of them is verified. A reliable representative reaction equation is required for predictions of chemical equilibria and strategies for salt stabilization. Systemizing the proposed equilibrium reactions and identifying the key differences is one part of **paper III**. Constant oxide ion concentrations over time due to chemical equilibrium are not reported in the literature for molten nitrate salts. Such results give insights on the reversibility of the oxide formation, and in the composition of the liquid-gas system that is required

for chemical equilibrium. Experiments that prove chemical equilibria are the main objective of **paper III**.

Previous studies indicate that the formation of oxide ions increases with temperature. Quantitative data on the reaction kinetics potentially enables the localization of fast salt decomposition in a molten salt system, and could allow for specific stabilizing measures in those areas. However, the necessary experiments and data are not presented by the literature. **Paper II** intends to fill this gap by providing experimental data and a model description of the oxide ion formation kinetics.

The approach and the methods in this thesis are chosen with regard to the technological application of Solar Salt in energy storage systems and the developments in the CSP and potentially new application fields. For example, temperature ranges (450-620 °C) and atmospheres (mainly air or synthetic air) similar to the (prospective) storage and HTF system conditions are chosen. Thermal decomposition processes often are complex sequences or networks of reaction steps. Their descriptions are simplified by appropriate approximations, and by prioritizing technologically relevant decomposition products and reaction directions.

2 Theoretical background and experimental methods

2.1 Chemical thermodynamics

Thermodynamics of chemical reactions

The thermodynamically most favorable state of a system at given temperature and pressure (isobar and isotherm closed system) is characterized by a minimum in the Gibbs free energy $G_{p,T}$. Changes of the system (in terms the amounts of substance or the composition of the phases) away from this state would always cause an increase of the Gibbs free energy. The condition for the thermodynamic state is therefore expressed in equation (6). Spontaneous processes in such a system are related to a decrease of the Gibbs free energy, see equation (7).

$$dG_{p,T} = 0 \tag{6}$$

$$\Delta G_{p,T} < 0 \tag{7}$$

When gas dissolves in a liquid phase or when a chemical reaction takes place, the amounts of the considered particles change. These changes affect the Gibbs free energy. Thermodynamics refer to those changes of the Gibbs free energy caused by changing numbers of particles i (n_i) as chemical potential μ_i. It is shown as the partial derivative in equation (8). The chemical potential is also termed partial molar Gibbs free energy since it refers to the amount of particles (moles) of one specific substance assuming that all other substances remain unchanged. In a closed system, changes in the amounts of particles due to distribution among phases or due to chemical reactions depend on each other. They are linked by the stoichiometric coefficients ν_i of the regarded process via equation (10c). The correlation is shown for an exemplary reaction in table 2.1. Accordingly, equation (8) is transformed to a more general form in equation (9). Equation (9) describes changes in the Gibbs free energy of a closed system due to processes that alter the compositions.

$$\left(\frac{dG}{dn_i}\right)_{T,p,n_{j\neq i}} = \mu_i \tag{8}$$

$$\left(\frac{dG}{d\xi}\right)_{T,p} = \sum_i \nu_i \mu_i \tag{9}$$

Table 2.1: Relating the reaction stoichiometry to the conversion ξ, and to changes in the amounts of particles dn_i.

Exemplary reaction of A and B to C and D with stoichiometry $\nu_A = -3, \nu_B = -1, \nu_C = 1, \nu_D = 2$.	$3\,A + B \rightarrow C + 2\,D$	(10a)
Changes in the amounts of particles n_A, n_B, n_C and n_D when the reaction happens 100 mol times (conversion progress $d\xi = 100\ mol$).	$dn_i = \nu_i \cdot d\xi$	(10b)
	$\rightarrow \boldsymbol{dn_A = -300\ mol}, \boldsymbol{dn_B = -100\ mol}, \boldsymbol{dn_C = 100\ mol}, \boldsymbol{dn_D = 200\ mol}$	
Correlation of the changes in the amounts of particles	$d\xi = \frac{dn_i}{\nu_i} = \frac{dn_A}{\nu_A} = \frac{dn_B}{\nu_B} = \cdots$	(10c)

The chemical potential of a substance i in ideal solutions is given in equation (11). It includes the chemical potential of this substance at a reference state μ_i^*, and a logarithmic term of the molar ratio x_i, which is the amount of particles of i relative to all particles in the regarded phase.

$$\mu_i = \mu_i^* + RT \ln x_i \tag{11}$$

In order to describe the thermodynamic equilibrium of a reaction, equations (6), (9) and (11) are combined to equation (12a) with the intention to find the minimum of the Gibbs free energy. The chemical potential is expressed by equation (11). In equation (12b), all constant terms are shifted to the left side of the equation, and summarized to the equilibrium constant of the regarded reaction $K_{(R)}$ in equation (12c). The right side of equation (12c) is the quotient of reaction products and reactants, each to the power of their stoichiometric coefficients. Equation (12c) is termed 'law of mass action'. It describes the thermodynamically favorable compositions, which are the chemical equilibria of a reaction. At chemical equilibrium, macroscopically, the reaction does not proceed in one (forward) or the other direction.

$$0 = \left(\frac{dG}{d\xi}\right)_{T,p} = \sum_i \nu_i \mu_i = \sum_i \nu_i \mu_i^* + RT \sum_i \nu_i \ln x_{i,eq} \tag{12a}$$

$$\frac{-\sum_i \nu_i \mu_i^*}{RT} = \ln \prod_i {x_{i,eq}}^{\nu_i} \tag{12b}$$

$$exp\left(\frac{-\sum_i \nu_i \mu_i^*}{RT}\right) = K_{(R)} = \prod_i {x_{i,eq}}^{\nu_i} \tag{12c}$$

The sum of the chemical potentials at reference state multiplied by the stoichiometric coefficients is the Gibbs free energy of reaction $\Delta_{(R)}G$, and it can be split in two temperature independent parameters, which are the reaction enthalpy $\Delta_{(R)}H$ and the reaction entropy $\Delta_{(R)}S$, see equation (13). Combining equations (12c) and (13) to equation (14) reveals the temperature dependence of the equilibrium constant $K_{(R)}$. The logarithmic equilibrium constant is proportional to the inverse

temperature. The reaction energies ($\Delta_{(R)}G$, $\Delta_{(R)}H$ and $\Delta_{(R)}S$) can be determined based on experimental equilibrium results. The process is sketched in figure 2.1. The equilibrium compositions at different temperatures allow calculation of several equilibrium constants $K_{(R)}$. The logarithm of those constants is plotted versus the inverse temperature (according to equation (14)), and the data is fitted linearly. The two resulting fit parameters are transformed to the reaction energies (slope to reaction enthalpy, and y-intercept to reaction entropy, see equation (14) and figure 2.1). [61,62]

$$\sum_i \nu_i \mu_i^* = \Delta_{(R)}G = \Delta_r H - T \cdot \Delta_{(R)}S \tag{13}$$

$$\ln K_{(R)} = \frac{-\Delta_{(R)}G}{RT} = T^{-1} \cdot \frac{-\Delta_{(R)}H}{R} + \frac{\Delta_{(R)}S}{R} = T^{-1} \cdot s + y_0 \tag{14}$$

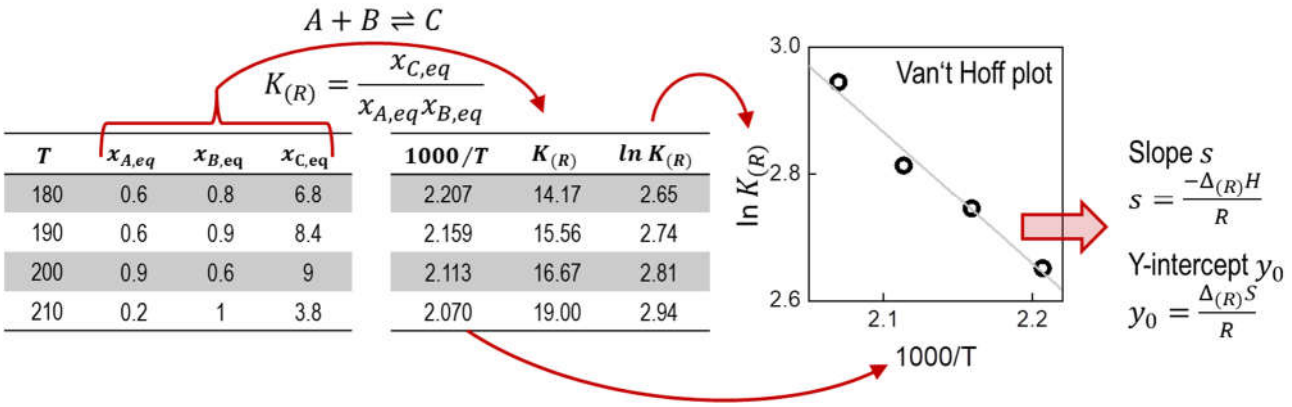

Figure 2.1: Evaluation of experimental equilibrium compositions $x_{i,eq}$ with regard to the equilibrium constants $K_{(R)}$, and the thermodynamic reaction parameters, enthalpy of reaction $\Delta_{(R)}H$ and entropy of reaction $\Delta_{(R)}S$.

Hess's law and calculation of chemical equilibria

Chemical reactions produce or consume energy. Most chemical substances can be formed via different reaction paths. According to Hess's law, the energy changes ($\Delta_{(R)}H$, $\Delta_{(R)}S$ and $\Delta_{(R)}G$) are the same, irrespective of the specific reaction path. An example (for the enthalpy) is given is figure 2.2. NO_2 can form on reaction path A in two steps. First, N_2 and O_2 react to NO which is characterized by the reaction enthalpy $\Delta_{A1}H$, and second, the NO further reacts to NO_2 with the reaction enthalpy $\Delta_{A2}H$. The second reaction path B is the direct reaction of N_2 and O_2 to NO_2 with the reaction enthalpy $\Delta_B H$. The total enthalpy of path A ($\Delta_{A1}H + \Delta_{A2}H$) is equal to the enthalpy of path B ($\Delta_B H$), see equation (15).

This thermodynamic principle (Hess's law) is applied in this thesis for calculations of reaction enthalpies and entropies, and equilibrium constants $K_{(R)}$. It can be an alternative to experimental investigations, and serves as comparison to experiments.

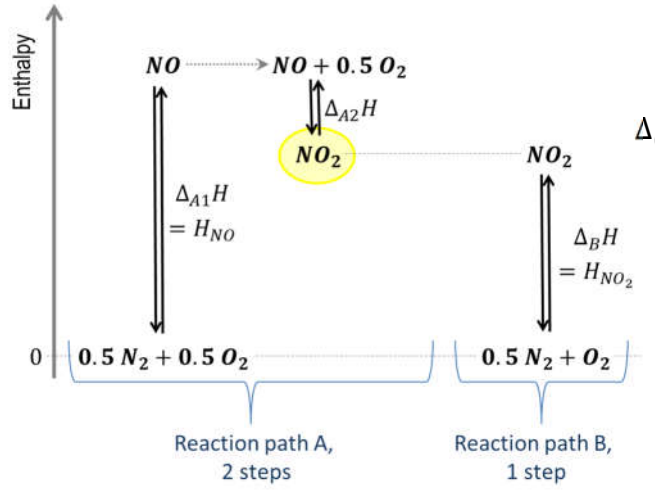

$$\Delta_{A1}H + \Delta_{A2}H = \Delta_B H \tag{15}$$

$$\Delta_{(R)}H_{NO\rightarrow NO_2} = H_{NO_2} - \left(H_{NO} + 0.5\, H_{O_2}\right) \tag{16}$$

Figure 2.2: Illustration of the Hess's law. NO_2 is formed in a two-step reaction (path A) or in a single step reaction (path B), and the overall energy change (e.g. the enthalpy change ΔH) does not depend on the particular reaction path.

The standard energies of formation (H_i, S_i, G_i) are listed for many pure chemical substances, e.g. in the references [44,52]. They refer to the reaction that describes their formation from the elements in their most stable form. For example, in figure 2.2, H_{NO} is the standard enthalpy of formation of NO, and H_{NO_2} is the standard enthalpy of formation of NO_2. Both describe the reaction of the most stable form of oxygen and nitrogen at a reference temperature and pressure (most commonly 289.15 K and 1 bar) which is gaseous O_2 and N_2 to NO or NO_2 at the regarded temperature. When those two standard enthalpies of formation are known, the enthalpy of the reaction from NO to NO_2 can be calculated via equation (16). Generally, reaction energies ($\Delta_{(R)}H$, $\Delta_{(R)}S$, $\Delta_{(R)}G$) are calculated according to equations (17) based on the standard energies of formation (H_i, S_i, G_i) of reactants and products. [61,62]

$$\Delta_{(R)}H = \sum_i \nu_i H_i \tag{17a}$$

$$\Delta_{(R)}S = \sum_i \nu_i S_i \tag{17b}$$

$$\Delta_{(R)}G = \sum_i \nu_i G_i \tag{17c}$$

Heterogeneous reactions

Chemical compounds can be restricted to one phase of a system, or they are distributed among two or more phases. The exemplary reaction (18) occurs in the liquid phase, and comprises a species B that is mainly located in the gas phase, but also dissolved in the liquid phase. In this case, two equilibria have to be considered. The first one is the solubility equilibrium of species B (equations (19a) and (19b)), and the second one is the reaction equilibrium in the liquid phase (equations (20a) and (20b)). Frequently, the solubility description of a gas in the regarded liquid (that allows calculation of $x_{B_{(l)}}$ in equation (19b) and (20b)) is not available in the literature and difficult to access experimentally, which prevents calculation of the reaction equilibrium via equation (20b). Analyzing or controlling the composition of the gas phase (resulting in a known partial pressure p_B) is commonly more feasible. It therefore makes sense to combine the two equilibrium descriptions (19b) and (20b) to the overall equilibrium expression (21) which describes the reaction equilibrium in terms of molar ratios and partial pressures, that are accessible. A similar discussion for the particular case of reaction (N) can be found in **paper I**. [61,62]

$$A + B \rightleftharpoons C \tag{18}$$

$$B_{(g)} \rightleftharpoons B_{(l)} \tag{19a}$$

$$K_{(19a)} = \frac{x_{B_{(l)}}}{p_B/p^0} \tag{19b}$$

$$A_{(l)} + B_{(l)} \rightleftharpoons C_{(l)} \tag{20a}$$

$$K'_{(18)} = \frac{x_{C_{(l)}}}{x_{A_{(l)}} x_{B_{(l)}}} \tag{20b}$$

$$K_{(18)} = K'_{(18)} \cdot K_{(19a)} = \frac{x_{C_{(l)}}}{x_{A_{(l)}}\, p_B/p^0} \tag{21}$$

2.2 Reaction kinetics

Reaction kinetics addresses the time dependence of a reaction. More precisely, it describes how often a reaction occurs per unit time.

Elementary reactions

The mechanism of an elementary reaction happens at once, and cannot be subdivided into several steps. For such reactions, the common description of the reaction kinetics in a liquid or in a gas is based on the following approach. First, the probability of collision of the reacting particles is

described. For a chemical reaction, the participating molecules, atoms or ions must be in close proximity, which is also termed a collision. This probability is proportional to the concentrations of the particles. The collision probability of the exemplary reaction (18) in the forward direction is included by ${c_A}^{\nu_A} \cdot {c_B}^{\nu_B}$ in equation (22). Second, the probability of reaction is considered. The colliding particles must have a certain energy that enables the chemical reaction. The energy barrier is known as the activation energy of a reaction $E_{a,f,(18)}$. Not all particles in a system have the same energy. Instead, the energy is distributed according to the Maxwell-Boltzmann distribution. The colliding particles sometimes have the required energy and the reaction happens, and sometimes the collision is not accompanied by a chemical reaction. With rising temperature, the particle energy distribution is shifted towards higher energies, the reaction probability increases, and reactions between particles become more frequent. This temperature dependence is included in the reaction constant $k_{f,(18)}$ in equation (22), which is further defined in equation (23). The reaction constant increases with an increasing temperature, or with a decreasing activation energy $E_{a,f,(18)}$. Multiplying the collision probability (collisions per unit time and volume) with the reaction probability (reactions per collision) results in the reaction rate (reactions per unit time and volume). Multiplication with the regarded volume finally results in the reaction rate $r_{(R)}$, which describes the number of reactions per unit time. The reaction rate is linked to changes in the amounts of particles in equation (24). [63,64]

$$r_{f,(18)} = {c_A}^{\nu_A} \cdot {c_B}^{\nu_B} \cdot k_{f,(18)} \cdot V \tag{22}$$

$$k_{f,(18)} = A_{f,(18)} \cdot exp\left(-E_{a,f,(18)}/RT\right) \tag{23}$$

$$\frac{1}{\nu_i}\frac{dn_i}{dt} = r_{(R)} \tag{24}$$

Multistep reactions

Frequently, chemical reactions summarize a reaction mechanism that can be expressed in terms of several steps. Each of those steps is supposed to be an elementary reaction. For reaction kinetics, the slowest elementary reaction of the regarded process must be identified (or assumed), because this slowest step determines and limits the reaction kinetics of the entire process. This procedure is called the ‘rate determining step approximation’. The other reaction steps are fast compared to the slowest step, and are assumed to be infinitely fast and complete, or in chemical equilibrium (‘quasi steady state approximation’).

An example for those approximations is given in equations (25a)-(25d). Equation (25a) shows the elementary steps of the reaction of A to D. The second step (reaction of B to C) is the slowest step, and is considered the rate determining step. The kinetic rate law (equation (25b)) therefore refers to

this elementary reaction and includes the concentration of B c_B (which is the 'rate determining step approximation'). Species A is in equilibrium with species B, and the reversible A-B reaction is relatively fast. Consequently, it is assumed that the equilibrium description in equation (25c) is always valid, and c_B can be replaced by $K_{(25)}c_A$ in equation (25d) (which is the 'quasi steady state approximation'). Finally, the reaction of C to D is relatively fast, and the reaction rate is related to changes in the amount of D (instead to C) in equation (25d) because an instantaneous reaction to D can be assumed. [63,64]

$$\begin{matrix} & K_{(25)} & k_{(25)} & \\ A & \rightleftharpoons & B & \longrightarrow & C & \longrightarrow & D \\ & fast & slow & & fast & & \end{matrix} \tag{25a}$$

$$r = c_B \cdot k_{(25)} \cdot V \tag{25b}$$

$$K_{(25)} = c_B / c_A \tag{25c}$$

$$r = K_{(25)} c_A \cdot k_{(25)} \cdot V = \frac{dn_D}{dt} \tag{25d}$$

Reversible reactions

For reversible elementary reactions, the reaction kinetics of both reaction directions can be described in one rate law. For the exemplary reaction (18), the first term of the kinetics equation (26) refers to the forward reaction, and is characterized by the forward rate constant $k_{f,(18)}$. The second term with the reverse rate constant $k_{r,(18)}$ corresponds to the reverse reaction, and has a different (negative) sign. Both reactions (forward and reverse) occur simultaneously on a molecular level. If the first term predominates, the forward reaction is observed macroscopically, and the reaction rate is positive (and vice versa). At chemical equilibrium, the overall reaction rate equals zero, and no reaction is observed (macroscopically). This situation is agreement with equation (26) when the two terms compensate each other. On a molecular level, the forward reaction is equally frequent than the reverse reaction. At chemical equilibrium, the kinetic rate law can be transformed into the quotient of products and reactants, see equations (27a) and (27b), and equals the law of mass action (compare equation (12c)) which is the thermodynamic equilibrium description of the reaction. Equation (27b) finally shows that the thermodynamics and kinetics of an elementary reversible reaction are linked. The equilibrium constant $K_{(18)}$ is related to the two reaction rate constants $k_{f,(18)}$ and $k_{r,(18)}$. [63,64]

$$r_{(18)} = {c_A}^{\nu_A} {c_B}^{\nu_B} \cdot k_{f,(18)} \cdot V - c_C \cdot k_{r,(18)} \cdot V \tag{26}$$

$$r_{(18)} = 0 = {c_{A,eq}}^{\nu_A} {c_{B,eq}}^{\nu_B} \cdot k_{f,(18)} \cdot V - c_{C,eq} \cdot k_{r,(18)} \cdot V \tag{27a}$$

$$\frac{k_{f,(18)}}{k_{r,(18)}} = \frac{c_{C,eq}}{{c_{A,eq}}^{\nu_A} {c_{B,eq}}^{\nu_B}} = K_{(18)} \tag{27b}$$

Intrinsic kinetics and macrokinetics

Regarding multiphase reaction, the macroscopically observable reaction progress is not only depending on the intrinsic kinetics (also termed microkinetics). Especially in real scale systems, mass transport (e.g. diffusion) can be crucial. An exemplary case is a liquid phase reaction producing a gas, which initially accumulates in the liquid phase. At the liquid-gas interface, the gas is released to the gas phase to obtain the thermodynamic solubility equilibrium. The resulting concentration gradient drives diffusion of dissolved gas through the liquid phase to the interface. However, diffusion might be a slower process than the intrinsic reaction kinetics. In times of oversaturation, the reaction product (gas) concentration is higher in the liquid phase than it should be according to the solubility equilibrium, and suppresses the progress of the reaction according to the law of mass action. The reaction kinetics measured for the entire liquid phase consequently differ from the intrinsic kinetics, and are termed macrokinetics. The macrokinetics describe the interplay of intrinsic kinetics and mass transport effects, and strongly depend on the system geometry (e.g. surface-to-volume ratio) and reaction conditions (e.g. stirring, fluid flow). [65-69]

2.3 Experimental methods in comparison

The section provides an overview of the experimental methods that are used in this thesis. The aims are to trace the progress of chemical reactions and the resulting composition changes over time, and to analyze the salt compositions at chemical equilibria. During the reactions, it is necessary to create defined reaction conditions for the molten salt, especially with regard to temperature and atmosphere. Also, mass transport phenomena and the consequent limitations regarding the reaction kinetics have to be considered. The reactions are either traced in-situ, e.g. by mass changes that are continuously recorded, or salt samples are extracted and subsequently analyzed (‘post-analysis’). The analysis methods are addressed in the subsequent paragraphs, which are followed by descriptions of the thermal treatment methods.

Analyzing the salt composition

Ion chromatography (IC) is a method that separates and detects ions in an aqueous sample. The concept of this method is sketched in figure 2.3. A small volume of sample (typically some µL) is injected into a column whose inner walls are covered with a charged material. The sample is carried through the column by a liquid eluent. Analytes that are attracted to the charged column walls due to intermolecular interactions are retarded, and need a longer time to flow through the column. The intensity of those interactions depends on the ionic strength of the analytes which is mainly affected by charge, polarizability and size, of the ions. At the end of the column, the analytes are detected by a conductivity detector. The conductivity is plotted versus time in a chromatogram. Calibration allows a quantitative calculation of the amounts of analytes in the sample based on the peaks in the chromatogram. The IC method is used for analysis of the Solar Salt samples with regard to nitrate and nitrite ions in **papers I, II and III**.

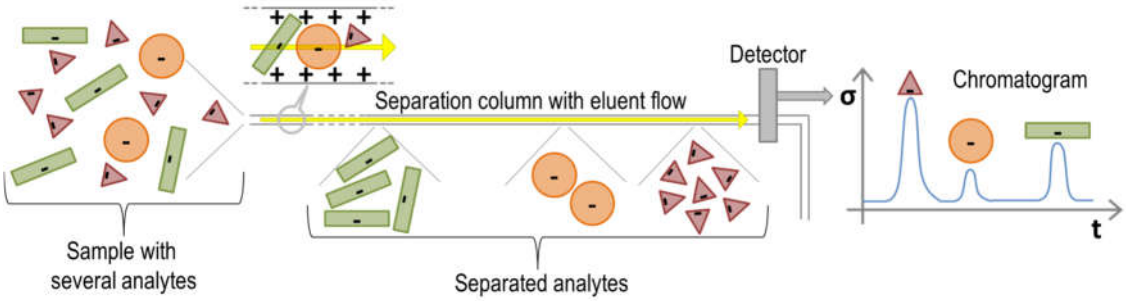

Figure 2.3: Separation principle of ion chromatography. The interaction of the analytes with the separation column depends on the charge, polarizability and size of the ions.

The applied **titration analysis** in this thesis is based on acid-base reactions. In such a reaction, a proton (hydrogen cation H^+) is transferred from an acid HA (compound that is able to donate a proton, according to the Brønsted-Lowry acid-base theory) to a base B^- (which is a compound that accepts a proton), see equation (28). During titration, defined amounts of acid are stepwise added to an unknown amount of base (or vice versa). The acid-base reaction is traced (usually by a pH electrode) to detect the completion of the reaction. The amount of added acid allows the calculation of the unknown amount of base, which is the intention of this analysis method. In **papers II and III**, acid-base titration is applied to analyze oxide ions and carbonate ions, and the process is explained for oxide ions in detail. When the salt sample (about 1 g) is dissolved in water, the oxide ions react with water to hydroxide ions via reaction (29). Then, hydrochloric acid HCl is added to the sample solution, until completion of the acid-base reaction (30), which is characterized by a sudden decrease of the pH value. The amount of oxide ions equals half of the amount of added HCl according to the 1:2

($\nu_{O^{2-}}/\nu_{OH^-}$) stoichiometry in reaction (29), and is calculated via equation (31). The carbonate ion is analyzed in a similar way according to reaction (32).

$$HA + B^- \rightarrow A^- + BH \tag{28}$$

$$O^{2-} + H_2O \rightarrow 2\,OH^- \tag{29}$$

$$HCl + OH^- \rightarrow Cl^- + H_2O \tag{30}$$

$$n_{O^{2-}} = 1/2 \cdot n_{HCl} = 1/2 \cdot V_{HCl} \cdot c_{HCl} \tag{31}$$

$$CO_3^{2-} \xrightarrow{+H^+} HCO_3^- \xrightarrow{+H^+} H_2CO_3 \tag{32}$$

Thermal treatment methods

Thermogravimetric analysis (TGA) is a standard analysis method for thermal processes, and it is applied in **paper I** to investigate the nitrate-nitrite reaction (N) in Solar Salt. The set-up of the commercial apparatus is sketched in figure 2.4. The sample (typically in the mg range) in a small platinum crucible is put in a larger crucible to avoid salt creeping over other parts of the apparatus. Those two crucibles are positioned on a scale with a sample holder to detect mass changes. The sample environment is purged with a defined gas flow (synthetic air), and the temperature is controlled. The temperature is raised from room temperature to the target temperature (450-550 °C), which is hold for the isothermal measurements. The raw data is the sample mass over time, which is recorded by the scale. It can be converted into e.g. evaporation rates or the progress of reactions with absorption or release of gases. After the TGA measurement, the salt samples are analyzed by IC, which reveals the nitrate ion and nitrite ion content. Due to the small sample quantities, mass transport limitations can be avoided, which makes TGA an appropriate method for intrinsic kinetics measurements.

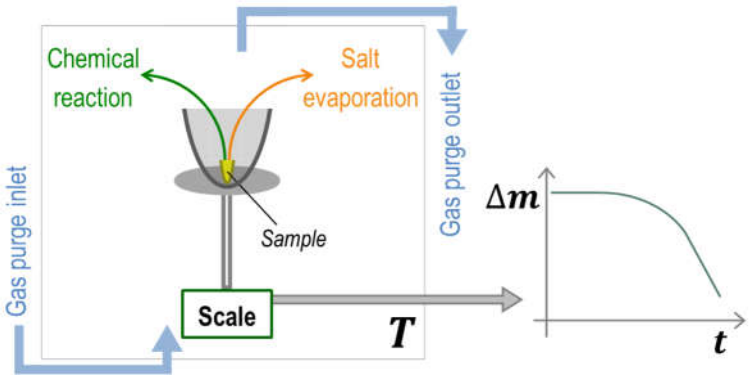

Figure 2.4: Thermogravimetric analysis set-up for Solar Salt investigations. Mass changes of the salt sample Δm are measured under defined atmospheric and temperature conditions over time t.

The **chamber furnace** sketched in figure 2.5(a) is equipped with four heating elements (SiC rods). Two small openings allow inflow and outflow of ambient air, which is driven by natural convection. The chamber is accessible by a swivel-type door. Two alumina crucibles of 4 cm diameter with salt samples are inserted into the furnace at 300 °C, and then heated to the target temperature (560-630 °C). This procedure avoids excessive temperature shocks and material breakage. The target temperature is hold for several hours. Afterwards, the temperature is reduced back to 300 °C, the crucibles are taken out of the chamber, and the sample is poured into small aluminum beakers where the salt instantly solidifies and the reaction ceases. Part of the sample is dissolved in water for acid-base titration, and a smaller part is used for IC analysis, which is illustrated in figure 2.5 (b). The results of those two analysis methods reveal the reaction progress during the temperature treatment in the furnace.

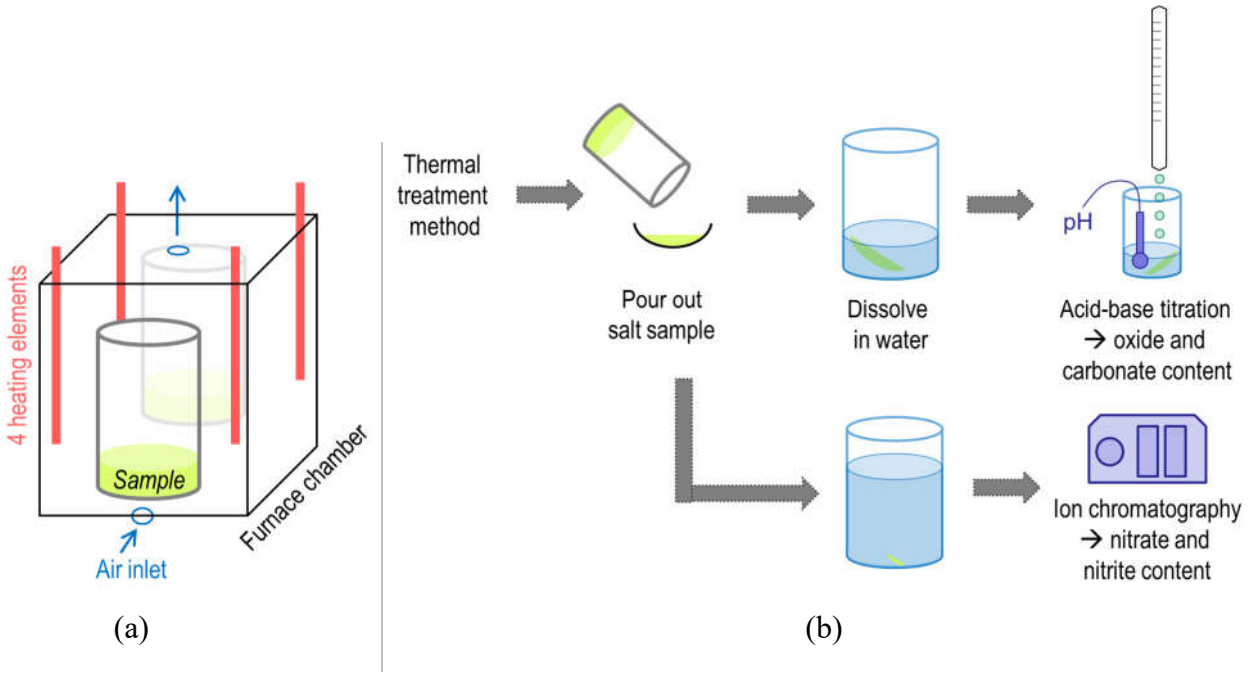

Figure 2.5: Sketch of the chamber furnace set-up (a), and the ensuing salt sample analysis procedure (b). Salt aging is performed in the furnace (thermal treatment), and the composition of the sample is subsequently analyzed by titration and ion chromatography. A similar figure is included in **paper II**.

Compared to the crucibles used in TGA, the crucibles in this method allow investigation of larger sample quantities at similarly thin sample films. The sample geometry is important to exclude mass transport limitations of liquid-gas reactions (see paragraph 'Intrinsic kinetics and macrokinetics' in section 2.2). However, a certain amount of sample (about 1 g) is required for the analysis of oxide ions and carbonate ions (acid-base titration). In brief, the larger crucibles in this method enable investigation of the intrinsic kinetics addressed in **paper II** due to the relatively large sample quantity, and thin molten salt layers (films) in this geometry.

The **autoclave test rig** sketched in figure 2.6 enables exposure of salt samples to defined temperatures and atmospheres. An alumina crucible is filled with about 100 g of salt, which is a large amount of salt compared to the previous two thermal treatment methods. The sample is heated from the walls, and a temperature sensor measures the salt temperature, which is used for the heating control system. A stirrer accelerates the transport of soluble gases through the liquid phase, and development of chemical equilibria. Horizontal plates act as shields, and prevent the flow of evaporated salt or salt dust into the gas outlet tubes, which could lead to problematic clogging. The gas phase is constantly purged. Compared to the chamber furnace set-up, the purge gas and the flow rate are precisely adjustable by flow control devices. Salt samples are extracted over the course of the experiments by opening a valve, and a pipette-like process with a stainless steel tube. Analyzing the salt composition is identical with the procedure described above for the furnace chamber experiments (compare figure 2.5(b)). The autoclave test rig allows extraction of multiple samples from the same batch without interruption of the experiment until the chemical composition remains constant, and is applied in **paper III**.

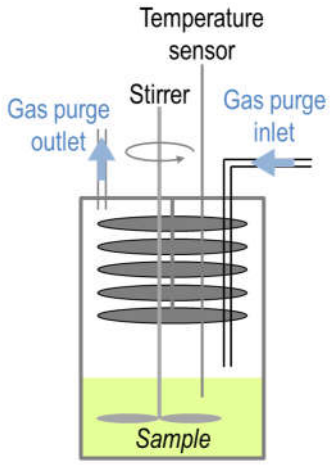

Figure 2.6: Autoclave test rig set-up for thermal treatment of salt samples in the 100 g scale. The molten salt in an alumina crucible is heated from the walls, and the atmosphere is controlled by a gas purge. The five horizontal plates are installed to retain evaporated salt.

An overview of the key features of the three presented thermal treatment methods is given in table 2.2. The methods used in the papers (2nd row) are chosen with regard to the scientific intention (3d row). The intrinsic kinetics and chemical equilibrium of reaction (N) are investigated in **paper I**. The TGA method is chosen since it controls temperature and atmosphere most accurately, and at the same time allows IC post-analysis. Also, the relatively small sample quantity excludes mass transport limitations, which makes TGA a suitable method for intrinsic kinetics measurements. The intrinsic kinetics of the oxide ion formation are addressed in **paper II**. The chamber furnace is applied in the respective experiments because it allows measurement of the intrinsic kinetics of reaction (O) due to the temperature limit, and the possibility to analyze the oxide and carbonate content of the salt

samples via acid-base-titration. **Paper III** aims to demonstrate the chemical equilibrium of reaction (O). The autoclave test rig is the appropriate method, because it allows addition of nitrous gases to the gas purge, as well as titration analysis of oxide ions and carbonate ions.

Table 2.2: Overview and comparison of the thermal treatment methods applied in this thesis. Depending on the scope of research, the adequate method is selected for each series of experiments.

Method	**Thermogravimetric analysis (TGA)**	**Chamber furnace**	**Autoclave test rig**
Applied in	Paper I	Paper II	Paper III
Intention	Intrinsic kinetics and equilibrium of reaction (N)	Intrinsic kinetics of reaction (O)	Reaction (O) equilibrium
Apparatus	Netzsch STA 449	Nabertherm HTCT 01/16, controller P330	Custom designed
Sample quantity	~50 µg	~1.5 g	~100 g
Accessible reaction characteristics	Intrinsic kinetics and equilibrium of reaction (N)	Intrinsic kinetics and equilibrium of reaction (N); Intrinsic kinetics of reaction (O)	Macrokinetics and equilibrium of reaction (N); Macrokinetics and equilibrium of reaction (O)
Upper temperature limit	~560 °C for Solar Salt	1000 °C	~650 °C
Atmospheres in this work	Synthetic air	Ambient air	Mixtures of N_2, O_2 and NO_x
In-situ analysis	Mass change	-	-
Post-analysis of the salt composition	IC (NO_3^-, NO_2^-) after the TGA experiments	IC (NO_3^-, NO_2^-); Titration (O^{2-}, CO_3^{2-})	IC (NO_3^-, NO_2^-); Titration (O^{2-}, CO_3^{2-})

3 Summarizing the results

The fundamental results of the three papers of this thesis are summarized and discussed in the subsequent sections. It is elucidated, that the results complement and influence each other. Also, links and effects among the publications are explained. Details and in-depth discussion can be found in the particular papers in the appendix. In section 3.1, the reaction steps of the decomposition process that are investigated in the papers are assembled to a consistent network. Sections 3.2-3.5 summarize the main results of the four principal research topics, which are the chemical equilibrium and the intrinsic kinetics of reactions (N) and (O), respectively.

3.1 Guide through the journal publications

The conclusions derived from literature reviews, and the results of this thesis allow combination of the molten salt components and reactions to a consistent network of reaction steps. This network visualizes the relations and dependences of the reactions, and is sketched in figure 3.1. Starting from a mixture of solid sodium nitrate (60 wt.%) and potassium nitrate (40 wt.%), molten Solar Salt is formed by increasing the temperature above the melting range. The molten Salt is comprised of nitrate anions (NO_3^-), and sodium and potassium cations (Na^+, K^+).

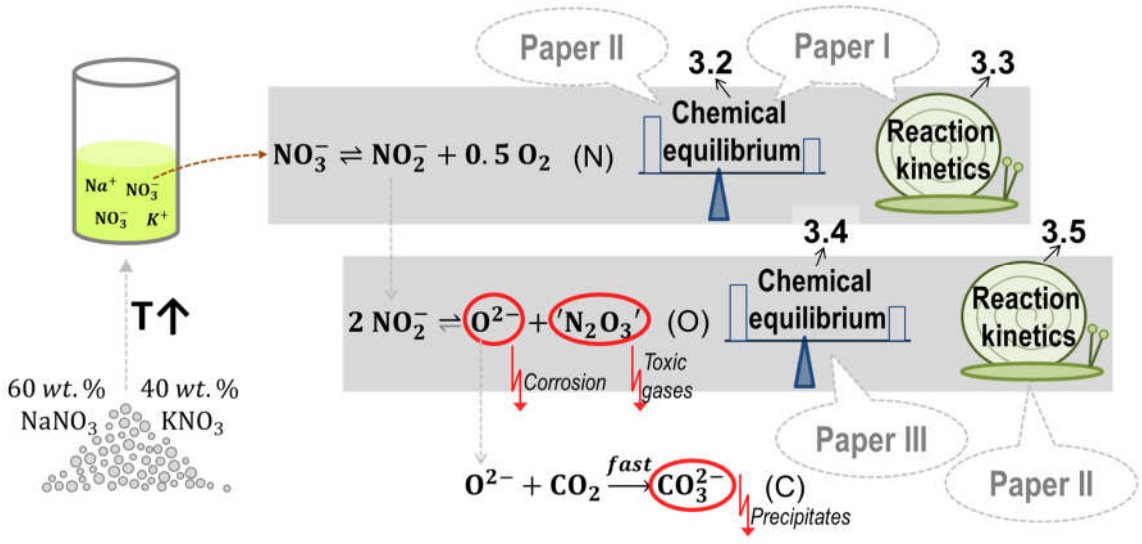

Figure 3.1: Schema of composition changes and the thermal decomposition process of Solar Salt. The three decomposition steps are linked via the nitrite ions and oxide ions. The chemical equilibria (illustrated by the balance symbol) and reaction kinetics (snail symbol) of the first and second step are investigated in this thesis (**papers I, II and III**), and the numbers refer to the corresponding sections. The problematic decomposition products are marked with red circles and lightning symbols.

The nitrate ions are converted to nitrite ions and oxygen gas in the first step reaction (N). The chemical equilibrium of this reaction is investigated in **papers I** and **II** in two temperature ranges (450-550 °C

and 560-630 °C, respectively). The results are summarized in the following section 3.2. The reaction kinetics of reaction (N) are focused in **paper I**, and reported in section 3.3. Reaction (N) is investigated in **paper I** independently from the other reactions, since those are negligible in the applied temperature range (450-550 °C).

The nitrite ions that evolve from reaction (N) can decompose further to oxide ions and decomposition gases in reaction (O), which is the second step in figure 3.1. Many details of the oxide ion formation reaction in molten nitrate salts are lacking in the literature. The chemical equilibrium and the reaction kinetics are investigated separately in two papers in this thesis. **Paper III** (and section 3.4) addresses questions regarding the equilibrium compositions of molten Solar Salt including oxide ions, and the necessary gas atmosphere. The time dependence of the oxide formation (forward reaction (O)) is investigated and described in **paper II**, and in section 3.5.

In the presence of carbon dioxide, the oxide ions react to carbonate ions in reaction (C). The results indicate that this reaction is fast compared to the other reactions of the network, and thermodynamically favored. Therefore, the reaction is approximated as a complete and instantaneous reaction in **paper II**. In **papers I and III**, the carbonate formation is excluded by the use of CO_2 free atmospheres. Detailed research on reaction (C) is not within the scope of this thesis since the formation of carbonates can be approximated reasonably.

The most problematic decomposition products are oxide ions, nitrous gases, and carbonate ions, according to the state-of-knowledge. Those compounds are formed in the second and third step of the decomposition process shown in figure 3.1. However, the first step (reaction (N)) is equally important. It enables further decomposition by forming nitrite ions, and influences other reactions via salt composition changes. Therefore, detailed knowledge and an exact description of reaction (N) is acquired in **papers I and II**.

3.2 Chemical equilibrium of the nitrite forming reaction (N) (Papers I and II)

Chemical equilibrium requires that all compounds that participate in a regarded reaction can reach constant concentrations. In the case of reaction (N), the liquid-gas system must comprise nitrate ions and nitrite ions in the liquid phase, and oxygen molecules in the gas phase as well as in the liquid phase (in terms of dissolved oxygen). This situation including the relevant equilibrium constants K is sketched in figure 3.2. The reaction equilibrium in the liquid phase with the constant K_{melt} (equation (34)), and the solubility equilibrium of oxygen with the constant K_H (equation (33)) are merged to the overall equilibrium constant $K_{(N)}$ (equation (35)). Using $K_{(N)}$ is favorable, because it can be

calculated by experimentally accessible quantities, which are the nitrate and nitrite ion content in the liquid phase, $x_{NO_3^-,eq}$ and $x_{NO_2^-,eq}$, resp., and the partial pressure of oxygen $p_{O_2,eq}$ in the gas phase.

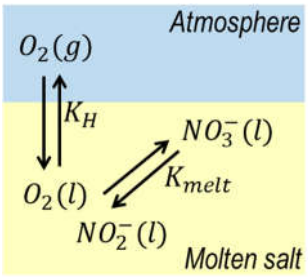

$$K_H = x_{O_2,eq} / \frac{p_{O_2,eq}}{p_0} \tag{33}$$

$$K_{melt} = x_{NO_2^-,eq} \cdot x_{O_2,eq}^{0.5} / x_{NO_3^-,eq} \tag{34}$$

$$K_{(N)} = K_{melt} / K_H^{0.5} = x_{NO_2^-,eq} \cdot \left(\frac{p_{O_2,eq}}{p_0}\right)^{0.5} / x_{NO_3^-,eq} \tag{35}$$

Figure 3.2: Chemical equilibria related to reaction (N) in a liquid-gas system. Species in the molten salt are marked with (l) which refers to the liquid phase, and species in the atmosphere are marked with (g) for gas phase. The equilibrium constants are described in equations (33)-(35). A similar figure is included in **paper I**.

The gas phase of the experiments in **papers I and II** is purged with synthetic air and ambient air, respectively, with the intention to assure constant oxygen partial pressure in all experiments. Nitrate ions are a major component of Solar Salt, and the nitrite ions form via reaction (N). Both ions are analyzed by ion chromatography (IC) in the experimental processes. Thus, all components of reaction (N) are comprised in the liquid-gas systems of **papers I and II**, and chemical equilibrium is achievable.

The experimentally measured nitrate ions and the nitrite ion contents at chemical equilibrium at different temperatures are reported in **papers I and II**. Those ion contents are used to calculate the equilibrium constants $K_{(N)}$ of reaction (N) at the considered temperatures. The equilibrium constants are shown in the van't Hoff plot in figure 3.3 together with results from the literature. The results of **paper II** are also included in figure 3.3, but should be considered with care, because full equilibrium of reaction (N) might be prevented by mass transport effects in the larger scale (~100 g) experiments. The results of **papers I and II** are in between the literature results for pure sodium salt and pure potassium salt, which is reasonable because Solar Salt ($Na_{0.64}K_{0.36}$) is a mixture of both. The literature results for mixtures of sodium salt and potassium salt are closer to the results of this thesis than the values for pure salts. Investigations including lower temperatures (533-866 K, Tracey et al. [42], blue square symbols and purple solid line in figure 3.3) showed lower $K_{(N)}$ values than the fit line of higher temperature data points (500-600 °C, Nissen and Meeker [39], pink dashed fit line of the pink rhombus symbols) predicts. This effect is confirmed by the results of this thesis. The fit line of the high temperature results (black dotted line) overestimates the $K_{(N)}$ values measured at lower temperatures (unfilled circle symbols); or vice versa: the fit line of low temperature results (black dashed line) underestimates the $K_{(N)}$ values measured at higher temperatures (partly filled circle symbols). In other words, assuming that the nitrite concentrations at lower (≤550 °C) temperatures are correct, measurements at high temperatures reveal too high nitrite concentrations. Linearity over

the entire temperature range would be expected according to reaction thermodynamic considerations. The deviations maybe arise from reactions that occur parallel to reaction (N), which could be more pronounced in the higher temperature range.

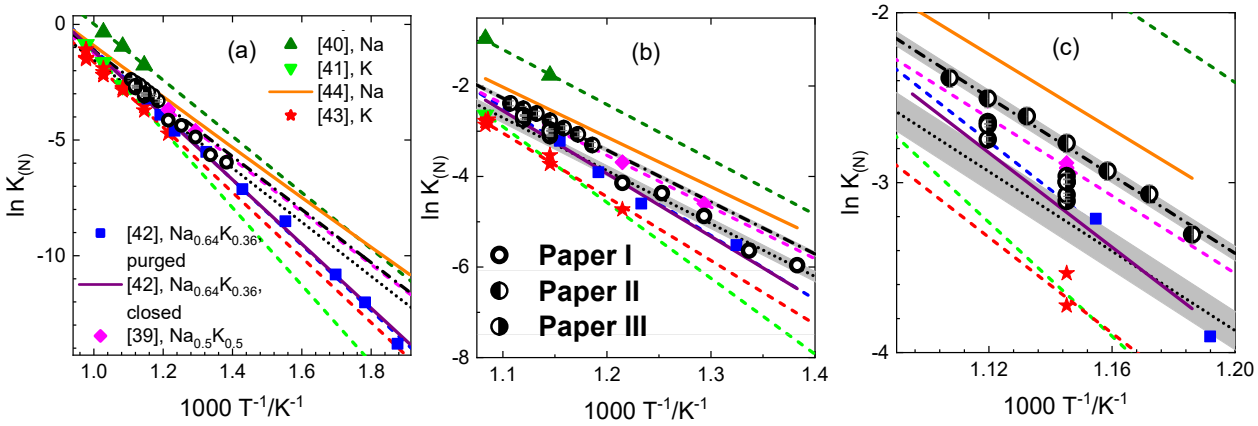

Figure 3.3: Van't Hoff plots of equilibrium constants of reaction (N) $K_{(N)}$ obtained in **papers I, II and III**, and from the references [39-44]. Note that the constants are plotted on a logarithmic scale. (a) shows the overall diagram, and (b) and (c) are enlargements of (a).

The enthalpies and entropies of reaction (N) ($\Delta_{(N)}H$ and $\Delta_{(N)}S$, resp.) resulting from this thesis, and from the literature references are listed in table 3.1. The reaction enthalpies and entropies of **papers I and II** agree with each other considering the uncertainties. Both also agree with the values from Barin [44] and Nissen and Meeker [39]. Differences to the remaining references are ascribed to diverging cation compositions and temperature ranges, as described in the above paragraph along with the discussion of figure 3.3.

Table 3.1: Thermodynamic parameters of reaction (N) regarding the chemical equilibrium. The reaction enthalpies $\Delta_{(N)}H$ and entropies $\Delta_{(N)}S$ of **papers I and II**, and appropriate references are collected. An extended version of this table can be found in **paper I**.

Reference		Cations	$\Delta_{(N)}H/kJ\cdot mol^{-1}$	$\Delta_{(N)}S/J\cdot mol^{-1}\cdot K^{-1}$
Paper I		**$Na_{0.65}K_{0.35}$**	**97 ± 9**	**85 ± 12**
Paper II		**$Na_{0.65}K_{0.35}$**	**95 ± 4**	**86 ± 5**
Freeman [40]		Na	101 ± 5	101 ± 5
Freeman [41]		K	139 ± 6	129 ± 6
Barin [44]		Na	97.5	87.4
Bartholomew [43]		K	117 ± 4	103 ± 5
Tracey et al.[42]	Closed system	$Na_{0.65}K_{0.35}$	115.5	105.9
	Purged system		117 ± 3	109 ± 4
Nissen and Meeker [39]		$Na_{0.5}K_{0.5}$	95 ± 3	84 ± 3

3.3 Intrinsic kinetics of the nitrite forming reaction (N) (Paper I)

The time dependence of the nitrite and nitrate formation in Solar Salt is investigated and described by means of reaction kinetics. The thermogravimetric analysis (TGA) experiments presented in **paper I** trace the formation of nitrite ions over time at five temperatures. The results are shown in the diagram in figure 3.4 in terms of the nitrite concentration $c_{NO_2^-}$ over time. The reaction is fast in the beginning when the molten Solar Salt is mostly undecomposed, meaning that a relatively high amount of nitrite ions is formed per time step, and the curve is steep. When nitrite ions accumulate in the molten salt, the observable reaction becomes slower. On a microscopic level, the rate of the nitrite formation reaction remains constant, but the reverse reaction that forms nitrate ions intensifies until it is equally frequent, and chemical equilibrium is obtained. The finally obtained equilibrium concentration of nitrite is described and discussed in the previous section 3.2. The experiments show faster nitrite formation with increasing temperatures. This relation is in agreement with the reaction kinetics theory (see section 2.2) saying that the ratio of nitrate ions with sufficient energy to overcome the energy threshold of the reaction (activation energy) increases with temperature.

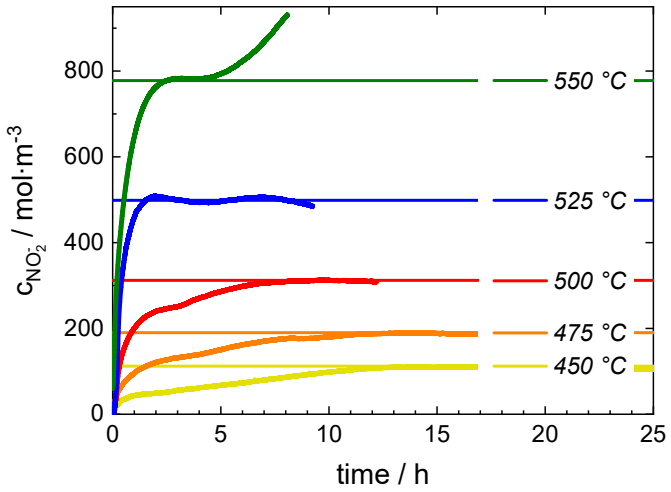

Figure 3.4: Thermogravimetric analysis (TGA) results of **paper I**. The nitrite concentration $c_{NO_2^-}$ in molten Solar Salt is plotted over time. The temperatures represent the experiment temperature. The horizontal lines illustrate the chemical equilibrium at the respective temperatures. A similar figure is presented in **paper I**.

For a quantitative description of the reaction kinetics, a differential rate law is developed. The type of rate law is based on literature findings, and focusses on the nitrite formation (forward reaction) with the intention to precisely describe the decomposition process. The derived rate law (equation (36a)) expresses changes in the amount of nitrite $c_{NO_2^-}$ over time t by two terms. The first term with a positive sign belongs to the forward reaction (N) (nitrite formation), which increases the amount of nitrite, and is characterized by the forward rate constant $k_{f,(N)}$. The second term with a negative sign belongs to the reverse reaction (N) (nitrate formation), which consumes nitrite ions and therefore

decreases the amount of nitrite, and is characterized by the reverse rate constant $k_{r,(N)}$. Depending on the actual salt concentration, one or the other term predominates, and causes an overall increase or decrease of nitrite ions. For the presented experiments, the nitrite concentration is small at the beginning ($c_{NO_2^-} \approx 0$, undecomposed Solar Salt), which makes the second term in equation (36a) small compared to the first term. Accordingly, an overall formation of nitrite ions is described by equation (36a), and also observed in the experiments. In equation (36b), the rate constants of equation (36a) are replaced by the Arrhenius expressions (equation (23)), which reveals the temperature dependence of the reaction kinetics.

$$\frac{dc_{NO_2^-}}{dt} = k_{f,(N)} \cdot c_{NO_3^-} - k_{r,(N)} \cdot c_{NO_2^-} p_{O_2}^{0.5} \tag{36a}$$

$$\frac{dc_{NO_2^-}}{dt} = A_{f,(N)} \cdot exp\left(-E_{a,f,(N)}/RT\right) \cdot c_{NO_3^-} - A_{r,(N)} \cdot exp\left(-E_{a,r,(N)}/RT\right) \cdot c_{NO_2^-} p_{O_2}^{0.5} \tag{36b}$$

The experimental results (figure 3.4) are fitted according to the derived differential rate law (equation (36a)). The fit results combined with the existing equilibrium description of reaction (N) allow calculation of the rate constants $k_{f,(N)}$ and $k_{r,(N)}$. The experiments are made at five different temperatures, and consequently, $k_{f,(N)}$ and $k_{r,(N)}$ are determined for five temperatures. The temperature dependence of the rate constants is evaluated by means of the Arrhenius diagrams in figure 3.5, which plot the logarithmic rate constants versus the inverse temperature. $k_{f,(N)}$ and $k_{r,(N)}$ increase with increasing temperature, as discussed earlier. The rate constants measured in **paper I** are higher than the literature values. The applied TGA method was developed with the intention to exclude mass transport limitations, and therefore thin salt samples (<1 mm) are investigated. Probably, diffusion of oxygen through the molten salt is included in the kinetics description of some literature references. The published values then describe reaction macrokinetics, which is a combination of the intrinsic reaction kinetics and mass transport effects, and are valid for the particular sample geometry and experiment conditions.

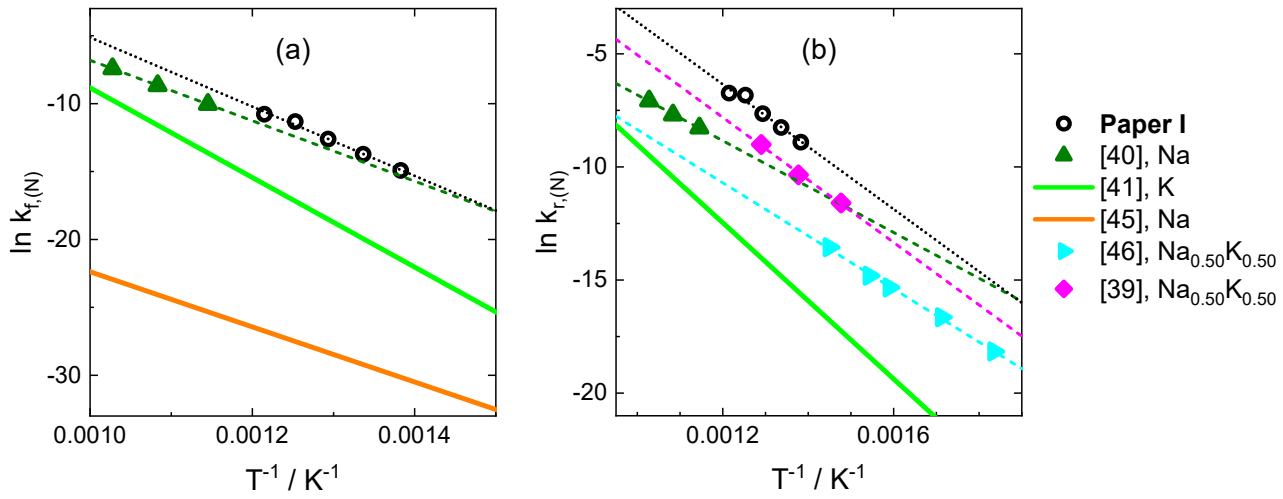

Figure 3.5: Arrhenius diagrams of the reaction rate constants of reaction (N), determined in **paper I**. The forward rate constants $k_{f,(N)}$ are plotted in (a), and the reverse rate constants $k_{r,(N)}$ are plotted in (b). The numbers is brackets refer to the literature that is consulted for comparison. The figures are taken from **paper I**.

The activation energies $E_{a,f,(N)}$ and $E_{a,r,(N)}$ and pre-exponential factors $A_{f,(N)}$ and $A_{r,(N)}$ for both forward (reduction) and reverse (oxidation) reaction are extracted from the linear fit (black dotted lines in figure 3.5), according to the Arrhenius equation (23). The results are listed in table 3.2 together with literature values. The activation energy for the reverse reaction $E_{a,r,(N)}$ found in this thesis agrees with the results of Nissen and Meeker [39]. However, comparability of the results is limited due to different experimental set-ups, and varying differential rate laws. The parameters of table 3.2 can be inserted in equation (36b) to obtain a temperature independent model equation for the reversible kinetics of reaction (N).

Table 3.2: Parameters of the intrinsic kinetics of reaction (N) in molten nitrate salts. An extended version of this table can be found in **paper I**.

Reference	Cations	$E_{a,f,(N)}$/kJ·mol^{-1}	$A_{f,(N)}$/s^{-1}	$E_{a,r,(N)}$/kJ·mol^{-1}	$A_{r,(N)}$/s^{-1}
Paper I	**$Na_{0.65}K_{0.35}$**	**212 ± 11**	**694546727 ± 6**	**115 ± 11**	**25770 ± 6**
Freeman [40]	Na	185 ± 2	5104230 ± 11	84 ± 5	27 ± 1
Freeman [41]	K	274	3.16E+10	144	3801.90
Bond and Jacobs [45]	Na	169	0.122		
Paniccia and Zambonin [46]	$Na_{0.50}K_{0.50}$			98 ± 2	29 ± 2
Nissen and Meeker [39]	$Na_{0.50}K_{0.50}$			115 ± 7	6376 ± 3

3.4 Chemical equilibrium of the oxide forming reaction (O) (Paper III)

The literature on molten nitrate salts indicates that the formation of oxide ions is accompanied by the evolution of reaction gases (see section 1.3). Most frequently, the nitrous gases NO and NO_2, O_2 and N_2 are observed or postulated. The oxide formation is expected to be a reversible reaction that ceases at chemical equilibrium, but no experimental confirmation could be found. Those findings are summarized to reaction (O) where the particular reaction gases are replaced by $'N_2O_3'$ due to lacking results on the exact types and stoichiometry or the gases.

According to the state-of-knowledge, experimental demonstration of a chemical equilibrium with oxide ions in molten nitrate salt should be possible under specific atmospheric conditions. The experiments in **paper III** are designed with the intention to create a liquid-gas system, which contains all species that are relevant for the reaction (O). More precisely, the aim is to provide a gas phase that comprises the reaction gases (represented by $'N_2O_3'$ in reaction (O)). The gas volume of the experimental set-up is purged with a gas mixture of N_2, O_2 and NO. The formation of NO_2 according to reaction (G) is fast according to the references [57-59], and therefore the presence of NO_2 in the purge gas is reasonably assumed. NO_2^- and O^{2-} are formed in the liquid phase by the chemical reactions (N) and (O). The liquid-gas system thus comprises all ions and gases that are discussed to participate in reaction (O), which enables chemical equilibrium.

The experimental results gained at two temperatures are shown in terms of the oxide ion content $x_{O^{2-}}$ over time in figure 3.6 for 600 °C and 620 °C. Blank experiments, which are purged with synthetic air (but without the nitrous gases NO and NO_2), are included in the diagrams for both temperatures. Nitrous gases are considered as products of reaction (O). Therefore, a steady removal of nitrous gases by the synthetic air gas flow in the blank experiments pushes reaction (O) constantly in the forward direction, which means a release of nitrous gases and the formation of oxide ions. In agreement with this theoretical consideration, both blank experiments (square symbols in figure 3.6) show a steady increase of the oxide ion content over the course of the experiments. Less oxide ions are formed in the experiments with NO_x in the purge gas, compared to the blank experiments without NO_x purge. In addition, the oxide content seems to stabilize at a certain level, which is not the case in the blank experiments. The presented curves demonstrate the stabilizing effect of NO_x addition to the purge gas. Obviously, the purge mixture of N_2, O_2, NO and NO_2 indeed comprises the gases that are relevant in reaction (O), and no by-product of the oxide formation is missing in the liquid-gas system. The reaction ceases when the equilibrium composition in terms of a particular nitrite and oxide content is reached.

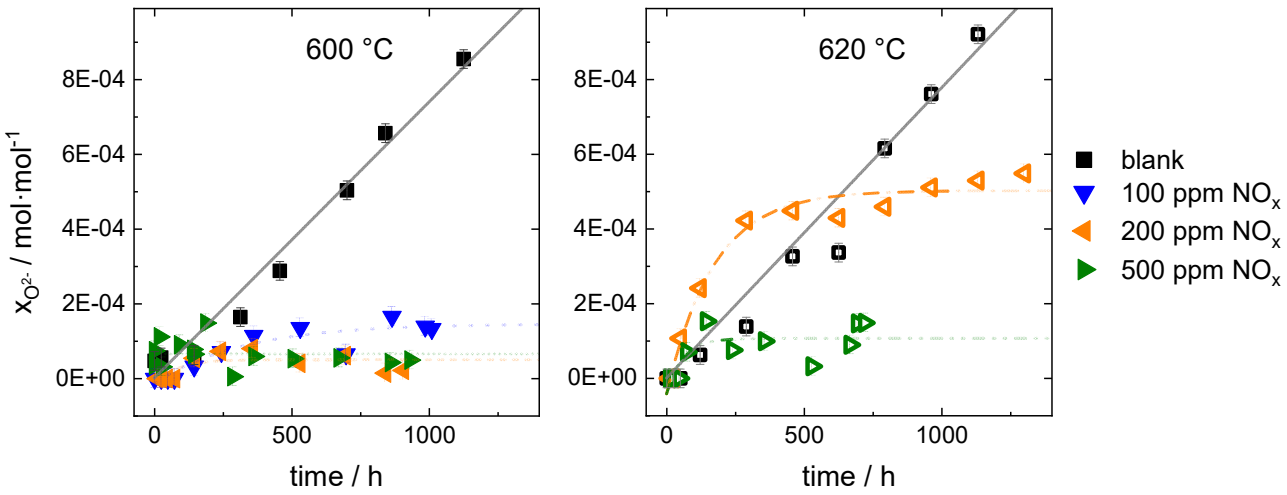

Figure 3.6: Effect of NO_x in the purge gas on the oxide content in Solar Salt. At two temperatures, a blank experiment with synthetic air purge, and experiments with different concentrations of nitrous gases are presented. The lines serve as a guide for the eye. The figures in extended versions are included in **paper III**.

Comparing the steady oxide levels towards the end of the experiments reveals general trends. First, with increasing temperature, the oxide content increases at a given NO_x pressure. For 200 ppm NO_x, the oxide content stabilizes at ~ 0.5E-4 mol·mol^{-1} at 600 °C, and at 5.5E-4 mol·mol^{-1} at 620 °C. This relation agrees with the thermodynamics of an endothermic reaction predicting increasing contents of reaction product with increasing temperature. Second, increasing the NO_x pressure decreases the oxide content at constant temperature, which is shown by the curves in figure 3.6 for the temperature 620 °C. This observation follows the law of mass action of reaction (O) indicating that chemical equilibrium can be preserved when the content of one reaction product (in this case the oxide content) increases, while the content of another product (in this case the NO_x pressure) decreases.

A precise reaction equation for the oxide formation instead of the general reaction (O) is required for the prediction of equilibrium salt compositions at varying temperatures and atmospheric conditions. The reaction equations available in the literature differ in the stoichiometric ratio $\nu_{N_2}/\nu_{O^{2-}}$, which expresses the amount of nitrogen molecules that are formed per oxide ion. Examples of reaction equations with stoichiometric ratios $\nu_{N_2}/\nu_{O^{2-}}$ of 0, 0.5 and 1 are taken from the literature, and listed in table 3.3. The stoichiometric ratio of NO, NO_2 and O_2 in those reaction equations is not relevant for equilibrium calculations, because the gas phase equilibrium of these three gases is sufficiently described by the thermodynamics of reaction (G), and gas phase equilibrium is assumed.

3.4 Chemical equilibrium of the oxide forming reaction (O) (Paper III)

Table 3.3: Reaction equations proposed in the literature for oxide ion formation. The reactions differ in the stoichiometric ratio $\nu_{N_2}/\nu_{O^{2-}}$, and are combined with reactions (N) and (G) (in grey) to model the chemical equilibrium of the entire liquid-gas system. A similar table is included in **paper III**.

$\boldsymbol{\nu_{N_2}/\nu_{O^{2-}}} =$	Reaction equation		References
0	$2\ NO_2^- \rightleftharpoons \boldsymbol{O^{2-}} + NO_2 + NO$		20,35-37,48-53
0.5	$2\ NO_2^- \rightleftharpoons \boldsymbol{O^{2-}} + NO + O_2 + \boldsymbol{0.5\ N_2}$		34
1	$2\ NO_2^- \rightleftharpoons \boldsymbol{O^{2-}} + \boldsymbol{N_2} + 1.5\ O_2$		48,51,52
	+		
	$2\ NO_3^- \rightleftharpoons 2\ NO_2^- + O_2$	(N)	
	+		
	$NO + 0.5\ O_2 \rightleftharpoons NO_2$	(G)	

In addition to one of the oxide forming reactions, reactions (N) and (G) also have to be considered to describe the equilibrium state of the entire liquid-gas system, see table 3.3. Overall, thermodynamic data (enthalpies and entropies of formation) of the pure substances, and the laws of mass action of the reactions (N), (O) and (G) are combined. This procedure enables calculation of the equilibrium oxide contents (and also nitrate and nitrite contents) at different temperatures, NO_x pressures, and stoichiometric ratios $\nu_{N_2}/\nu_{O^{2-}}$. Details of the calculations e.g. selection of the applied data and assumptions can be found in **paper III**. The calculated oxide contents are shown in figure 3.7 for the conditions that are applied in the experiments, e.g. 600 and 620 °C, 0.8 bar N_2 and 0.2 bar O_2. The diagrams allow comparison of calculated equilibrium oxide contents (striped columns) and experimentally measured equilibrium oxide contents (grey columns). The calculations based on reactions with stoichiometric ratio $\nu_{N_2}/\nu_{O^{2-}}$ of 0 differ notably from the experimental results. Although reaction equations without N_2 formation are predominantly reported in the literature, the results gained in this thesis indicate that these reactions are not suitable to describe the reaction equilibrium of the oxide formation in Solar Salt. For all parameter combinations, the experimental results are in between the calculations with stoichiometric ratios $\nu_{N_2}/\nu_{O^{2-}}$ of 0.5 and 1. The reaction with $\nu_{N_2}/\nu_{O^{2-}}$ equal 1 can be excluded, because it predicts the existence of chemical equilibrium with oxide ions under nitrogen-oxygen atmospheres (without nitrous gases), which was never observed in experiments. Based on the results of this thesis, an appropriate reaction equation for the oxide formation in Solar Salt with a stoichiometric ratio $\nu_{N_2}/\nu_{O^{2-}}$ between 0.5 and 1 is recommended. For example, equation (37) with $\nu_{N_2}/\nu_{O^{2-}}$ equal 0.75 is proposed.

$$2\ NO_2^- \rightleftharpoons O^{2-} + 0.5\ NO + 1.25\ O_2 + 0.75\ N_2 \qquad (37)$$

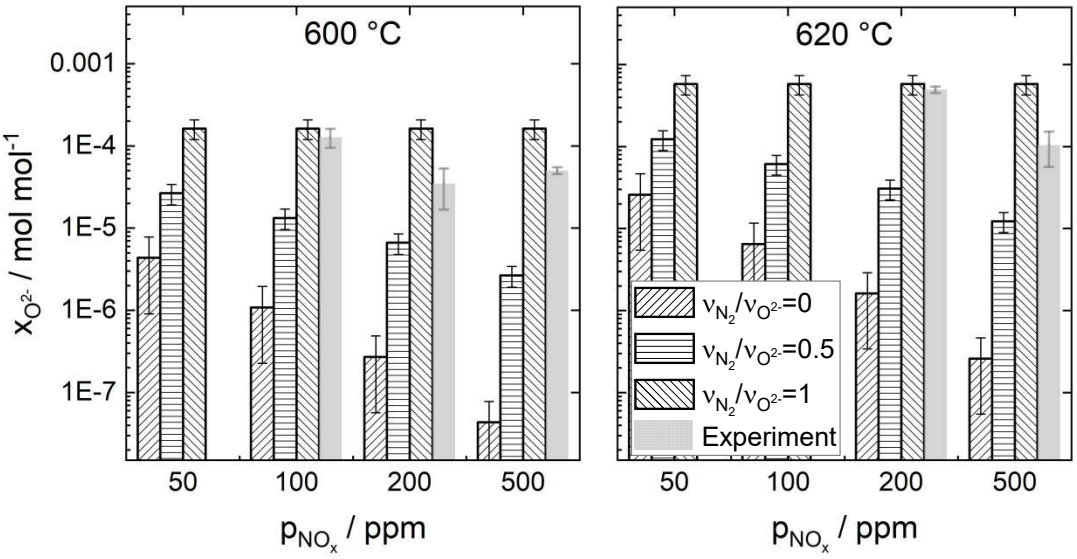

Figure 3.7: Calculated and experimental equilibrium oxide contents in Solar Salt. The calculated results depend on the chosen stoichiometric ratio $\nu_{N_2}/\nu_{O^{2-}}$, on the temperature (600 °C for the left diagram, and 620 °C for the right diagram), and on the NO_x partial pressure p_{NO_x}. The experimental results (grey columns) are obtained under the corresponding experiment conditions. The figures can also be found in **paper III**.

3.5 Intrinsic kinetics of the oxide forming reaction (O) (Paper II)

Paper II focuses on the time dependence of the oxide ion formation in Solar Salt. In a series of experiments, salt composition changes are monitored over time at temperatures between 560 and 630 °C, which is the temperature range of interest for future molten salt energy storage technologies. The experiment durations are chosen with respect to two major experimental constrains. First, the applied furnace method requires heating and cooling times of ~30 min each. The isothermal segments, which are considered for kinetics evaluation, are chosen ≥2 h to minimize the contribution of the heating and cooling periods to the overall measured composition changes. Second, the content of reaction products increases with time. Exceeding the solubility limit of the reaction products causes the formation of solid precipitates. Experiment durations ≤5 h are chosen to avoid inhomogeneities in the salt samples, and erroneous analysis results.

The experiments are performed with ambient air purge, which contains carbon dioxide (~400 ppm), and allows reaction (C) to follow on reaction (O). Indeed, carbonate ions are measured in the salt samples, whereas no oxide ions are found. This observation corresponds to a fast successiveness of reactions (O) and (C), see figure 3.1. It is also reported in the literature that reaction (C) is fast, compared to reaction (O). According to the rate determining step approximation (see section 2.2), the faster step of a sequence can be neglected for kinetics considerations, and therefore the oxide content (shown in figure 3.8) is recalculated from the carbonate content.

The nitrate and nitrite contents measured in the experiments are evaluated with regard to the chemical equilibrium of reaction (N), which is presented in section 3.2.

The oxide content x_{M_2O} $(M = Na, K)$ over time is plotted in figure 3.8. The experimental results reveal that the oxide content increases with time. According to reaction (O) and the results of section 3.4, nitrous gases evolve simultaneously to the oxide formation. Those gaseous by-products are steadily removed from the gas phase by the air purge, which drives the reaction in the forward direction. Under these atmospheric conditions, reaction (O) can be considered an irreversible reaction that forms oxide ions over the entire experiment durations.

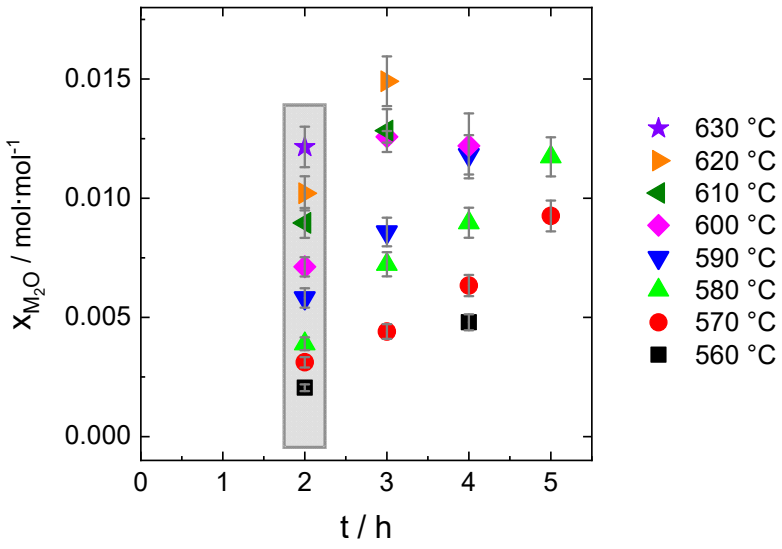

Figure 3.8: Oxide contents in Solar Salt after 2-5 h at temperatures up to 630 °C. Thermal treatment of Solar Salt in air atmosphere provokes chemical reactions that form oxide ions and carbonate ions. Each point represents one individual experiment. This figure is published in **paper II**.

The grey shaded area in figure 3.8 shows the oxide contents that have accumulated in the molten salt after 2 h at different temperatures. It reveals that the oxide content increases with increasing temperature. The sample stored at 560 °C contains 0.002 mol·mol^{-1} oxide ions, whereas 0.012 mol·mol^{-1} are formed at 630 °C. This increase is related to the kinetics theory. The fraction of reactant particles that are able to overcome the reaction energy barrier increases with temperature.

A kinetic rate law is formulated for a quantitative description of the reaction kinetics in terms of a mathematical equation. The literature indicates that the oxide formation in nitrate-nitrite salts is first order with respect to nitrite ions, meaning that the rate determining step is the decay of nitrite ions. Accordingly, the rate law expressed in equation (38) can be assumed. It describes changes in the oxide concentration c_{M_2O} over time in terms to the rate constant $k_{(O)}$ and the actual nitrite concentration c_{MNO_2}.

$$r_{(O)} = dc_{M_2O}/dt = k_{(O)} \cdot c_{MNO_2} \tag{38}$$

Rate constants $k_{(O)}$ at eight temperatures are obtained by fitting the experimental results at the respective temperature according to the rate law equation (38). The fitting process in detail is described in **paper II**. The temperature dependence of $k_{(O)}$ is accessed by plotting the constants in the Arrhenius diagram in figure 3.9. It illustrates that $k_{(O)}$ increases with increasing temperature, as discussed qualitatively above. The linear fit of the rate constants according to the Arrhenius equation (23) reveals the kinetics parameters, which are the activation energy $E_{a,(O)}$ of 42 ± 3 kJ·mol^{-1}, and the pre-exponential factor $A_{(O)}$ of 0.003 ± 0.001 s^{-1}. The obtained parameters are combined with equations (23) and (38) to finally present the 'ready-for-use' equation (39).

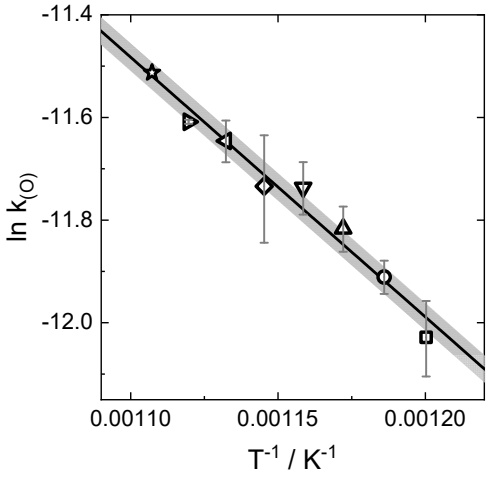

Figure 3.9: Rate constants of reaction (O) in Solar Salt shown in an Arrhenius plot. Each symbol corresponds to the rate constant at the respective temperature. The symbol shapes of this figure and figure 3.8 agree. The slope and intercept of the linear fit are transformed to the activation energy $E_{a,(O)}$, and the pre-exponential factor $A_{(O)}$ according to equation (23). This figure is published in **paper II**.

$$r_{(O)} = dc_{M_2O}/dt = 0.003 \pm 0.001\ s^{-1} \cdot exp(-42 \pm 3\ \text{kJ} \cdot mol^{-1}/RT) \cdot c_{MNO_2} \tag{39}$$

4 Comprehensive conclusions of papers I, II and III

The investigations presented in this thesis provide new insights regarding the methodology, and extend the state-of-knowledge of the reaction chemistry in Solar Salt. The results are appreciable in several application fields, and concern existing and future molten nitrate salt heat storage and heat transfer technologies. Conclusions with regard to those points are made in the following paragraphs.

Methodology to examine nitrate salt reactions

The difference between micro- and macrokinetiks has to be considered while selecting an experiment methodology. The chemical reactions addressed in this thesis all comprise gaseous reaction products, which are soluble in the liquid phase only to some extent, and primarily exist in the gas phase. Accordingly, **mass transport of dissolved gases** through the phases, and through the liquid-gas interface can affect the macroscopically observable reaction kinetics. To measure the intrinsic kinetics (microkinetics), mass transport limitations have to be negligible in the chosen sample quantities and geometries. For this reason, thin films of salt are used for intrinsic kinetics investigations in this thesis, and are recommended for similar investigations. Exclusion of mass transport limitations is not only favorable for intrinsic kinetics investigations, but can also be advantageous for measurements of reaction equilibria. Diffusion of reactants might be slow, so that the equilibrium composition may not be obtained within the experiment duration. The equilibrium results of larger scale experiments should be evaluated with regard to mass transport limitations.

Thermogravimetric analysis experiments reveal a significant **vapor pressure** of Solar Salt, which is challenging in a practical sense for the experiment set-up, and also for data evaluation. Salt evaporation and precipitation in cooler areas of the apparatus should be taken in consideration. Mass changes of the salt sample can be ascribed to, first, salt evaporation, which is mostly unintended but difficult to avoid, and second, release or uptake of reaction gases, which correlate with the reaction progress of interest. Separating those two effects that can occur simultaneously is crucial to gain reliable reaction results. For large-scale application of Solar Salt, salt evaporation is considered less critical than during laboratory testing due to the smaller surface-to-volume ratio.

The **atmosphere** in contact with molten Solar Salt greatly influences the reactions in the liquid phase. In most published investigations, the gas phase is composed of nitrogen gas and oxygen gas. The results of this thesis emphasize that the presence of carbon dioxide and nitrous gases in the atmosphere is highly relevant as well. Carbon dioxide enables the formation of carbonates in the molten salt, which precipitate to carbonate rich solid phases, if the solubility limit is exceeded.

Analyzing inhomogeneous salt samples is sensitive to errors, and should be avoided by using carbon dioxide free atmospheres. Otherwise, experiment durations have to be restricted to keep the carbonate concentration below the solubility limit.

Some decomposition reactions in Solar Salt are vanishingly weak and slow at low temperatures, but become significant at higher temperatures. Those high temperature reactions such as the oxide ion formation can be neglected at low temperatures. At high temperatures, several reactions occur in parallel in Solar Salt. Under certain conditions, instantaneous equilibrium can be assumed for reactions with relatively fast reaction kinetics, e.g. for the nitrate-nitrite reaction at high temperatures. In general, appropriate selection of the **experiment temperatures** allows assumptions regarding the relevant reactions, reaction kinetics and equilibria.

Reaction chemistry of nitrate salt reactions

The decomposition reactions in Solar Salt are combined to a **comprehensive network** of three chemical reactions in this thesis. Nitrate ions react to nitrite ions in reaction (N). Reaction (O) describes the decomposition of nitrite ions to oxide ions. In the presence of carbon dioxide, oxide ions react to carbonate ions in reaction (C). On an intrinsic level, this network suitably represents the chemistry of Solar Salt for the molten salt technology. Dispensable information such as the detailed reaction mechanisms are not included to keep the reaction network simple and effective. The model description contains the relevant steps of the decomposition process as well as the verified decomposition products, which makes it appropriate and adequate for the prediction of Solar Salt stability without mass transport limitations. Depending on the experimental and application conditions, the network can be further simplified. For example, reaction (C) can be neglected in the absence of carbon dioxide, and reaction (N) can be approximated with chemical equilibrium at high temperatures due to comparably fast reaction kinetics.

The ratio of nitrite ions to nitrate ions is defined by the **chemical equilibrium of reaction (N)**. The ratio increases with increasing temperature, and with decreasing oxygen partial pressure. To maintain Solar Salt close to its native (undecomposed) composition, low temperatures and high oxygen partial pressures are favorable. The equilibrium of reaction (N) is described in a model description in terms of the law of mass action and the equilibrium constants, which can be applied for predictions of equilibrium compositions of nitrate ions and nitrite ions in Solar Salt. The thermodynamic reaction parameters (reaction enthalpy and reaction entropy) vary over the investigated temperature range, probably due to minor parallel reactions. Using the parameters that are determined for the regarded temperature range is advisable.

The **intrinsic kinetics of reaction (N)** are relevant for the entire decomposition process, because this reaction is considered the first step in the reaction network. Quantitative experimental data confirm that the nitrite formation becomes faster with increasing temperatures. The model description comprises terms for the forward and reverse reaction, which entails several advantages. Reaction kinetics and the chemical equilibrium are both covered by this combined description. The kinetic rate constants are directly included, and the equilibrium constant of reaction (N) is indirectly included. The model description is applicable to Solar Salt irrespective of the decomposition level, and regardless of whether the forward or reverse reaction predominates macroscopically. The kinetic parameters are most precise in the investigated temperature range (450-550 °C). Extrapolation to lower or higher temperatures is possible, but probably increases the uncertainties.

The oxide content in molten Solar Salt continuously increases over time in synthetic air atmosphere. Addition of nitrous gases to the atmosphere significantly reduces the oxide content, and keeps it at a constant level. Liquid-gas systems with nitrate, nitrite and oxide ions, and nitrogen, oxygen and nitrous gases are found to fulfill the **equilibrium requirements of reaction (O)**. To maintain a low oxide level, an increasing partial pressure of nitrous oxides is needed with increasing temperatures. The quantitative experiment results at 600 and 620 °C serve as reference points for the selection of the appropriate atmosphere condition for Solar Salt under varying conditions. For a model description of Solar Salt, oxide ions included, and the connected gas phase, all relevant reactions must be considered. Those reactions are the reversible nitrate-nitrite reaction (N), the gas phase reaction (G) of the nitrous gases, and an oxide forming reaction (O). Based on the results of this thesis, oxide forming reactions that state between 0.5 and 1 equivalents nitrogen gas per oxide ion are recommended. Reaction equations with those stoichiometries lead to the best agreements of thermodynamic calculations and experimental results. Therefore, it is reasonable to assume that nitrogen is formed together with oxide ions, or, that nitrogen plays a role in the oxide formation reaction mechanism.

The **intrinsic kinetics of the oxide formation** is found to accelerate with temperature. The experiment results are satisfyingly described with a differential rate law, which is first order with respect to nitrite. Consequently, the rate determining step in reaction (O) is assumed to be a decay of nitrite ions. The resulting model description, and the associated kinetics parameters are relevant in a technological sense, because oxide ions are regarded as primarily responsible for steel corrosion in Solar Salt. Also, the release of nitrous gases is undesired. The model description for the oxide formation kinetics is suitable for combination with descriptions of further reactions.

Relevance for research and technology

The results of this thesis serve as a basis for **future research**. The investigated reactions are fundamental for all processes in molten nitrate salts and remain relevant, e.g. if further high temperature reactions are revealed. Moreover, extended knowledge about the reaction chemistry and its model description affect scientific fields apart from the pure reaction chemistry, such as corrosion processes, changing material properties and gas solubility.

The developed network of decomposition reactions and the corresponding model descriptions enable prediction and specific manipulation of the Solar Salt chemistry for **technological applications**. For large-scale molten salt systems, the reaction chemistry description can be combined with existing models for e.g. mass transport and fluid flow to integrate the relevant characteristics of the system. Such a multi-phenomenon-model can be applied to prolong the lifetime of Solar Salt material in state-of-the art heat storage systems. The model helps to adjust the operating conditions including temperature profiles and atmosphere compositions with the intention to ensure material stability. For example, it can predict the amount of stabilizing gases that needs to be added to the atmosphere to restrict the accumulation of corrosive oxide ions and the evolution of toxic nitrous gases to acceptable levels. For the next generation of heat storage systems, the model supports the increase of the maximum operating temperature, which finally increases the performance of the energy storage unit. It is mandatory to estimate and compare the potential of stabilizing measures such as regeneration of salt and temperature limits in specific zones of the molten salt loop. For example, the decomposition to oxide ions can occur at the heat sources in the molten salt system (e.g. solar receiver). The kinetic description of the oxide formation developed in this thesis can give guidance to design parameters such as hold-up times, and surface temperatures of hot heat source parts.

The results of this thesis constitute a significant progress in the field of Solar Salt energy storage. Economic and ecological benefits are expected when the storage material remains stable for a longer time period. Decisions regarding the developments of the storage technology are facilitated by nuanced stability predictions and recommendations. The competitiveness of Solar Salt energy storage with increased material stability can be compared to other energy storage technologies. Finally, knowledge about the changing salt composition is crucial to select appropriate materials that are in contact with the molten salt, such as steels.

5 Summary

The socially and politically intended transition to renewable energy sources that fluctuate over time entails a growing demand of energy storage options. Thermal energy storage with the storage material Solar Salt (a mixture of sodium nitrate and potassium nitrate) is currently implemented in concentrating solar power plants to store the heat generated from the solar radiation. The existing storage systems with a maximum storage temperature of 565 °C have proven technological feasibility. At the time of writing, operation experience is collected over some years for large-scale systems. A development of the technology towards higher temperatures is intended for the following reasons. Increasing the maximum temperature while retaining the minimum temperature broadens the usable temperature range, and improves the storage capacity. Hence, more energy can be stored in the same amount of storage material, and capital costs of the storage unit are reduced. Additionally, the conversion of thermal to electrical energy via steam turbines becomes more efficient with increasing temperature. Besides, research that enables a temperature increase likewise allows prolonged lifetime at the state-of-the-art temperature. Those three aspects induce the **development of molten salt heat storage towards increased temperatures**. However, **maintaining the material stability** is challenging when the temperature is raised. Thermal decomposition intensifies and becomes faster, leading to higher amounts and concentrations of decomposition products. Those products comprise corrosive ions in the molten salt, and toxic gases released to the atmosphere. Knowledge about the decomposition process of Solar Salt is required to maintain material stability at increased molten salt temperatures, and finally contributes to safe, sustainable, economic and long lasting heat storage systems.

The **decomposition process of molten nitrate salts** comprises several chemical reactions. It is well accepted that the nitrate ion decomposes to nitrite ions and oxygen gas. This reaction is known to obtain chemical equilibrium when the connected gas atmosphere contains oxygen gas. The thermodynamics of the reaction are sparsely published for Solar Salt. The intrinsic kinetics of the reversible nitrite forming reaction are not described in the literature. The formation of oxide ions is described in differing reaction equations. However, reversibility of those reactions, and chemical equilibrium of molten nitrate salt containing oxide ions has not been proven. Experimental studies in the literature concluded that oxide ions amplify corrosion of steel that is in contact with molten salt, which entail technical risks.

This thesis aims to create a consistent model for the decomposition process on a reaction level. The relevant reactions are investigated regarding temperature, atmosphere and time dependence. The results are condensed to model descriptions that can be combined with each other, and also to

macroscopic physical-chemical phenomena that are beyond the scope of this thesis. Emphasis is put on elementary parts of the decomposition reactions that are lacking or little reported in the literature, or showed contradicting results. In particular, the **contributions of the presented thesis** are:

- Thermodynamic equilibrium data of the nitrite forming reaction up to 630 °C is generated by evaluation of experiments.
- A consistent intrinsic kinetics description of the reversible reaction from nitrate ions to nitrite ions is presented.
- The chemical equilibrium with oxide ions is proven experimentally, and an appropriate reaction equation is identified.
- The intrinsic kinetics of the oxide formation is characterized based on quantitative experimental data.

Two fields of chemistry are fundamental for this thesis, which are the thermodynamics and the reaction kinetics. The **thermodynamics** allow for the description of the equilibrium composition of the molten salt system including the gas atmosphere at a certain temperature and pressure. In this state, the Gibbs free energy of the system is minimized, the compositions of both liquid phase and gas phase are constant, and no chemical reaction is observed macroscopically. The equilibrium composition can be calculated when the relevant chemical reactions and the thermodynamic data of the pure substances in the regarded state of matter are known. The **reaction kinetics** focus on the time dependence of the reaction progress. The reaction rate is described in terms of the collision frequency of the reacting particles, and in terms of the reaction probability. The mathematical description of the reaction rate in liquid phases is usually referred to as the differential rate law. To measure the intrinsic kinetics of a reaction, mass transport limitations must be excluded in the applied experimental set-up.

The **experimental methods** applied in this thesis mainly differ in scale. When the focus is on intrinsic reaction kinetics, thin films of molten salt are investigated to minimize mass transport effects. The chemical equilibrium with oxide ions is investigated in a larger scale (~100 g) set-up, which allows precise gas purge, and the extraction of several salt samples to track the salt composition changes over time. Subsequent to three methods to carry out experiments at elevated temperatures, two methods namely ion chromatography and acid-base-titration are used to analyze the salt composition with regard to nitrate ions, nitrite ions, and oxide ions after experiments.

The results of this thesis and literature findings are assembled to a **reaction network** that includes the relevant reactions and products of thermal decomposition of Solar Salt. Undecomposed Solar Salt

is comprised of nitrate anions, and sodium and potassium cations. The first step is the formation of nitrite ions. The second step is the reaction of nitrite ions to oxide ions, and the third step is the reaction of oxide ions to carbonate ions. The carbonate formation (third step) is fast compared to the oxide formation, and therefore can be assumed instantaneous for kinetics considerations. In the absence of carbon dioxide, the carbonate formation can be excluded.

The thermogravimetric analysis experiments showed that the **chemical equilibrium of the nitrite forming reaction** is shifted towards higher nitrite contents with increasing temperature, which is in agreement with the endothermic reaction thermodynamics. The reaction parameters (enthalpy and entropy of reaction) are determined, and amount to 97 ± 9 kJ·mol^{-1} and 85 ± 12 J·mol^{-1}·K^{-1} in the lower temperature range (450-550 °C), and 95 ± 4 kJ·mol^{-1} and 86 ± 5 J·mol^{-1}·K^{-1} in the higher temperature range (560-630 °C), respectively.

The **time dependent formation of nitrite ions** is investigated at 450-550 °C in synthetic air atmosphere, and the reaction rate is found to increase with rising temperature. To quantify the reaction kinetics, the experiment curves are fitted according to a differential rate law that focuses on a precise description of the forward (nitrite forming) reaction. The resulting activation energies for the forward and reverse reaction amount to 212 ± 11 kJ·mol^{-1} and 115 ± 11 kJ·mol^{-1}, respectively. The obtained model description for the intrinsic kinetics of the nitrite forming reaction comprises the dependency on the oxygen partial pressure, and also indirectly includes the thermodynamics in terms of the temperature dependent reaction equilibrium.

Salt aging experiments with synthetic air purge are compared to similar experiments with addition of nitrous gases (in particular nitrogen monoxide) to the purge gas at 600 and 620 °C. The nitrous gases have a remarkable stabilizing effect on the molten Solar Salt, and affect the decomposition to oxide ions. The oxide level remains stable over the experiment duration with nitrous gases, whereas a steady accumulation of oxide ions is observed under synthetic air atmosphere. An increasing pressure of nitrous gases reduces the oxide level. With increasing temperature, the oxide level increases at a given pressure of nitrous gases. The presented experiments are the first experimental prove of **oxide content stabilization** in Solar Salt by a defined gas atmosphere. The results are promising for the applicability of Solar Salt at temperatures above the state-of-the-art (>565 °C), because the content of corrosive oxide ions was lowered consciously. The equilibrium oxide content was not only measured in experiments, but also calculated based on thermodynamic data and several proposed reaction equations. The stoichiometric amount of nitrogen gas coupled with the oxide ion formation affects the predicted equilibrium oxide content. For reaction equations that describe the evolution of 0.5 equivalents nitrogen gas per oxide ion, the oxide content is higher and closer to the experiments than

the calculation results for reaction equations without evolution of nitrogen gas. Formation of 1 equivalent nitrogen gas per oxide ion can be excluded for logical reasons. Best agreement of calculations and experiments was found for reaction equations that include between 0.5 and 1 equivalent nitrogen gas per oxide ion.

The **intrinsic kinetics of the oxide ion formation** are investigated in the range 560-630 °C. The reverse reaction is excluded by purging the atmosphere with air, thereby removing some of the gaseous reaction products (presumably nitrous gases) to focus on the forward reaction. Quantitative experimental data reveals the increase of the formation rate with increasing temperature. A rate law that assumes a decay of nitrite ions as the rate determining step is applied for fitting of the experimental data. The intrinsic kinetics of the oxide formation are characterized by kinetics parameters, which are the activation energy of 42 ± 3 kJ·mol^{-1}, and a pre-exponential factor of 0.003 ± 0.001 s^{-1}.

The model descriptions gained in each part of this thesis pertain to particular steps in the decomposition process, and can be combined and adapted to the conditions (temperature, atmosphere, degree of decomposition) of a specific Solar Salt system. As a whole, quantification and prediction of the thermal decomposition on an intrinsic level is possible. The reaction model is universally usable, and allows integration of existing models that describe other phenomena, e.g. fluid flow, heat transfer and mass transport in molten salt, and in the gas phase. The **extended state-of-knowledge** constitutes a significant progress for the technological application of Solar Salt in heat storage and heat transfer systems. It provides necessary data and parameters to estimate the stabilizing effect of different gas phases at elevated temperatures, and to quantify the reduction of decomposition products. The work presented manifests that the maximum operation temperature of Solar Salt can be increased significantly above 565 °C when decomposition reactions are suppressed using nitrous gases. Steel materials in the molten salt loop, and measures against decomposition can be selected to unite a temperature increase above the state-of-the-art temperature, and long term stability of the materials. From an overall perspective, this thesis contributes to a future efficient, economic, safe and long lasting operation of thermal energy storage based on molten nitrate salts.

References

1 (BMWi), B. f. W. u. T. Energie in Deutschland - Trends und Hintergründe zur Energieversorgung. 67 (Berlin, 2013).

2 iea, I. E. A. Germany 2020. (Paris, 200).

3 iea, I. E. A. Technology Innovation to Accelerate Energy Transitions. (Paris, 2019).

4 iea, I. E. A. Global Energy & CO2 Status Report 2019. (Paris, 2019).

5 Pfleger, N., Bauer, T., Martin, C., Eck, M. & Wörner, A. Thermal energy storage – overview and specific insight into nitrate salts for sensible and latent heat storage. *Beilstein Journal of Nanotechnology* **6**, 1487-1497 (2015).

6 Bauer, T., Steinmann, W. D., Laing, D. & Tamme, R. in *Annual Review of Heat Transfer* Vol. 15 (ed G. Chen) Ch. 5, 131-177 (Begell, 2012).

7 Tian, Y. & Zhao, C. Y. A review of solar collectors and thermal energy storage in solar thermal applications. *Applied Energy* **104**, 538-553 (2013).

8 iea, I. E. A. Technology Roadmap - Solar Thermal Electricity. (2014).

9 Mehos, M. *et al.* Concentrating solar power Gen3 demonstration roadmap. (2017).

10 Vignarooban, K., Xu, X., Arvay, A., Hsu, K. & Kannan, A. M. Heat transfer fluids for concentrating solar power systems--a review. *Applied Energy* **146**, 383-396 (2015).

11 Nunes, V. M. B., Queirós, C. S., Lourenço, M. J. V., Santos, F. J. V. & De Castro, C. A. N. Molten salts as engineering fluids--a review: Part I. Molten alkali nitrates. *Applied Energy* **183**, 603-611 (2016).

12 Bauer, T. *et al.* Material aspects of Solar Salt for sensible heat storage. *Applied Energy* **111**, 1114-1119 (2013).

13 Wang, K., He, Y.-L. & Zhu, H.-H. Integration between supercritical CO2 Brayton cycles and molten salt solar power towers: A review and a comprehensive comparison of different cycle layouts. *Applied Energy* **195**, 819-836 (2017).

14 Bonk, A., Sau, S., Uranga, N., Hernaiz, M. & Bauer, T. Advanced heat transfer fluids for direct molten salt line-focusing CSP plants. *Progress in Energy and Combustion Science* **67**, 69-87 (2018).

15 SolarPaces. *CSP Projects Around the World*, <https://www.solarpaces.org/csp-technologies/csp-projects-around-the-world/> (2017).

16 Steinmann, W. D. in *Concentrating Solar Power Technology: Principles, Developments and Applications* (eds K. Lovegrove & W. Stein) (Woodhead Publishing, Ltd., Cambridge, UK, 2012).

17 Turchi, C., Vidal, J. & Bauer, M. Molten salt power towers operating at 600–650 °C: Salt selection and cost benefits. *Solar Energy* **164**, 38-46, doi:10.1016/j.solener.2018.01.063 (2018).

18 Bonk, A. *et al.* Influence of different atmospheres on molten salt chemistry and its effect on steel corrosion. *AIP Conference Proceedings* **2033**, 090003, doi:10.1063/1.5067097 (2018).

19 Bonk, A., Martin, C., Braun, M. & Bauer, T. Material investigations on the thermal stability of solar salt and potential filler materials for molten salt storage. *AIP Conference Proceedings* **1850**, 080008 (2017).

20 Federsel, K., Wortmann, J. & Ladenberger, M. High-temperature and corrosion behavior of nitrate nitrite molten salt mixtures regarding their application in concentrating solar power plants. *Energy Procedia* **69**, 618-625 (2015).

21 McConohy, G. & Kruizenga, A. Molten nitrate salts at 600 and 680 °C: Thermophysical property changes and corrosion of high-temperature nickel alloys. *Solar Energy* **103**, 242-252 (2014).

22 Fernández, Á. G. & Cabeza, L. F. Molten salt corrosion mechanisms of nitrate based thermal energy storage materials for concentrated solar power plants: A review. *Solar Energy Materials and Solar Cells* **194**, 160-165 (2019).

23 Fernández, A. G., Lasanta, M. I. & Pérez, F. J. Molten Salt Corrosion of Stainless Steels and Low-Cr Steel in CSP Plants. *Oxidation of Metals* **78**, 329-348 (2012).

24 Kramer, C. M. & Wilson, C. J. The Phase Diagram of NaNO3-KNO3. *Thermochimica Acta* **42**, 253-264 (1980).

25 Janz, G. J., Allen, C. B., Bansal, N. P., Murphy, R. M. & Tomkins, R. P. T. Physical properties data compilations relevant to energy storage. II. Molten salts: data on single and multi-component salt systems. (1979).
26 Pacheco, J. E. *et al.* Results of molten salt panel and component experiments for solar central receivers: cold fill, freeze/thaw, thermal cycling and shock, and instrumentation tests. (1995).
27 Fernández, A. G., Galleguillos, H. & Pérez, F. J. Thermal influence in corrosion properties of Chilean solar nitrates. *Solar Energy* **109**, 125-134, doi:10.1016/j.solener.2014.07.027 (2014).
28 Goods, S. H., Bradshaw, R. W. & Chavez, J. M. Corrosion of Stainless and Carbon Steels in Molten Mixtures of Industrial Nitrates. *Sandia Report*, 1-38 (1994).
29 Grosu, Y., Bondarchuk, O. & Faik, A. The effect of humidity, impurities and initial state on the corrosion of carbon and stainless steels in molten HitecXL salt for CSP application. *Solar Energy Materials and Solar Cells* **174**, 34-41 (2018).
30 Prieto, C. *et al.* Effect of the impurity magnesium nitrate in the thermal decomposition of the solar salt. *Solar Energy* **192**, 186-192, doi:10.1016/j.solener.2018.08.046 (2019).
31 Prieto, C. *et al.* Study of corrosion by Dynamic Gravimetric Analysis (DGA) methodology. Influence of chloride content in solar salt. *Solar energy materials and solar cells* **157**, 526-532 (2016).
32 Bonk, A., Rückle, D., Kaesche, S., Braun, M. & Bauer, T. Impact of Solar Salt aging on corrosion of martensitic and austenitic steel for concentrating solar power plants. *Solar Energy Materials and Solar Cells* **203**, 110162-110162 (2019).
33 Ortega-Fernández, I. *et al.* New insights into the corrosion mechanism between molten nitrate salts and ceramic materials for packed bed thermocline systems: A case study for steel slag and Solar salt. *Solar Energy* **173**, 152-159, doi:10.1016/j.solener.2018.07.040 (2018).
34 Protsenko, P. I. & Bordyushkova, E. A. Kinetics and mechanism of the thermal dissociation of the nitrites of calcium, strontium, and barium. *Russian Journal of Physical Chemistry* **39**, 1048-1051 (1965).
35 Lee, A. K. K. & Johnson, E. F. The Stoichiometry and Kinetics of the Thermal Decomposition of Molten Anhydrous Lithium Nitrite. *Inorganic Chemistry* **11**, 782-787 (1972).
36 Hoshino, Y., Utsunomiya, T. & Abe, O. The Thermal Decomposition of Sodium Nitrate and the Effects of Several Oxides on the Decomposition. *Bulletin of the Chemical Society of Japan* **54**, 1385-1391 (1981).
37 Wei, X. *et al.* NOx emissions and NO2- formation in thermal energy storage process of binary molten nitrate salts. *Energy* **74**, 215-221 (2014).
38 Yang, C. *et al.* NOx emissions and the component changes of ternary molten nitrate salts in thermal energy storage process. *Applied Energy* **184**, 346-352 (2016).
39 Nissen, D. A. & Meeker, D. E. Nitrate/Nitrite Chemistry in NaN03-KN03 Melts. *Inorganic Chemistry* **22**, 716-721 (1983).
40 Freeman, E. S. The Kinetics of the Thermal Decomposition of Sodium Nitrate and of the Reaction between Sodium Nitrite and Oxygen. *The Journal of Physical Chemistry* **60**, 1487-1493 (1956).
41 Freeman, E. S. The Kinetics of the Thermal Decomposition of Potassium Nitrate and of the Reaction between Potassium Nitrite and Oxygen. *Journal of the American Chemical Society* **79**, 838-842 (1957).
42 Tracey, T. R., Tyner, C. E. & Weber, E. R. Conceptual Design of Advanced Central Receiver Power System. *Martin Marietta Corporation, final report for contract EG77-C-03-1724* (1978).
43 Bartholomew, R. F. A Study of the Equilibrium KNO3(l)=KNO2(l)+1/2O2(g) over the Temperature Range 550-750°. *The Journal of Physical Chemistry* **70**, 3442-3446 (1966).
44 Barin, I. *Thermochemical Data of Pure Substances*. (Wiley-VCH Verlag GmbH, 2008).
45 Bond, B. D. & Jacobs, P. W. M. The thermal decomposition of sodium nitrate. *Journal of the Chemical Society A: Inorganic, Physical, Theoretical* **A**, 1265-1268 (1966).
46 Paniccia, F. & Zambonin, P. G. Redox Mechanisms in an Ionic Matrix. III. Kinetics of the Reaction N02- + 1/2 O2 = NO3- in Molten Alkali Nitrates. *The Journal of Physical Chemistry* **77**, 1810-1813 (1973).
47 Villada, C., Bonk, A., Bauer, T. & Bolivar, F. High-temperature stability of nitrate/nitrite molten salt mixtures under different atmospheres. *Applied Energy* **226**, 107-115 (2018).

48 Olivares, R. I. The thermal stability of molten nitrite/nitrates salt for solar thermal energy storage in different atmospheres. *Solar Energy* **86**, 2576-2583 (2012).
49 Abe, O., Utsunomiya, T. & Hoshino, Y. The Reaction of Sodium Nitrite with Silica. *Bulletin of the Chemical Society of Japan* **56**, 428-433 (1983).
50 Abe, O., Utsunomiya, T. & Hoshino, Y. Acid-base and redox reactions in fused sodium nitrite. *Thermochimica Acta* **74**, 131-141 (1984).
51 Wright, S., Tran, T., Chen, C., Olivares, R. I. & Sun, S. in *Ninth International Conference on Molten Slags, Fluxes and Salts (Molten12), Beijing.*
52 Stern, K. H. High Temperature Properties and Decomposition of lnorganic Salts. Part 3. Nitrates and Nitrites. *Journal of Physical Chemical Reference Data* **1**, 747-771 (1972).
53 Olivares, R. I. & Edwards, W. LiNO3–NaNO3–KNO3 salt for thermal energy storage: Thermal stability evaluation in different atmospheres. *Thermochimica Acta* **560**, 34-42 (2013).
54 White, S. H. & Twardoch, U. M. Study of the interactions of molten sodium nitrate-potassium nitrate 50 mol% mixture with water vapor and carbon dioxide in air. Final report, June 2, 1980-June 30, 1981. (1981).
55 Bradshaw, R. W. & Siegel, N. P. in *Energy Sustainability 2008.*
56 Tsukahara, H., Ishida, T. & Mayumi, M. Gas-Phase Oxidation of Nitric Oxide: Chemical Kinetics and Rate Constant. *Biology and Chemistry* **3**, 191-198 (1999).
57 Tipper, C. F. H. & Williams, R. K. The effect of sulphur dioxide on the combustion of some inorganic compounds. Part 2.—The nitric oxide+ sulphur dioxide+ oxygen system. *Transactions of the Faraday Society* **57**, 79-86 (1961).
58 Ashmore, P. G., Burnett, M. G. & Tyler, B. J. Reaction of nitric oxide and oxygen. *Transactions of the Faraday Society* **58**, 685-691 (1962).
59 Olbregts, J. Termolecular reaction of nitrogen monoxide and oxygen: A still unsolved problem. *International journal of chemical kinetics* **17**, 835-848 (1985).
60 Olsson, L. *et al.* A kinetic study of oxygen adsorption/desorption and NO oxidation over Pt/Al2O3 catalysts. *The Journal of Physical Chemistry B* **103**, 10433-10439 (1999).
61 Atkins, P. W. & de Paula, J. *Physikalische Chemie*. (Wiley, VCH, 2013).
62 Wedler, G. & Freund, H.-J. *Lehrbuch der physikalischen Chemie*. Vol. 1 (John Wiley & Sons, 2012).
63 Connors, K. A. *Chemical Kinetics: The Study of Reaction Rates in Solution*. (Wiley-VCH, 1990).
64 Quack, M. & Jans-Buerli, S. Molekulare Thermodynamik und Kinetik, Teil 1: Chemische Reaktionskinetik. *Verlag der Fachvereine, Zuerich* (1986).
65 van Swaaij, W. P. M. & Versteeg, G. F. Mass transfer accompanied with complex reversible chemical reactions in gas—liquid systems: an overview. *Chemical Engineering Science* **47**, 3181-3195 (1992).
66 Versteeg, G. F., Kuipers, J. A. M., Beckum, F. P. H. V. & Swaaij, W. P. M. V. Mass transfer with complex reversible chemical reactions—I. Single reversible chemical reaction. *Chemical Engineering Science* **44**, 2295-2310 (1989).
67 van Krevelen, D. W. Micro- and macro-kinetics. *Chemical Engineering Science* **8**, 5-17 (1958).
68 van Krevelen, D. W. & Hoftijzer, P. J. Kinetics of gas-liquid reactions part I. General theory. *Recueil des Travaux Chimiques des Pays-Bas* **67**, 563-586 (1948).
69 van de Vusse, J. G. Mass transfer with chemical reaction. *Chemical Engineering Science* **16**, 21-30 (1961).

Appendix

List of journal publications and copyright information

Paper I

This article was published in

Thermochimica Acta, **678**, Sötz, V. A., Bonk, A., Forstner, J. & Bauer, T, Microkinetics of the reaction $NO_3^- \rightleftharpoons NO_2^- + 0.5\ O_2$ in molten sodium nitrate and potassium nitrate salt, 178301, Copyright Elsevier (2019).

https://doi.org/10.1016/j.tca.2019.178301

Paper II

This article was published in

Solar Energy Materials and Solar Cells, **212**, Sötz, V. A., Bonk, A. & Bauer, T, With a view to elevated operating temperatures in thermal energy storage - Reaction chemistry of Solar Salt up to 630 °C, 110577, Copyright Elsevier (2020).

https://doi.org/10.1016/j.solmat.2020.110577

Paper III

This article was published in

Solar Energy, **211**, Sötz, V. A., Bonk, A., Steinbrecher, J. & Bauer, T, Defined purge gas composition stabilizes molten nitrate salt - Experimental prove and thermodynamic calculations, 453-462, Copyright International Solar Energy Society (2020), Published by Elsevier Ltd.

https://doi.org/10.1016/j.solener.2020.09.041

Thermochimica Acta 678 (2019) 178301

Contents lists available at ScienceDirect

Thermochimica Acta

journal homepage: www.elsevier.com/locate/tca

Microkinetics of the reaction $NO_3^- \rightleftharpoons NO_2^- + 0.5\,O_2$ in molten sodium nitrate and potassium nitrate salt

Veronika Anna Sötz[a,*], Alexander Bonk[b], Jochen Forstner[b], Thomas Bauer[a]

[a] Institute of Engineering Thermodynamics, German Aerospace Center (DLR), Linder Höhe, 51147 Köln, Germany
[b] Institute of Engineering Thermodynamics, German Aerospace Center (DLR), Pfaffenwaldring 38-40, 70569 Stuttgart, Germany

ARTICLE INFO

Keywords:
Concentrating solar power (CSP)
Thermal energy storage (TES)
Nitrate salt melts
Thermogravimetric analysis
Chemical equilibrium
Intrinsic kinetics

ABSTRACT

Latest development in the concentrating solar power (CSP) tower technology for energy production and storage intends to find a heat transfer and storage material that provides stability at elevated temperatures. The binary nitrate salt mixture Solar Salt (sodium nitrate, 60 wt.% and potassium nitrate, 40 wt.%) is utilized up to its state-of-the-art temperature limit of 560 °C. Knowledge of the ongoing reactions is demanded to assess the potential of Solar Salt for higher temperature applications. The reversible reaction $NO_3^- \rightleftharpoons NO_2^- + 0.5\,O_2$ is fundamental in a sequence of decomposition reactions. It is investigated by thermogravimetric experiments and ion chromatography post-analysis with regard to the chemical equilibrium, and to reaction kinetics. The reaction enthalpy and entropy of 97 +/- 9 kJ mol^{-1} and 85 +/- 12 J·mol^{-1} K^{-1}, respectively, coincide with literature values. A detailed reaction mechanism based on literature findings is drafted and discussed. The corresponding kinetic rate law is simplified by means of rate law approximations and by focusing on the reduction reaction path. The kinetic rate constants of this study exceed previous findings, probably due to successful exclusion of mass transport limitations in the < 1 mm thin salt samples. The activation energies and pre-exponential factors amount to 212 +/- 11 kJ·mol^{-1} and 694546727 +/- 6 s^{-1}, and 115 +/- 11 kJ·mol^{-1} and 25770 +/- 6 s^{-1} for the reduction and oxidation reaction, respectively.

Nomenclature

Symbol	Description	Unit
A_i	Pre-exponential factor in the Arrhenius equation	Varying
C_i	Molar concentration of i	$mol \cdot m^{-3}$
$C_{i,0}$	Molar concentration of i at time zero	$mol \cdot m^{-3}$
$C_{i,eq}$	Molar concentration of i at chemical equilibrium	$mol \cdot m^{-3}$
$E_{a,i}$	Activation energy of reaction i	$kJ \cdot mol^{-1} \cdot K^{-1}$
f_i	Mechanism term in a kinetic rate law, for i see description of k_i	k_i
ΔH	Reaction enthalpy	$kJ \cdot mol^{-1}$
I	Reacting or product atom or molecule	
K	Equilibrium constant	1
K_H	Henry constant, solubility equilibrium constant	1
K_{melt}	Equilibrium constant of the homogeneous reaction in the melt	1
K_{atm}	Equilibrium constant, where pressure is not normalized	$atm^{0.5}$
K_{exp}	Equilibrium constant from the IC post analysis of this study	1
K_{fit}	Equilibrium constant predicted by the van't Hoff fit of this study	1
k_i	Reaction rate constant, $i = Red$: Reduction rate constant, $i = Ox$: Oxidation rate constant, $i = f$: Forward rate constant, $i = r$: Reverse rate constant, $i = RRP$: Reduction on Reduction Path, $i = ORP$: Oxidation on Reduction Path, $i = ROP$: Reduction on Oxidation Path, $i = OOP$: Oxidation on Oxidation Path	Varying
M_i	Molar mass of i, $M_O = 0.01600\,kg \cdot mol^{-1}$ $M_{Na_{0.65}K_{0.35}NO_3} = 0.09076\,kg \cdot mol^{-1}$	$kg \cdot mol^{-3}$
Δm	Mass difference	mg
m_{total}	Total mass of the salt sample at time zero	mg
N	Number of data points	
n_i	Amount of substance of i	mol
P	Total pressure	bar
p_{O_2}	Partial pressure of oxygen	bar
P_{atm,O_2}	Partial pressure of oxygen	atm
p_0	Reference pressure, $p_0 = 1\,bar$	bar
R	Ideal gas constant, $8.314\,J \cdot mol^{-1} \cdot K^{-1}$	$J \cdot mol^{-1} \cdot K^{-1}$
r	Reaction rate	$mol \cdot m^{-3} \cdot s^{-1}$
ΔS	Reaction entropy	$J \cdot mol^{-1} \cdot K^{-1}$
T	Temperature	K

* Corresponding author.
E-mail address: Veronika.Soetz@dlr.de (V.A. Sötz).

https://doi.org/10.1016/j.tca.2019.178301
Received 8 November 2018; Received in revised form 9 May 2019; Accepted 29 May 2019
Available online 31 May 2019

x_i	Molar ratio of i relative to the total amount of substance	1
α	Extent of conversion, $0 < \alpha < 1$	
ν_I	Stoichiometric coefficient of I	1
ρ_{SoSa}	Density of Solar Salt, $\rho_{SoSa} = 2268.9\,kg{\bullet}m^{-3} - 0.6395\,kg{\bullet}m^{-3}{\bullet}K^{-3}{\bullet}T$	$kg{\bullet}m^{-3}$

1. Introduction

Concentrating solar power (CSP) plants frequently include energy storage units that enable electricity production during the night, or during sunless times. The state-of-the-art storage technology [1] is sensible heat storage with the storage material Solar Salt, which is a mixture of sodium nitrate (60 wt.%, 64 mol%) and potassium nitrate (40 wt.%, 36 mol%). Currently, a maximum storage temperature of 560 °C is widely accepted. CSP development in the field of solar power tower systems aims to transfer higher temperature heat [2] to the heat transfer fluid, and eventually to the heat storage material. Solar Salt is an option for both heat transfer fluid and storage material. Under common gas atmospheres such as air, synthetic air, or inert gases, the nitrate ions are known to decompose significantly at elevated temperatures [3]. Issues related to the decomposition products comprise intensified corrosion [4,5] of the storage tank material that is in contact with molten salt, and the formation of harmful gases [6]. Still, the underlying chemical reactions are not fully understood. Due to this lack of knowledge, the potential of preventing the salt from decomposition cannot be estimated. Time-dependent mathematical descriptions of the chemical reactions in Solar Salt are needed to predict changes in the salt composition at different temperatures, and at various locations in the heat transfer and storage system.

The most pronounced reaction in nitrate salt melts is the reaction (1) of nitrate ions to nitrite ions and oxygen [7]. Further reactions (2) to (4) describe the formation of oxide ions and nitrous gases [6–12]. Often, nitrite ions are assumed to be the reactants, e.g. Eqs. (2) and (3). But also, reaction equations such as reaction (4) with nitrate ions as reactants can be found in the literature.

$$NO_3^- \rightleftharpoons NO_2^- + 0.5\,O_2 \tag{1}$$

$$2\,NO_2^- \rightleftharpoons O^{2-} + NO + NO_2 \tag{2}$$

$$2\,NO_2^- \rightleftharpoons O^{2-} + 2\,NO + 0.5\,O_2 \tag{3}$$

$$2\,NO_3^- \rightleftharpoons O^{2-} + 2\,NO_2 + O_2 \tag{4}$$

Reactions (1) to (4) illustrate that the chemistry in molten nitrates is not about individual and isolated reactions, but rather sequences or a network of reactions. Reaction (1) can be seen as the starting reaction, because it occurs already at relatively low temperatures, and because it produces the reactants (nitrite ions) of subsequent reactions. Hence, characterization of this reaction is of fundamental importance. Besides, investigation of reaction (1) irrespective of reaction (2) to (4) is possible, because the oxide forming reactions are comparably slow, and a negligible amount of oxide is formed at temperatures up to about 550 °C [7,13,14].

This study makes a unique contribution to the field of sensible heat storage by combining the following requirements.

- Use of technically relevant Solar Salt material
- Experimental investigation of nitrite formation, because this species contributes to salt decomposition and eventually to damages of the storage system
- Investigation of the chemical equilibria under relevant oxygen pressure
- Investigation of microkinetics (mass transport effects excluded), because microkinetics are independent of system geometries and can be combined with mass transport descriptions
- Examination of the microkinetics temperature dependence in a relevant temperature range

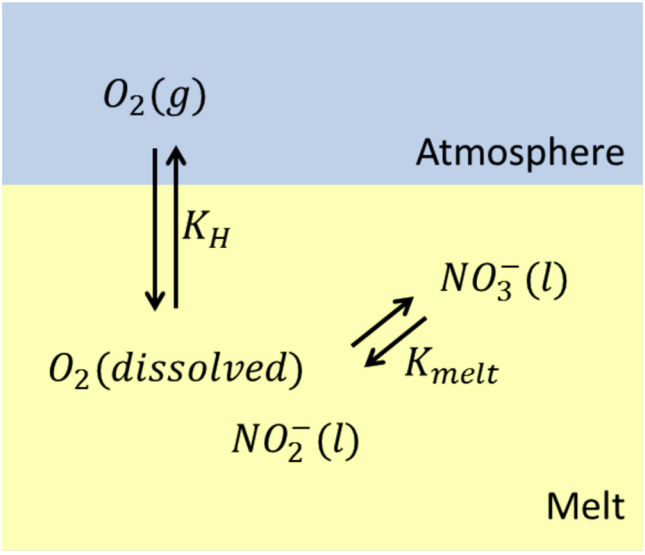

Fig. 1. Sketch of chemical nitrate-nitrite equilibria in molten nitrate salt in contact with an oxygen containing gas atmosphere.

- Mathematical description of the reaction kinetics, that enables stability predictions of Solar Salt in the future

The applied experimental methods and the data evaluation are chosen with regard to the above listed requirements. Some of the requirements where already addressed in previous publications (see chapters 1.1 and 1.2). However, this paper addresses multiple effects in a combined approach to provide reliable data for predictions of chemical compositions in Solar Salt.

1.1. Thermodynamics

The chemical equilibrium of reaction (1) can be separated into two equilibria, which are sketched in Fig. 1. The solubility equilibrium of oxygen in the atmosphere above the melt, and dissolved oxygen (Eq. (5a)) is described by Henry's law (Eq. (5b)) with a temperature dependent Henry constant K_H [15]. The dissolved oxygen is in chemical equilibrium with nitrate and nitrite ions [13,16–19], see Eqs. (6a) and (6b). The partial pressure of oxygen p_{O_2} in the atmosphere can be set or measured in an experiment, and is more easily accessible than the ratio of dissolved oxygen x_{O_2}. Therefore, the two equilibria are commonly merged to an overall equilibrium constant K (Eq. (7b)), which describes the chemical equilibrium of the formal reaction (7a).

$$O_2(g) \rightleftharpoons O_2(diss.) \tag{5a}$$

$$\mathrm{K_H} = \frac{x_{0_{2,\mathrm{eq}}}}{\frac{p_{0_2}}{p_2}} \tag{5b}$$

$$K_{melt} = \frac{x_{NO_2^-,eq} \bullet x_{O_2}^{0.5}}{x_{NO_3^-,eq}} \tag{6a}$$

$$NO_3^-(l) \rightleftharpoons NO_2^-(l) + 0.5\,O_2\ (\mathrm{diss.}) \tag{6b}$$

$$NO_3^-(l) \rightleftharpoons NO_2^-(l) + 0.5\ O_2\ (\mathrm{gas}) \tag{7a}$$

$$K = \frac{K_{melt}}{K_H^{0.5}} = \frac{x_{NO_2^-,eq} \bullet (\frac{p_{O_2}}{p_0})^{0.5}}{x_{NO_3^-,eq}} \tag{7b}$$

The thermodynamics of reaction (1) can be found in the literature for several pure salts and cation compositions. Table 3 lists the reaction enthalpies and entropies of salts, which are similar to Solar Salt. Often, the equilibrium constants in the literature are calculated according to

Eq. (8) and with the unit $atm^{0.5}$. The fundamental thermodynamic equilibrium constant K is defined according to Eq. (7) with regard to a reference pressure $p_0 = 1\,bar$ [20]. For better comparability, all thermodynamic parameters in Table 3 originate from the nondimensional.

$$K_{atm} = \frac{c_{NO_2^-,eq} p_{atm,O_2}^{0.5}}{c_{NO_3^-,eq}} \tag{8}$$

The equilibrium constants K are plotted in Fig. 3 according to Eq. (9) in a van't Hoff diagram, and the reaction enthalpy ΔH and entropy ΔS were extracted from linear fits.

$$\ln K = -\frac{\Delta H - T\Delta S}{RT} \tag{9}$$

1.2. Kinetics

Reaction kinetics describes the time-dependent progress of a chemical reaction. When the reaction is heterogeneous, meaning that two or more phases participate, kinetics can be divided into micro- and macrokinetics [21–25]. Microkinetics, also called intrinsic kinetics, describes the reaction kinetics in an infinitesimally small volume element with respect to the actual and local concentrations of reactants and products. Macrokinetics intends to describe the overall reaction velocity, and is valid for special system geometries and reaction conditions.

The commonly accepted treatment for thermogravimetric analysis data [26] is based on Eq. (10). This kinetic rate law describes changes in the extent of conversion α over time in terms of a temperature dependent term $k(T)$, a mechanism related term $f(\alpha)$, and a pressure term $h(P)$. For the specific investigations of this study, we transformed Eq. (10) into Eq. (11), in consideration of the following points [27,28]. First, the effect of the total pressure P is negected. Partial pressures of gaseous reactants can be included in the mechanism term, and can be converted into concentrations of dissolved gases, e.g. via Henry's law. Second, using concentrations instead of the extent of conversion is preferred for a mechanistic approach. Reversible reactions are described by two terms (see positive and negative term in Eq. (11)) which represent the forward (with indices f) and reverse reaction (with indices r), respectively. When the two terms compensate each other, the forward and reverse reactions are equally frequent, the system composition is constant, and chemical equilibrium is established.

In the particular case of an elementary reaction, the mechanism terms can be directly derived from the reaction equation, and vice versa [27,28]. Multiplication of all reagent concentrations of the forward reaction $c_{I,(I=A,B,...)}$ to the power of their stoichiometric coefficient $\nu_{I,(I=A,B,...)}$ results in the forward mechanism term, and the same applies to the reverse mechanism term. This correlation is exemplified in the Eqs. (12a) and (12b). The reaction orders (exponents) in the rate law (12b) correspond to the stoichiometric coefficients ν_I in the elementary reaction Eq. (12a).

Mechanism terms that belong to elementary reaction steps refer to the collision probability. They describe the likelihood in which the reacting particles are in close proximity, which is required for chemical reaction. In the case of collision, the energy of the reacting particles must be high enough to overcome the activation energy barrier, which is represented by the temperature dependent reaction rate constants $k(T)$. The rate constants can be viewed as a reaction probability of colliding reagents [27,28]. The collision probability multiplied by the reaction probability of a collision finally results in the reaction rate r (compare Eq. (12b)).

$$\frac{d\alpha}{dt} = k(T) \bullet f(\alpha) \bullet h(P) \tag{10}$$

$$\frac{dc_I}{dt} = k_f(T) \bullet f_f\left(c_{I,(I=A,B,...)}, \nu_{I,(I=A,B,...)}\right) - k_r(T) \bullet f_r\left(c_{I,(I=A,B,...)}, \nu_{I,(I=A,B,...)}\right) \tag{11}$$

$$\nu_A A + \nu_B B \underset{k_r}{\overset{k_f}{\rightleftharpoons}} \nu_C C + \nu_D D \tag{12a}$$

$$r = -\frac{1}{\nu_A}\frac{dc_A}{dt} = -\frac{1}{\nu_B}\frac{dc_B}{dt} = \frac{1}{\nu_C}\frac{dc_C}{dt} = \frac{1}{\nu_D}\frac{dc_D}{dt} = k_f(T) \cdot c_A^{\nu_A} \cdot c_B^{\nu_B} - k_r(T) \cdot c_C^{\nu_C} \cdot c_D^{\nu_D} \tag{12b}$$

Frequently, chemical reactions are a sequence of elementary reactions. They occur in one single step without any intermediates. The elementary reactions of the reaction (1) are not ultimately confirmed, and the reaction orders in an appropriate rate law remain unclear. Several hints can be found in the literature: Freeman [17] says that the kinetics comprises a reversible reaction that is first order with respect to both nitrate and nitrite. Bond and Jacobs [29] state that the presence or absence of oxygen does not influence the reduction of nitrate, meaning that the reduction reaction is zeroth order on the oxygen concentration. Paniccia and Zambonin [14] stated that they found first-order dependence of the nitrate formation (oxidation reaction) both on nitrite and oxygen concentration. Furthermore, Nissen and Meeker [18] found first-order dependence of the nitrite oxidation with respect to both nitrite concentration and oxygen partial pressure. All these findings lead to the elementary reactions (13) and (14). Nissen and Meeker [18] derived a rate law of the overall reaction (see Eq. (15)) from the two elementary reactions. Therein, k_{Red} and k_{Ox} are the reduction and oxidation rate constants, respectively.

$$\text{Reduction reaction } NO_3^- \overset{k_{Red}}{\rightarrow} NO_2^- + O \tag{13}$$

$$\text{Oxidation reaction } NO_2^- + O_2 \overset{k_{Ox}}{\rightarrow} NO_3^- + O \tag{14}$$

$$\frac{dc_{NO_2^-}}{dt} = k_{Red} c_{NO_3^-} - k_{Ox} c_{NO_2^-} p_{O_2} \tag{15}$$

2. Methods

The thermogravimetric analysis (TGA) experiments were executed in a Netzsch STA 449 apparatus. The TGA sample holder was equipped with a thermocouple type S Pt10Rh-Pt. Around 50 mg of salt (60 wt.% NaNO3, 40 wt.% KNO3, both > 99% purity, Merck) were filled in a small platinum crucible, which itself was put in a larger aluminum oxide crucible to prevent the molten salt from spreading or creeping over the sample holder and other areas of the thermogravimetric system. Table 1 lists the labelling, temperature settings and exact masses of the experiments. The apparatus was purged with synthetic air at 100 mL·min^{-1} (80 mL·min^{-1} nitrogen and 20 mL·min^{-1} oxygen, both Linde 5.0 grade) to ensure a constant oxygen partial pressure in the gas phase.

Five experiments were executed for this study, see Table 1. In every experiment, the salt was heated to 300 °C, which is 70 °C above the

Table 1
Details on the TGA experiments.

Experiment label	Temperature program	Sample mass m_{total} /mg
TGA450	300 °C (5 h) – 450 °C (30 h)	52.722
TGA475	300 °C (5 h) – 475 °C (20 h)	51.444
TGA500	300 °C (5 h) – 500 °C (12 h)	51.535
TGA525	300 °C (5 h) – 525 °C (9 h)	53.542
TGA550	300 °C (5 h) – 550 °C (8 h)	53.327

liquidius temperature of solar salt [30] and in the range of the melting points of the pure salts $NaNO_3$ and KNO_3 [31]. The temperature was kept for 5 h for melting and equilibration. Chemical equilibrium cannot be established within this short period. However, the mass loss at 300 °C compared to the initial salt mass amounts to only 0.001 wt.% (whereas it ranges from 0.083 to 0.576 wt.% at 450 to 550 °C), and is therefore negligible. Then, the sample is heated to the desired temperature (450 to 550 °C) with a heating rate of 20 K·min^{-1}, followed by isotherms between 8 to 30 h, depending on the final temperature.

Post-analysis via ion chromatography (IC) revealed the ion composition of the salt samples after the TGA experiments. After TGA experiment was completed, the platinum crucible with the remaining salt was weighed. Then, it was inserted in ultrapure water (HiPerSolv, VWR, Germany), and dissolution of the salt was accelerated by use of an ultrasonic bath. The crucible was rinsed with water, dried and weighed again to determine the mass of salt that was transferred from the crucible to the aqueous solution. The collected aqueous sample was filled up to an exact volume in a volumetric flask. The amount of salt obtained in the solution was measured in a *Metrohm model 930 Compact IC Flex* (Metrohm, Switzerland) IC apparatus. It is equipped with a *Metrosep A Supp* analytical column (5 x 250 mm), a *Metrosep RP2* guard column, and a suppressed conductivity detector, as also described in the reference [32]. The molar ratios nitrite-to-nitrate $n_{NO_2^-,eq}/n_{NO_3^-,eq}$ are converted into mass differences Δm via Eq. (16). The first term of this equation expresses the amount of substance ratio of nitrite with respect of the total amount of anions and the second term describes the total amount of anions in the salt sample. The resulting amount of nitrite is finally multiplied by the molar mass of oxygen to obtain the mass difference Δm.

$$\Delta m = -\frac{n_{NO_2^-,eq}/n_{NO_3^-,eq}}{n_{NO_2^-,eq}/n_{NO_3^-,eq}+1} \cdot \frac{m_{total}}{M_{Na_{0.65}K_{0.35}NO_3}} \cdot M_O \tag{16}$$

It is assumed that the measured ion compositions are the equilibrium compositions at the maximum temperature of the TGA temperature program. Equilibrium constants K are calculated with Eq. (7), and an oxygen partial pressure of $p_{O_2,eq} = 0.2\,bar$. The logarithmic equilibrium constants are plotted versus the inverse temperature in a van't Hoff plot, according to Eq. (9) [33]. A linear regression analysis (method of least squares) of the data points allows calculation of the reaction enthalpy ΔH and entropy ΔS. The uncertainties of ΔH and ΔS are calculated by quadratic error propagation of the standard errors of the linear fits. The error of $\ln(K)$ is calculated by the root mean square error (RMSE) formula, see Eq. (17). The RMSE is used for further error propagation calculations, which include K. The enthalpy and entropy of this study are used to calculate equilibrium values that are needed for TGA data evaluation. Those values are hereafter referred to as predicted equilibrium concentrations.

$$RMSE = \sigma(\ln K) = \sqrt{\frac{\sum(\ln K_{exp} - \ln K_{fit})^2}{N}} \tag{17}$$

The experimentally (TGA) measured mass difference curves are corrected with regard to salt evaporation [34,35]. The procedure is demonstrated exemplarily for the *TGA500* experiment in Fig. 2a. The experimental mass difference, which includes a buoyancy correction, is the dotted curve in Fig. 2a. The linear part at the end of the curve shaded in grey is assumed to originate from salt evaporation, and this part is fitted linearly [36]. The slope of the fit corresponds to the evaporation rate at 500 °C, and an evaporation correction curve (dashed line in Fig. 2a) is calculated with this result. Negligible salt evaporation is assumed for the 300 °C segment and during heating. The correction curve is subtracted from the experiment curve, and the resulting curve is labeled as EC (evaporation-corrected) in Fig. 2a.

The EC mass difference curve of Fig. 2a is converted into a nitrite concentration curve, see EC in Fig. 2b, via Eq. (18). The numerator of this equation converts the mass difference Δm into the amount of substance of nitrite, and the denominator converts the total mass m_{total} into the sample volume. Volume changes due to reaction (1) are thereby neglected. The EC curve exposes a difference between the equilibrium nitrite concentration that originates from the experimentally measured mass difference (around 420 mol·m^{-3}), and the predicted equilibrium nitrite concentration (312 mol·m^{-3}, dashed line in Fig. 2b). We assume that this deviation originates from the sensitivity of the weighing unit to e.g. temperature, which is relevant at small mass losses. In contrast, the predicted equilibrium nitrite concentrations that are based on IC post-analysis of the salt samples are reliable, as discussed later. The EC curve is shifted along the x-axis with the result that the high temperature segment begins at time zero. Also, the EC curve is shifted along the y-axis so that the nitrite concentration at time zero is the predicted equilibrium concentration at 300 °C. The nitrite concentration axis is linearly corrected with the result that the final nitrite concentration equals the predicted equilibrium nitrite concentration at 500 °C. The resulting curve is denoted as FC (final correction) in Fig. 2b. The grey shaded part of the FC curve is used for fitting the reaction kinetics later on.

$$c_{NO_2^-} = \frac{\Delta m/M_O}{m_{total}/\rho_{SoSa}} \tag{18}$$

The reaction rate constants k are plotted in Arrhenius diagrams. The uncertainties of the rate constants are calculated via quadratic error propagation, which consider the errors of the equilibrium constants K, and the standard errors of the kinetic fit parameters. Linear regression analysis with the method of least squares gives fit parameters, which can be transformed to the activation energy E_a and the pre-exponential factor. The uncertainties of E_a and A are calculated by quadratic error propagation of the standard errors of the linear fits. The error of $\ln k$ is calculated by the root mean square error (RMSE) formula, analogous to Eq. (17).

3. Results and discussion

3.1. Equilibrium

Post-analysis of the nitrite and nitrate concentrations in the salt samples after the TGA experiments by ion chromatography revealed the equilibrium anion compositions at 450, 475, 500, 525 and 550 °C. The

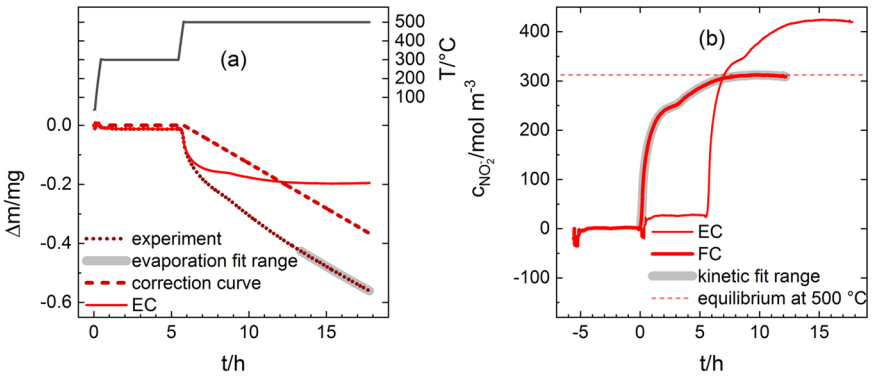

Fig. 2. Data treatment procedure for the *TGA500* experiment (exemplarily). Note that the y-axis is different in the two diagrams. (a): The experimentally measured mass difference is corrected with regard to salt evaporation at 500 °C, resulting in the evaporation corrected (EC) curve. (b): For the FC (final correction) curve, the EC curve is shifted along the time-axes. Linear correction along the concentration-axis brings the curve in agreement with the equilibrium nitrite concentrations.

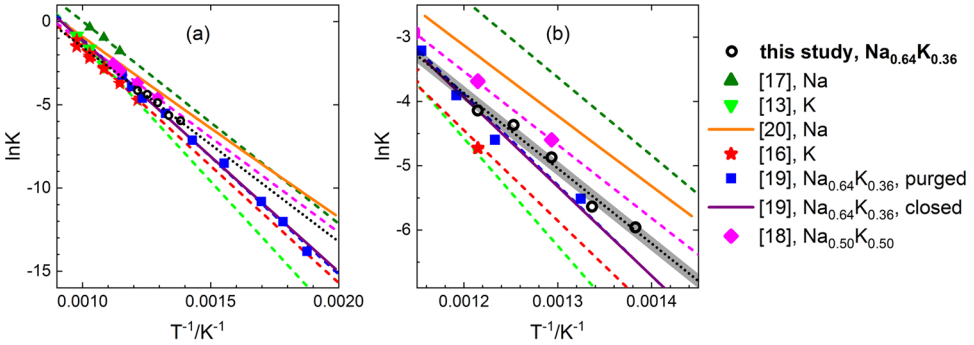

Fig. 3. Van't Hoff plots of logarithmic equilibrium constants versus inverse temperature. The filled symbols are equilibrium constants which are published in the indicated literature, and re-fitted in this study (dashed lines). The solid lines are equilibrium functions (Eq. (9)), which are calculated with reaction enthalpies and entropies from the indicated literature. The black circles and the dotted line are the equilibrium results of this study (IC post-analysis of the TGA experiments) and their linear fit, respectively. The RMSE amounts to 0.11, and is illustrated as grey tunnel behind the fit line. Diagram (b) is the enlargement of the framed area in diagram (a) with the temperature range of this work (450–550 °C).

molar ratios nitrite-to-nitrate $n_{NO_2^-,eq}/n_{NO_3^-,eq}$, the equilibrium constants K, and the ratios of mass difference to the total sample mass $\Delta m_{eq}/m_{total}$ are listed in Table 2, column 2, 3 and 4. The experimentally obtained equilibrium constants K are plotted as black circles in a van't Hoff diagram in Fig. 3. The linear fit leads to the enthalpy ΔH and entropy ΔS of reaction (1), which are listed in Table 3 together with the literature values. Next, the results are compared first with regard to enthalpy and entropy, which are the temperature-independent equilibrium parameters, and second with regard to the temperature dependent equilibrium constants.

The enthalpy and entropy results of this study agree with those of Freeman [17], Barin [20], and Nissen and Meeker [18] in consideration of the uncertainties. Deviations to the other literature values might be due to different cation compositions (pure potassium instead of sodium-potassium-mixtures or pure sodium). In the case of Tracey [19], experiments were executed at low temperatures (e.g. 533 K), where chemical equilibrium requires long isotherms, making measurements sensitive to errors.

For the temperature range 450–550 °C, the equilibrium constants K are closer to the van't Hoff fit of Tracey [19] (deviations of 5–37% to the K values of this study) than to the van't Hoff fit of Nissen [18] (deviations of 41–48%). For the following data evaluation and discussion of the reaction kinetics, the enthalpy ΔH of 97 +/- 9 kJ·mol^{-1} and entropy ΔS of 85 +/- 12 J·mol^{-1} K^{-1} of this study are used. The values in bold in Table 2, column 5–8 ('predicted values') are based thereon. The bold equilibrium constants K (column 9) correspond to the dotted fit line in Fig. 3.

3.2. Kinetics

Eq. (15) shows the kinetic rate law published by Nissen and Meeker [18]. It can be inferred that it does not belong to an elementary reversible reaction, because the reaction equation deduced from the rate law $NO_3^- \rightarrow NO_2^- + O_2$ reveals erroneous stoichiometry. Furthermore, the rate law contradicts the equilibrium description given in the reference [18] (see Table 4). The rate law can therefore only be applied for a specific and constant oxygen partial pressure, or if at least one of the constants K, k_{Red} and k_{Ox} depends on the oxygen partial pressure.

One possible alternative to avoid these contradictions is to think of reactions (13) and (14) as reversible elementary reactions. Then, the overall reaction (6) comprises three elementary reversible reactions (19), (20) and (21), which are sketched in Fig. 4. The three reactions build a consistent network of reactions. Yet, oxygen species such as O_2^{2-} and O_2^- are ignored, although their presence in molten nitrate salt is also reported [37]. According to reaction (13) and forward reaction (20) (orange path in Fig. 4), nitrate ions decompose to nitrite and atomic oxygen. The results found in the literature [14,29] indicate that this reaction is the predominating path for the reduction of nitrate ions, and the reaction is therefore abbreviated RRP (Reduction reaction on the main Reduction Path). The associated oxidation reaction (back reaction (20), blue path in Fig. 4) is the combination of nitrite and atomic oxygen to form nitrate, and it is abbreviated ORP (Oxidation reaction on the main Reduction Path). The predominating path for the oxidation reaction (reaction (14) and forward reaction (21), purple in Fig. 4) is found [18] to be the reaction of nitrite and molecular oxygen (OOP). The associated back reaction (reverse reaction (14), green in Fig. 4) is the reduction reaction of nitrate with atomic oxygen, where nitrite and molecular oxygen are formed. The rate law for nitrite that follows from the postulated sequence of reversible elementary reactions is noted in Eq. (22). Similar rate laws can be derived for the other involved species. Those differential equations cannot be solved analytically, and experimental determination of the numerous parameters (k_{RRP}, k'_{ORP}, k'_{OOP}, k'_{ROP}) is challenging or not feasible with the available experimental methods.

A few kinetics principles are available to simplify rate laws, namely the rate determining step (rds) approximation and the quasi steady state (qss) approximation [27,28]. When a particular product is formed by several elementary reaction steps, the limiting step is always the slowest step, namely the rds. It is sufficient to analyze the kinetics of the rds in order to describe the time dependence of the product formation. Previous experimental studies revealed that the rate law of the reduction of nitrate is first-order with respect to nitrate [17,29]. The rate law of the nitrite oxidation was found to be first order with respect to both nitrite and oxygen [14,18]. That indicates that the reactions (20) and (21) are slower than reaction (19) and therefore the rds.

The qss approximation is applied to reaction mechanisms that comprise a first quick equilibrium reaction. This reaction, in turn, provides the intermediate reagent of a second irreversible and slower reaction that produces the final reaction product. Then, the concentration of the intermediate reagent can be assumed constant, and expressed by reaction rate constants or equilibrium constants. In that way, the number of variables in the rate law is reduced.

Rds and qss approximation are applied to the full description of the rate law in Eq. (22). First, the oxygen concentration is replaced by Eq. (5) which results in Eq. (23). Eq. (23) can be solved analytically for a constant oxygen partial pressure, leading to an analytical equation with four unknown parameters (k_{RRP}, k_{ORP}, k_{ROP}, k_{OOP}). The equilibrium conditions (Eq.s (24) and (25)) are in accordance with Eq. (7). Eqs. (23–25) build a set of three equations and four unknown parameters, which cannot be solved by means of the available experimental data.

$$O_{2(diss.)} \rightleftharpoons 2\,O \tag{19}$$

$$NO_3^- \underset{k'_{ORP}}{\overset{k_{RRP}}{\rightleftharpoons}} NO_2^- + O \tag{20}$$

$$NO_2^- + O_{2(diss.)} \underset{k'_{ROP}}{\overset{k'_{OOP}}{\rightleftharpoons}} NO_3^- + O \tag{21}$$

Table 2
Equilibrium composition data of reaction (1).

$T/°C$	IC post-analysis of TGA experiments			Predicted from van't Hoff fit (Figure 3 and table 3, last row)			
	$\frac{n_{NO_2^-,eq}}{n_{NO_3^-,eq}}/mol \cdot mol^{-1}$	K^*	$\frac{\Delta m_{eq}}{m_{total}}/mg \cdot mg^{-1}$ †	$\frac{n_{NO_2^-,eq}}{n_{NO_3^-,eq}}/mol \cdot mol^{-1}$	$c_{NO_2^-,eq}/mol \cdot m^{-3}$	K^*	$\frac{\Delta m_{eq}}{m_{total}}/mg \cdot mg^{-1}$ †
300	/	/	/	**8.0E-5**	**1.671**	**3.56E-5**	**1.41E-5**
450	0.0058	0.00258	1.01E-3	**0.0055**	**109.9**	**0.00246**	**9.63E-4**
475	0.0080	0.00357	1.39E-3	**0.0094**	**187.8**	**0.00422**	**1.65E-3**
500	0.0172	0.00767	2.97E-3	**0.0156**	**310.4**	**0.00699**	**2.71E-3**
525	0.0283	0.01268	4.86E-3	**0.0251**	**498.9**	**0.01123**	**4.32E-3**
550	0.0355	0.01589	6.05E-3	**0.0392**	**782.8**	**0.01752**	**6.65E-3**

*: Eq. (7), $p_{O_2} = 0.2\,bar$. †: Eq. (16).

$$\frac{dc_{NO_2^-}}{dt} = k_{RRP} \cdot c_{NO_3^-} - k'_{ORP} \cdot c_{NO_2^-} c_O + k'_{ROP} \cdot c_{NO_3^-} c_O - k'_{OOP} \cdot c_{NO_2^-} c_{O_{2(diss.)}} \quad (22)$$

$$\frac{dc_{NO_2^-}}{dt} = k_{RRP} c_{NO_3^-} - k_{ORP} c_{NO_2^-} p_{O_2}^{0.5} + k_{ROP} c_{NO_3^-} p_{O_2}^{0.5} - k_{OOP} c_{NO_2^-} p_{O_2} \quad (23)$$

$$K p_0^{0.5} = \frac{k_{RRP}}{k_{ORP}} = \frac{c_{NO_2^-} p_{O_2}^{0.5}}{c_{NO_3^-}} \quad (24)$$

$$K p_0^{0.5} = \frac{k_{ROP}}{k_{OOP}} = \frac{c_{NO_2^-} p_{O_2}}{c_{NO_3^-} p_{O_2}^{0.5}} \quad (25)$$

Precise description of the reduction reaction kinetics (instead of the oxidation reaction kinetics) is considered more important because its impact on salt decomposition (e.g. formation of oxides) is stronger. We decided to place importance on the reduction process combined with a correct equilibrium description, and to accept minor inaccuracies regarding the description of nitrite oxidation. The reduction reaction predominantly occurs via the reduction path [17,29]. The oxidation path is therefore neglected, which leads to the simplified rate law (Eq. (26)). The benefits are that the simplified rate law requires less kinetic parameters than an exact rate law, yet leads to accurate chemical equilibrium values. For a given oxygen partial pressure, the rate law (26) can be solved analytically, and Eq. (27) shows the time dependent nitrite concentration. In this paper, the simplified approach is chosen for analysis of experimental data.

$$\frac{dc_{NO_2^-}}{dt} = k_{RRP} c_{NO_3^-} - k_{ORP} c_{NO_2^-} p_{O_2}^{0.5} \quad (26)$$

$$c_{NO_2^-}(t) = c_{NO_2^-,eq} - (c_{NO_2^-,eq} - c_{NO_2^-,0}) \cdot exp\{-t(k_{ORP} p_{O_2}^{0.5} + k_{RRP})\} \quad (27)$$

Fig. 5 shows the results of the FC curves of the TGA experiments. In every curve, the nitrite concentration increases fast in the beginning, and slower towards the end of the reaction time when the composition approaches chemical equilibrium. This observation is in accordance with the rate laws (15), (22) and (26). The terms with positive sign represent reduction reactions that form nitrite ions. The terms with negative sign stand for the oxidation reaction. At chemical equilibrium, the terms compensate each other, and the nitrite concentration is constant over time. At the beginning of the decomposition process, when no or little nitrite is present in the melt, the oxidation reaction (terms with negative signs in the rate laws) insignificantly contributes to the concentration changes, and the reduction reaction (terms with positive signs) strongly dominates. In contrast, when the nitrite concentration increases, the oxidation reaction becomes more and more

Table 3
Thermodynamic data of reaction (1) from the literature and this study.

Author(s)	Cations	Experimental details measured quantity	$\Delta H/\frac{kJ}{mol}$	$\Delta S/\frac{J}{mol \cdot K}$
Freeman [17]	Na	~500 mg, thermobalance, 1 atm O_2, 600, 650 and 700 °C, consumed O_2-volume	101 +/- 5 *	101 +/- 5 *
Freeman [13]	K	~500 mg, thermobalance, 1 atm O_2, 650, 700 and 750 °C, consumed O_2-volume	139 +/- 6 *	129 +/- 6 *
Barin [20]	Na	/	97.5 #	87.4 #
Bartholomew [16]	K	~100 mg, thermobalance, 1 atm O_2, 550, 600, 648/650, 700, 750 °C, consumed O_2-volume and post-analysis	117 +/- 4 *	103 +/- 5 *
Tracey et al. [19]	$Na_{0.64}K_{0.36}$	~100 g, closed steel reaction chamber, determination of oxygen pressure at equilibrium	115.5 †	105.9 †
		~100 g, purged steel reaction chamber, 81.4 kPa oxygen, 533-866 K, post-analysis of nitrate nitrite (1- > 10 wt.%) and decomposition products	117 +/- 3 *	109 +/- 4 *
Nissen and Meeker [18]	$Na_{0.5}K_{0.5}$	~700 g, stirred melt in crucible, 0.33 to 1.0 atm O_2, 404, 453, 502 °C, nitrite concentration	95 +/- 3 *	84 +/- 3 *
this study	$Na_{0.64}K_{0.36}$	~50 mg, thermogravimetric analysis, 0.2 bar oxygen, 450, 475, 500, 525 and 550 °C, ion chromatography analysis	97 +/- 9	85 +/- 12

* : Equilibrium constants K_{atm} were taken from the reference, converted into the thermodynamic K, and re-fitted according to Eq. (9).
† : Values are not re-fitted, ΔH is directly taken from the reference, and ΔS is converted with respect to p_0.
# : Values are calculated from listed absolute enthalpies and entropies for the reactants and products.

Table 4
Considerations about the kinetic rate law of Nissen and Meeker [18]. At chemical equilibrium, the concentrations of nitrite, nitrate and oxygen are not changing over time, meaning that the rate law (Eq. (15)) equals zero, see (I). The equilibrium description of reaction (1) can be solved for the nitrite concentration at equilibrium, see Eq. (7) and (II). In (III), the nitrite concentration $c_{NO_3^-,eq}$ in (I) is substituted by the expression (II). The equation (III) can only be valid, if the term in the curly brackets equals zero, see (IV). Equation (IV) can directly be converted into the equilibrium expression (V). It is contradictory to the equilibrium expression (VI), which can directly be found in the reference [18].

(I) Rate law at equilibrium, see also Eq. (15)	$\left(\frac{dc_{NO_2^-}}{dt}\right)_{eq} = 0 = k_{Red} c_{NO_3^-,eq} - k_{Ox} c_{NO_2^-,eq} p_{O_2}$
(II) Consecutive equilibrium description	$K = \frac{c_{NO_2^-,eq} \cdot p_{O_2}^{0.5}}{c_{NO_3^-,eq}}$
	$c_{NO_3^-,eq} = \frac{c_{NO_2^-,eq} \cdot p_{O_2}^{0.5}}{K}$
(III) Substitution of $c_{NO_3^-,eq}$	$0 = k_{Red} \cdot \frac{c_{NO_2^-,eq} \cdot p_{O_2}^{0.5}}{K} - k_{Ox} c_{NO_2^-,eq} p_{O_2}$
	$0 = c_{NO_2^-,eq} p_{O_2}^{0.5} \left\{ \frac{k_{Red}}{K} - k_{Ox} p_{O_2}^{0.5} \right\}$
(IV)	$\frac{k_{Red}}{K} - k_{Ox} p_{O_2}^{0.5} = 0$
(V) Correlation between equilibrium constant and rate constants derived from the rate law	$\boldsymbol{K = \frac{k_{Red}}{k_{Ox} p_{O_2}^{0.5}}}$
(VI) Correlation between equilibrium constant and rate constants directly from the reference [18]	$\boldsymbol{K = \frac{k_{Red}}{k_{Ox}}}$

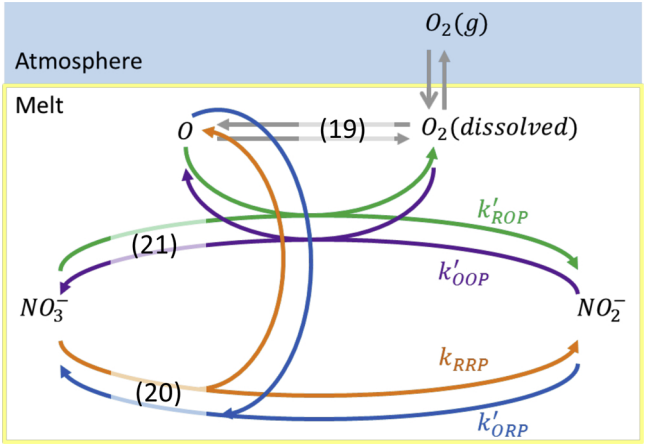

Fig. 4. Sketch of a potential set of elementary reactions for reaction (1). The numbers in brackets refer to the corresponding reaction equations, where nomenclature of the rate constants $\boldsymbol{k_i}$ is explained. Note that the transformation of nitrite to nitrate, and vice versa, can proceed on two reaction paths each.

pronounced, and the macroscopic formation of nitrite proceeds slower and eventually ceases.

With decreasing maximum temperature the system requires longer isotherms to reach steady state (horizontal lines in Fig. 5). Roughly estimated, at 450 °C isotherms of 12 h are needed, whereas, at 550 °C steady state is reached after only 3 h. This tendency is comprised in the Arrhenius Eq. (28), where the rate constant k increases with temperature.

$$k_i = A_i \cdot exp\left\{-\frac{E_{a,i}}{RT}\right\} \tag{28}$$

The FC curves are fitted according to Eq. (27), which is the analytical solution of the rate law (26). Fig. 6 shows the FC curves and the fit curve (black dotted lines) for all five TGA experiments. The 450, 475 and 500 °C experimental curves reveal a specific deviation from the fit

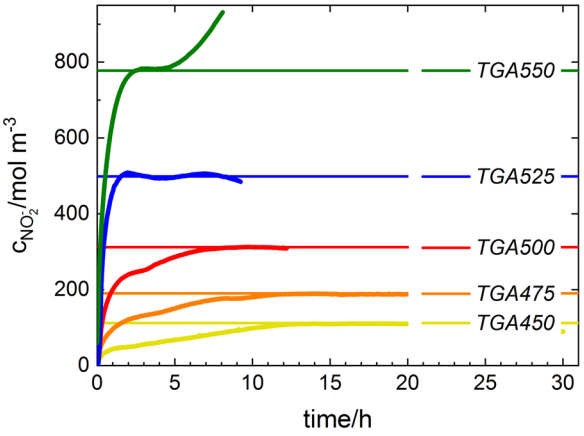

Fig. 5. FC curves of the experiments *TGA450*, *TGA475*, *TGA500*, *TGA525* and *TGA500*. The experimental curves are transformed to FC curve, as described in the methods section. The horizontal lines illustrate the equilibrium nitrite concentrations (see Table 2, column 8) at the respective temperature.

curves. The measured nitrite concentration increases faster than the fit curve at the very beginning. Then, the two curves intersect, and the fit curves describe higher nitrite concentration than the experiment curves, until they reach chemical equilibrium. It is assumed that these deviations arise from the oxidation reaction path, which is neglected in the applied rate law (26). For example, the formation of nitrite ions might not only proceed by forward reaction (20) (RRP), but also to a minor extent by reverse reaction (21) (ROP). The shapes of the experimental curves could be explained by overlapping of the two reactions. Also, these two reactions might have different temperature dependence, resulting in the different curve shapes at 525 and 550 °C.

The fit parameters and the derived reaction rate constants are listed in Table 5. In accordance with the Arrhenius equation and the previous observation, the rate constants decrease with increasing temperature. In Fig. 7, the logarithmic rate constants from this work and available literature data are plotted versus the inverse temperature. Comparison of the rate constants is not trivial, because they are determined for different rate laws, see Table 6. The studies of Freeman [13,17] refer to an oxygen pressure of 1 atm, and the rate law does not consider the oxygen partial pressure. However, the oxygen pressure is close to the reference pressure of 1 bar, and therefore hardly affects the rate constants. The rate law of Bond [29] only considers the reduction reaction, and the one of Paniccia [14] describes the oxidation reaction. In the Freeman [13,17] and Bond [29] studies, the temperatures that are chosen for investigation of reaction kinetics mainly exceed 600 °C. At these temperatures, reaction (1) is no longer the only reaction that has to be considered, because decomposition of nitrite ions to oxide species and various gases is observed. The rate law of Bond [29] describes the time dependent mass loss instead of molar concentrations.

The rate constants of this study are higher than the literature rate constants in the applied temperature range (450–550 °C). This can arise from the mentioned differences in the rate laws and chosen temperatures, and from the experimental scales. The experiments in this study are executed with about 50 mg of salt, whereas the salt samples in the literature studies are larger. In a series of TGA pre-experiments, mass transport limitations in the 50 mg samples were excluded. In the used TGA crucibles, this amount of salt forms a thin layer of approximately 0.8 mm, and mass transport limitations were found for sample thicknesses larger than 1.6 mm. The reduction rate constants of this study are closest to those of Freeman [17]. Depending on the temperature, the oxidation rate constants of this study are closest to those of Freeman [17] and Nissen [18].

Activation energies and pre-exponential factors of reduction and oxidation reaction are extracted from the linear fits in Fig. 7, according to the Arrhenius Eq. (28). They amount to 212 +/-11 kJ·mol^{-1} and

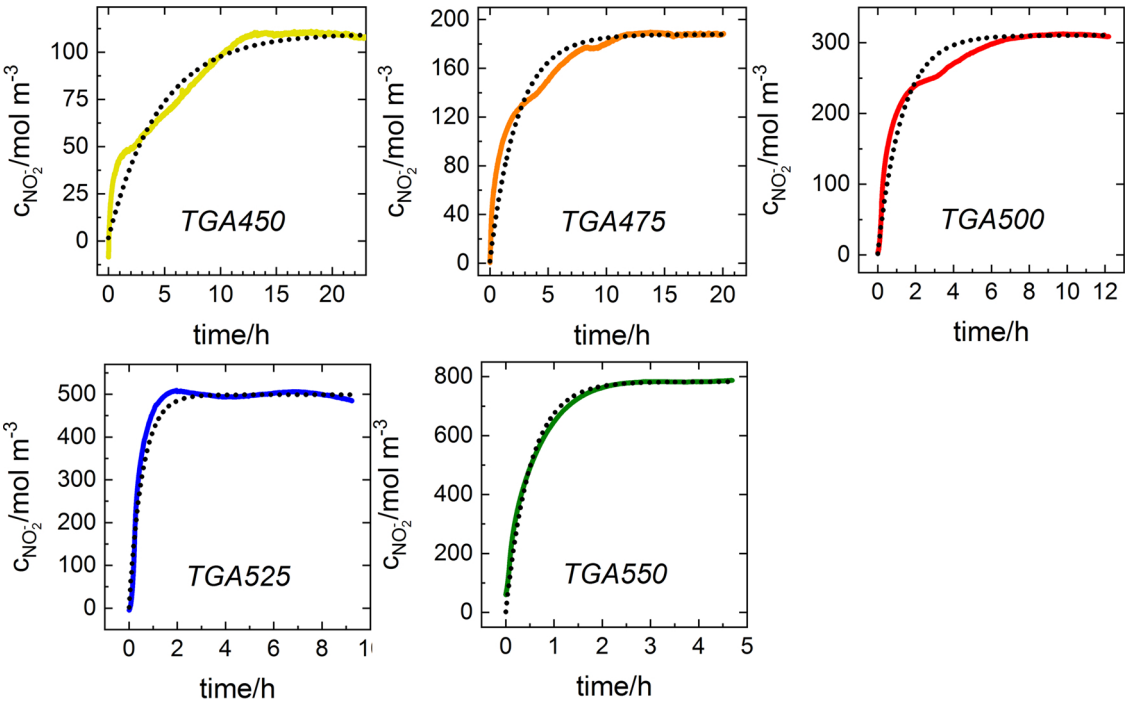

Fig. 6. Exponential fits (dotted lines) of the nitrite concentration curves of the experiments *TGA450, TGA475, TGA500, TGA525* and *TGA500.* The solid lines are the experimental curves, which are fitted according to the equation Table 5, column 2. The fit results can be found in Table 5, column 3.

Table 5
Fit functions and fit results of the TGA experiments. The exponential fits yield values for the term $k_{ORP}p_{O_2}^{0.5} + k_{RRP}$ (column 3). The rate constants k_{RRP} and k_{ORP} are calculated with the fit results.

T /°C	Fit function* all values /$mol{\bullet}m^{-3}$	$k_{ORP}p_{O_2}^{0.5} + k_{RRP}$ /s^{-1}	k_{RRP}† /s^{-1}	k_{ORP}† /s^{-1}
450	$c_{NO_2^-}(t) = 109.9 - 108.2{\bullet}exp\{-t(k_{Ox}p_{O_2}^{0.5} + k_{Red})\}$	6.07E-5	3.31E-7	1.35E-4
475	$c_{NO_2^-}(t) = 187.8 - 186.1{\bullet}exp\{-t(k_{Ox}p_{O_2}^{0.5} + k_{Red})\}$	1.17E-4	1.09E-6	2.59E-4
500	$c_{NO_2^-}(t) = 310.4 - 308.8{\bullet}exp\{-t(k_{Ox}p_{O_2}^{0.5} + k_{Red})\}$	2.16E-4	3.32E-6	4.76E-4
525	$c_{NO_2^-}(t) = 498.9 - 497.2{\bullet}exp\{-t(k_{Ox}p_{O_2}^{0.5} + k_{Red})\}$	4.95E-4	1.21E-5	1.08E-3
550	$c_{NO_2^-}(t) = 782.8 - 781.1{\bullet}exp\{-t(k_{Ox}p_{O_2}^{0.5} + k_{Red})\}$	5.49E-4	2.07E-5	1.18E-3

*: Based on Eq. (27), values from Table 2, column 6. †: Calculated with $Kp_0^{0.5} = \frac{k_{RRP}}{k_{ORP}}$ and $p_{O_2} = 0.2\,bar$.

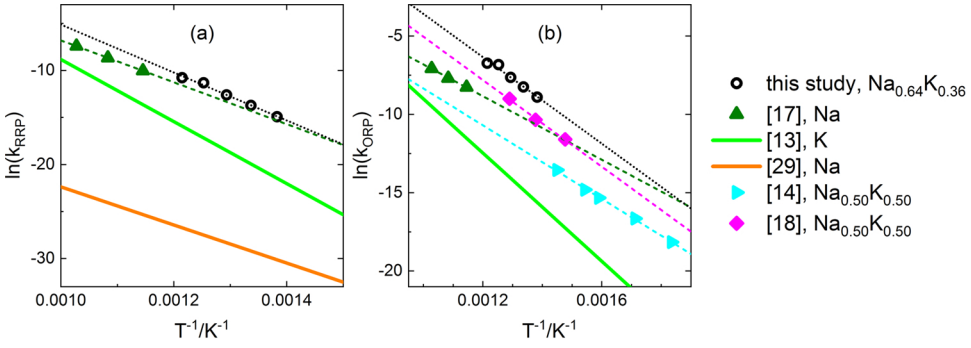

Fig. 7. Arrhenius plots of reduction (a) and oxidation (b) rate constants. The filled symbols are rate constants which are published in the indicated literature. The lines are Arrhenius functions with kinetic parameters published in the indicated literature (see also Table 6). The black circles are the results of this study and correspond to the fit results presented in Table 5. The RMSE amounts to 0.14, and is illustrated by the grey tunnel. The results of the linear fits allow calculation of activation energies and pre-exponential factors, which are listed in Table 6.

694546727 +/-6 s^{-1} (reduction, RRP), and 114.65 +/-11 kJ·mol^{-1} and 25770 +/-6 s^{-1} (oxidation, ORP), respectively. The results and the literature values are listed in Table 6. The activation energy of the reduction reaction in this study falls in between the values that Freeman [13,17] published for the pure salts (sodium nitrate and potassium nitrate), which is reasonable because Solar Salt is a mixture of these two salts. The activation energy of the oxidation reaction in this study is similar to the one that Nissen and Meeker [18] found, and again between the values of Freeman [13,17] for the pure salts. The difference to the values published by Bond [29] and Paniccia [14] could be attributed to the high temperatures and to the large scale of their experiments, respectively.

Table 6
Kinetic parameters of nitrate reduction and nitrite oxidation in sodium and potassium nitrate salt melts. Activation energies and pre-exponential factors from literature and this study are compared.

Author(s)	Experiment, measurement data	Applied kinetic equations	Oxidation/ reduction	Activation Energy E_a /kJ·mol^{-1}	Pre-exponential factor A /s^{-1}
Freeman [17]	~500 mg, inner diameter 1.6 cm, $NaNO_3$/$NaNO_2$, thermobalance, 1 atm O_2, 600, 650 and 700 °C, consumed O_2-volume	$\frac{dx/a}{dt} = k_{ox}\left(1 - x/a\right) - k_{red}x/a$ $k_{ox}t = \frac{x_e}{a}\ln\frac{x_e}{x_e - x}$	ox. red.	84 +/-5 † 185 +/-2 †	27 +/-1 † 5104230 +/-11 †
Freeman [13]	see above, KNO_3/KNO_2, 550 to 750 °C	x: mols sodium nitrate x_e: mols sodium nitrate at chemical equilibrium a: mols sodium nitrate plus sodium nitrite k_{ox}: oxidation rate constant k_{red}: reduction rate constant	ox. red.	144* 274*	3801.90* 3.16E+10*
Bond and Jacobs [29]	~100 mg, $NaNO_3$, thermobalance, air or argon, 628 to around 730 °C mass change	empirical equation: $[-\ln(1-\alpha)]^{\frac{1}{3}} = kt$ α: mass loss	red.	169*	0.122*
Paniccia and Zambonin [14]	~200 g, (Na,K)NO_2 in equimolar (Na,K)NO_3, 0.1 to 1.2 atm O_2, 545 to 690 K, pressure drop	$-\frac{dc_{NO_2^-}}{dt} = k_I c_{NO_2^-} c_{O_2}$ k_I: rate constant (oxidation)	ox.	98 +/-2†	29 +/-2†
Nissen and Meeker [18]	~700 g, $Na_{0.5}K_{0.5}NO_2$ in equimolar $Na_{0.5}K_{0.5}NO_3$, 0.33 to 1.0 atm O_2, 404, 453, 502 °C, nitrite concentration	$-\frac{dc_{NO_2^-}}{dt} = k_{ox}c_{NO_2^-}p_{O_2} - k_{red}c_{NO_3^-}$ analytical solution with simplification due to $k_{ox} \gg k_{red}$: $c_{NO_2^-} \cong c_{NO_2^-,0} \bullet \exp(-k_1 p_{O_2} t)$	ox.	115 +/-7 †	6376 +/-3 †
this study, TGA	~50 mg, $Na_{0.64}K_{0.36}NO_3$, 0.2 bar O_2, 450 to 550 °C, mass change	$\frac{dc_{NO_2^-}}{dt} = k_{RRP}c_{NO_3^-} - k_{ORP}c_{NO_2^-}p_{O_2}^{0.5}$ see Eq. (26)	red. ox.	212 +/-11 115 +/-11	694546727 +/-6 25770 +/-6

† Rate constants re-fitted (Fig. 7), and kinetic parameters calculated according to the Arrhenius Eq. (28).
* Kinetic parameters directly taken from the references.

4. Summary and conclusions

The thermodynamics and reaction kinetics of the reversible reaction $NO_3^- \rightleftharpoons NO_2^- + 0.5\,O_2$ in molten Solar Salt (60 wt.% sodium nitrate, 40 wt.% potassium nitrate) are investigated at temperatures from 450 to 550 °C. The applied experimental method is isothermal thermogravimetric analysis, and subsequent salt composition analysis by ion chromatography.

The chemical equilibrium is described by the reaction enthalpy and entropy, which are found to be close to the results of Nissen and Meeker [18]. In the investigated temperature range, the values of the equilibrium constant K are closest to the results of previous examinations of Tracey [19]. All three studies are deemed applicable with regard to future reaction equilibrium considerations of Solar Salt. The coinciding equilibrium outcome permits using the experiments for further evaluation with regard to reaction kinetics.

Mathematical description of the reaction kinetics in terms of different rate laws is discussed. Careful literature review reveals several potential elementary steps of the reversible reaction. First, those elementary steps are combined to a multi-path reaction mechanism, and to a rate law with numerous parameters, which are difficult to obtain experimentally. Second, several approximations are applied to derive a simplified rate law. The reduction reaction is regarded as the crucial direction of the reaction because it contributes to the problematic salt decomposition. Therefore, the presented work focuses on the reduction path which provides a highly accurate description of the nitrite formation. However, it might lead to deviations of predicted and actual salt compositions during the nitrate formation. The benefits are that the required parameters are experimentally accessible. Ultimately our work is the first describing intrinsic and temperature dependent kinetics of the nitrate-nitrite reaction in Solar Salt, which includes chemical equilibria, as well as forward and reverse reaction. In terms of kinetic analysis of the nitrite forming thermogravimetric experiments, the developed simplified rate law is applied.

The reduction and oxidation rate constants of this study are higher than those found in literature. Probably, the experimental method in this study successfully minimizes mass transport effects. The extracted kinetic parameters, activation energies and pre-exponential factors can be used for time dependent predictions of the reaction rate, and consequently of the stability of Solar Salt melts.

Declaration of competing interests

The authors have no competing interests to declare.

Acknowledgements

The authors thank the German Federal Ministry for Economic Affairs and Energy for the financial support given to this work in the MS-STORE project (Contract No. 0325497 A). We express our thanks to Ulrike Kröner and Markus Braun (DLR Stuttgart) for their support and expertise, especially during the experimental work.

References

[1] Y. Tian, C.Y. Zhao, A review of solar collectors and thermal energy storage in solar thermal applications, Appl. Energy 104 (2013) 538–553, https://doi.org/10.1016/j.apenergy.2012.11.051.
[2] M. Mehos, C. Turchi, J. Vidal, M. Wagner, Z. Ma, C. Ho, W. Kolb, C. Andraka, A. Kruizenga, Concentrating Solar Power Gen3 Demonstration Roadmap, NREL (National Renewable Energy Laboratory, CO United States), 2017.
[3] R.I. Olivares, The thermal stability of molten nitrite/nitrates salt for solar thermal energy storage in different atmospheres, Sol. Energy 86 (2012) 2576–2583, https://doi.org/10.1016/j.solener.2012.05.025.
[4] A.G. Fernández, M.I. Lasanta, F.J. Pérez, Molten salt corrosion of stainless steels and low-Cr steel in CSP plants, Oxid. Met. 78 (2012) 329–348, https://doi.org/10.1007/s11085-012-9310-x.
[5] G. McConohy, A. Kruizenga, Molten nitrate salts at 600 and 680 °C: thermophysical property changes and corrosion of high-temperature nickel alloys, Sol. Energy 103 (2014) 242–252, https://doi.org/10.1016/j.solener.2014.01.028.
[6] X. Wei, Y. Wang, Q. Peng, J. Yang, X. Yang, J. Ding, NOx emissions and NO2-formation in thermal energy storage process of binary molten nitrate salts, Energy 74 (2014) 215–221, https://doi.org/10.1016/j.energy.2014.05.064.
[7] Y. Hoshino, T. Utsunomiya, O. Abe, The thermal decomposition of sodium nitrate and the effects of several oxides on the decomposition, Bull. Chem. Soc. Jpn. 54 (1981) 1385–1391, https://doi.org/10.1246/bcsj.54.1385.
[8] O. Abe, T. Utsunomiya, Y. Hoshino, The reaction of sodium nitrite with silica, Bull. Chem. Soc. Jpn. 56 (1983) 428–433, https://doi.org/10.1246/bcsj.56.428.
[9] O. Abe, T. Utsunomiya, Y. Hoshino, Acid-base and redox reactions in fused sodium nitrite, Thermochim. Acta 74 (1984) 131–141, https://doi.org/10.1016/0040-6031(84)80013-1.
[10] A.K.K. Lee, E.F. Johnson, The stoichiometry and kinetics of the thermal

decomposition of molten anhydrous lithium nitrite, Inorg. Chem. 11 (1972) 782–787.
[11] R.I. Olivares, W. Edwards, LiNO3–NaNO3–KNO3 salt for thermal energy storage: thermal stability evaluation in different atmospheres, Thermochim. Acta 560 (2013) 34–42, https://doi.org/10.1016/j.tca.2013.02.029.
[12] P.I. Protsenko, E.A. Bordyushkova, Kinetics and mechanism of the thermal dissociation of the nitrites of calcium, strontium, and barium, Russ. J. Phys. Chem. 39 (1965) 1048–1051.
[13] E.S. Freeman, The kinetics of the thermal decomposition of potassium nitrate and of the reaction between potassium nitrite and oxygen, J. Am. Chem. Soc. 79 (1957) 838–842, https://doi.org/10.1021/ja01561a015.
[14] F. Paniccia, P.G. Zambonin, Redox mechanisms in an ionic matrix. III. Kinetics of the reaction N02- + 1/2 O2 = NO3- in molten alkali nitrates, J. Phys. Chem. 77 (1973) 1810–1813, https://doi.org/10.1021/j100633a018.
[15] E. Desimoni, F. Paniccia, P.G. Zambonin, Solubility and detection (down to 30 p.p.b.) of oxygen in molten alkali nitrates, J. Electroanal. Chem. Interfacial Electrochem. 38 (1972) 373–379, https://doi.org/10.1016/s0022-0728(72)80347-4.
[16] R.F. Bartholomew, A study of the equilibrium KNO3(l) = KNO2(l) + 1/2O2(g) over the temperature range 550-750°, J. Phys. Chem. 70 (1966) 3442–3446, https://doi.org/10.1021/j100883a012.
[17] E.S. Freeman, The kinetics of the thermal decomposition of sodium nitrate and of the reaction between sodium nitrite and oxygen, J. Phys. Chem. 60 (1956) 1487–1493, https://doi.org/10.1021/j150545a005.
[18] D.A. Nissen, D.E. Meeker, Nitrate/nitrite chemistry in NaN03-KN03 melts, Inorg. Chem. 22 (1983) 716–721, https://doi.org/10.1021/ic00147a004.
[19] T. Tracey, C. Tyner, W. ER, Conceptual Design of Advanced Central Receiver Power System. Martin Marietta Corporation, Final Report for Contract EG77-C-03-1724, (1978).
[20] I. Barin, Thermochemical Data of Pure Substances, third edition, Wiley-VCH Verlag GmbH, 2008, https://doi.org/10.1002/9783527619825.
[21] G.F. Versteeg, J.A.M. Kuipers, F.P.H.V. Beckum, W.P.M.V. Swaaij, Mass transfer with complex reversible chemical reactions—I. Single reversible chemical reaction, Chem. Eng. Sci. 44 (1989) 2295–2310, https://doi.org/10.1016/0009-2509(89)85163-2.
[22] Krevelen D.W. van, Micro- and macro-kinetics, Chem. Eng. Sci. 8 (1958) 5–17, https://doi.org/10.1016/0009-2509(58)80032-9.
[23] Krevelen D.W. van, P.J. Hoftijzer, Kinetics of gas-liquid reactions part I. General theory, Recl. Des Trav. Chim. Des Pays-bas 67 (1948) 563–586, https://doi.org/10.1002/recl.19480670708.
[24] Swaaij W.P.M. van, G.F. Versteeg, Mass transfer accompanied with complex reversible chemical reactions in gas—liquid systems: an overview, Chem. Eng. Sci. 47 (1992) 3181–3195, https://doi.org/10.1016/0009-2509(92)85028-A.
[25] Vusse J.G. van de, Mass transfer with chemical reaction, Chem. Eng. Sci. 16 (1961) 21–30, https://doi.org/10.1016/0009-2509(61)87003-6.
[26] S. Vyazovkin, K. Chrissafis, M.L.D. Lorenzo, N. Koga, M. Pijolat, B. Roduit, N. Sbirrazzuoli, J.J. Suñol, ICTAC kinetics committee recommendations for collecting experimental thermal analysis data for kinetic computations, Thermochim. Acta 590 (2014) 1–23, https://doi.org/10.1016/j.tca.2014.05.036.
[27] K.A. Connors, Chemical Kinetics: The Study of Reaction Rates in Solution, Wiley-VCH, 1990.
[28] M. Quack, S. Jans-Buerli, Molekulare Thermodynamik und Kinetik, Teil 1: Chemische Reaktionskinetik, Verlag Der Fachvereine, Zuerich, 1986.
[29] B.D. Bond, P.W.M. Jacobs, The thermal decomposition of sodium nitrate, J. Chem. Soc.: Inorg. Phys. Theor. (1966) 1265–1268, https://doi.org/10.1039/j19660001265.
[30] D.J. Rogers, G.J. Janz, Melting-crystallization and premelting properties of NaN03-KN03. Enthalpies and heat capacities, J. Chem. Eng. Data 27 (1982) 424–428.
[31] T. Jriri, J. Rogez, C. Bergman, J.C. Mathieu, Thermodynamic study of the condensed phases of NaNO3, KNO3, and CsNO3 and their transitions, Thermochim. Acta 266 (1995) 147–161, https://doi.org/10.1016/0040-6031(95)02337-2.
[32] A. Bonk, C. Martin, M. Braun, T. Bauer, Material investigations on the thermal stability of solar salt and potential filler materials for molten salt storage, AIP Conf. Proc. (2017) 1850, https://doi.org/10.1063/1.4984429.
[33] G. Wedler, H.-J. Freund, Lehrbuch der physikalischen Chemie 1 John Wiley & Sons, 2012.
[34] R. Carling, C. Kramer, R. Bradshaw, D. Nissen, S. Goods, R. Mar, J. Munford, M. Karnowsky, R. Biefeld, N. Norem, Molten Nitrate Salt Technology Development Status Report, Office of Scientific and Technical Information (OSTI), 1981, https://doi.org/10.2172/6853207.
[35] V.I. Glazov, G.P. Dukhanin, V.A. Losev, Saturated vapor pressure over the melts of the NaNO2 NaNO3 system, Russ. J. Appl. Chem. 75 (2002) 888–890, https://doi.org/10.1023/a:1020312024138.
[36] D.M. Price, Vapor pressure determination by thermogravimetry, Thermochim. Acta 367-368 (2001) 253–262, https://doi.org/10.1016/s0040-6031(00)00676-6.
[37] D.G. Lovering, Molten Salt Technology, Springer, 1982, https://doi.org/10.1007/978-1-4757-1724-2.

Solar Energy Materials & Solar Cells 212 (2020) 110577

Contents lists available at ScienceDirect

Solar Energy Materials and Solar Cells

journal homepage: http://www.elsevier.com/locate/solmat

With a view to elevated operating temperatures in thermal energy storage - Reaction chemistry of Solar Salt up to 630°C

Veronika Anna Sötz [a,*], Alexander Bonk [b], Thomas Bauer [a]

[a] Institute of Engineering Thermodynamics, German Aerospace Center (DLR), Linder Höhe, 51147 Köln, Germany
[b] Institute of Engineering Thermodynamics, German Aerospace Center (DLR), Pfaffenwaldring 38-40, 70569 Stuttgart, Germany

ARTICLE INFO

Keywords:
Concentrating solar power (CSP)
Thermal energy storage (TES)
Solar salt
Nitrate salt
Salt decomposition
Reaction kinetics

ABSTRACT

Sensible heat storage is a cost-efficient and scalable technology for energy storage. The state-of-the-art storage systems in concentrating solar power (CSP) plants use the storage material Solar Salt, which is a nitrate salt mixture. Chemical stability of this salt material is crucial for lifetime reliance, and for development of the storage technology towards higher temperatures. High temperatures enhance the storage capacity, but also promote decomposition reactions. For instance, harmful gases can evolve, and oxide ions are produced, which aggravate corrosion. Up to now, it is unclear how to describe the salt chemistry, and how to quantitatively predict the problematic decomposition products. The experimental method in this study is chosen with regard to the exclusion of mass transport limitations. Thin films of salt are heated to 560–630 °C. The salt composition is analyzed by ion chromatography and acid-base titration. The ratio of nitrite to nitrate ions stabilizes, which indicates chemical equilibrium of the nitrite forming reaction. The oxide content increases continuously over time, and is interpreted in terms of a kinetic rate law. A consistent mathematical description of Solar Salt chemistry at high temperatures (≥560 °C) in contact with air is presented. It includes thermodynamic parameters, in particular the reaction enthalpy of 95 ± 4 kJ·mol^{-1} and entropy of 86 ± 5 J·mol^{-1}·K^{-1} for the nitrate-nitrite reaction. The microkinetics of the oxide ion formation are characterized by an activation energy of 42 ± 3 kJ·mol^{-1}. The work presented finally contributes to a forecast of material stability at and above 560 °C.

1. Introduction

1.1. Motivation

Sensible heat storage in so-called Solar Salt is implemented in existing storage units, and it is a promising candidate for growing demands of energy storage [3–6]. For concentrating solar power plants combined with thermal energy storage, it is the state of the art technology [7–9]. To improve flexibility of the electricity market, sensible heat storage in nitrate salts is an option for the future. Based on energy conversions power-to-heat-to-power (P2H2P), electric energy can be stored temporarily in terms of heat, and subsequently re-converted to electric power [10].

Liquid storage materials feature tempting advantages such as effortless pumpability and high volumetric heat capacities. The lower operating temperature of a sensible heat storage system with a liquid material is restricted by the solidification temperature of the regarded storage material. The upper temperature limit has to be chosen with regard to thermal stability and system requirements. At the time of writing, commercial CSP plants restrict the Solar Salt temperature to a maximum of 560 or 565 °C [7] for several reasons. These include unacceptable corrosion and the alarming production of toxic gases, particularly nitrous gases, at higher temperatures.

On the contrary, higher storage temperatures are favorable from a technological point of view [11]. A higher maximum temperature basically improves the storage capacity, and the power block efficiency regarding the conversion heat-to-power. The storage capacity is proportional to the difference of maximum and minimum temperature. It increases with the maximum temperature if the minimum temperature remains constant. Hence, more energy can be stored in the same tanks when the temperature limit is raised. Furthermore, according to the Carnot efficiency description, the conversion of thermal energy to electricity is more efficient at high temperatures [12]. This can result in significant overall cost reductions of the storage system. Long-term stable, widely available and cost-efficient liquids with a broad range of operating temperatures are requested for the sensible energy storage technology.

* Corresponding author.
E-mail address: Veronika.Soetz@dlr.de (V.A. Sötz).

https://doi.org/10.1016/j.solmat.2020.110577
Received 15 January 2020; Received in revised form 2 April 2020; Accepted 19 April 2020
Available online 4 May 2020

Nomenclature

List of Symbols

A	Pre-exponential factor in the Arrhenius equation of reaction (O), s^{-1}
b_i	Molal concentration of i, $mol{\cdot}kg^{-3}$
C_{exp}	Constant derived from the experimental results of this study
C_{fit}	Constant predicted by the linear fit
c_i	Molar concentration of i, $mol{\cdot}m^{-3}$
$c_{i,m}$	Molar concentration of i in the sample m, $mol{\cdot}\ m^{-3}$
$\Delta_{\%}c_i(t)$	Standard deviation of the concentration of i for time t, %
$\Delta_{\%}c_i$	Uncertainty of the concentration of i, %
$c_{M_2O,exp}$	Oxide concentration measured in an experiment, $mol{\cdot}\ m^{-3}$
$c_{M_2O,mod}$	Oxide concentration predicted by a model, $mol{\cdot}\ m^{-3}$
E_a	Activation energy of reaction (O), $kJ{\cdot}mol^{-1}{\cdot}K^{-1}$
ΔH	Reaction enthalpy of reaction (N), $kJ{\cdot}mol^{-1}$
K	Equilibrium constant of reaction (N)
k	Reaction rate constant of reaction (O), s^{-1}
M_{CO_2}	Molar mass of carbon dioxide, 0.04400 $kg{\cdot}mol^{-1}$
N	Number of data points
p_{O_2}	Partial pressure of oxygen, bar
p_0	Reference pressure, 1 bar
Q	Reaction quotient of reaction (N), 1
R	Ideal gas constant, 8.314 $J{\cdot}mol^{-1}{\cdot}K^{-1}$
r	Reaction rate of reaction (O), $mol{\cdot}m^{-3}{\cdot}s^{-1}$
ΔS	Reaction entropy of reaction (N), $J{\cdot}mol^{-1}{\cdot}K^{-1}$
t	Time, h
T	Temperature, K
x_i	Molar ratio of i relative to the total amount of substance, $mol{\cdot}mol^{-1}$
$x_{i,eq}$	Molar ratio of i relative to the total amount of substance at chemical equilibrium, $mol{\cdot}mol^{-1}$
ρ_{SoSa}	Density of Solar Salt, $\rho_{SoSa} = 2268.9\ kg{\cdot}m^{-3} - 0.6395\ kg{\cdot}m^{-3}{\cdot}K^{-3}{\cdot}T$ [1,2]

These conditions might be fulfilled by new materials [13–20], or they are realized by innovative operating strategies for the well-established and reliable Solar Salt, which is addressed in this study. Widespread and detailed knowledge about the chemical reactions in Solar Salt is required to estimate its stability under manifold conditions at elevated temperatures. Besides, understanding of the salt chemistry provides a necessary basis for the assessment of compatibilities between molten salt and component materials [21–27] or filler materials [8, 28–30]. The latter are particularly important for the concept of thermocline filler storage systems [31–34]. Up to now, a deep comprehension of many reactions in Solar Salt is still lacking, although several studies on nitrate salt chemistry were published in the past.

1.2. Literature review

The formation of nitrites (MNO_2) was confirmed many times, and reaction equation (N) is generally accepted. The thermodynamics have been investigated in several studies [35–41]. The kinetics of this reaction can be found in the literature [36–38,42,43] for pure sodium nitrate $NaNO_3$ and potassium nitrate KNO_3, and for mixtures of both. Recently, the authors of this work have published the microkinetics of reaction (N) in the Solar Salt mixture [41].

$$MNO_3 \rightleftharpoons MNO_2 + 0.5\ O_2 \quad (M = Na, K) \tag{N}$$

The nature of nitrate and nitrite ions was investigated on a theoretical level by means of quantum mechanical methods. The calculated bond lengths *N-O*, and the total energies amount to 1.2552 Å and 1.2567 Å, and −289 hartree and −205 hartree for nitrate ions and nitrite ions, respectively, according to Wei et al. [44], which agrees with a previous publication [45], and with experimental values. The partial charges of the oxide atoms are −0.673 and −0.793 for nitrate ions and nitrite ions, respectively, according to ab initio calculation in reference [45].

It is also accepted that oxide ions O^{2-} form at high operating temperatures [14,22,46,47]. The underlying reaction equations, thermodynamics and kinetics, however, are far less understood. Some studies consider oxide formation kinetics in nitrite rather than nitrate salts. Protsenko and Bodyushkova [48] followed thermal decomposition kinetics of calcium, strontium and barium nitrite at 420 and 450 °C in a thermogravimetric apparatus. Thermal decomposition turned out to be influenced by the atmosphere (argon, vacuum and air). For argon atmosphere, equations (1)–(3) were proposed, demonstrating the formation of oxide and nitrate ions as well as the gases NO_2, NO and N_2. Rate constants of the decomposition kinetics were calculated, assuming a first-order rate law.

$$2\ NO_2^- \rightleftharpoons NO_2 + NO + O^{2-} \tag{1}$$

$$NO_2^- + NO_2 \rightleftharpoons NO_3^- + NO \tag{2}$$

$$NO_2^- + NO \rightleftharpoons NO_3^- + 0.5\ N_2 \tag{3}$$

Lee and Johnson [49] analyzed the gases evolving from lithium nitrite under argon atmosphere with a mass spectrometer, and reported salt composition changes. N_2, NO, O_2 and N_2O were detected at 250, 300 and 350 °C. NO_2 was assumed to be formed only at higher temperatures. With time, the nitrite content decreased, whereas the nitrate and oxide content increased up to 6 and 1 anion-mol%, respectively, at 350 °C. The underlying reaction mechanism was proposed to be composed of four steps, equations (4)–(7). The exact reaction order remained unclear, but approximation with first-order kinetics with respect to nitrite was reasonable due to a linear dependence of the logarithmic nitrite concentration on time. A rather sophisticated temperature dependence of the rate constants is expected because of the complex network of reaction steps.

$$3\ NO_2^- \rightleftharpoons O^{2-} + NO_3^- + 2\ NO \tag{4}$$

$$2\ NO_2^- \rightleftharpoons O^{2-} + N_2O + O_2 \tag{5}$$

$$2\ NO_2^- + 2\ NO \rightleftharpoons 2\ NO_3^- + N_2 \tag{6}$$

$$2\ NO_3^- \rightleftharpoons 2\ NO_2^- + O_2 \tag{7}$$

Hoshino et al. [50] analyzed the temperature dependent decomposition of sodium nitrate in argon atmosphere with a combined thermogravimetric analysis – gas chromatography set-up. From 500 °C upwards, O_2 was detected, and at slightly higher temperatures also NO gas was observed. Above 680 °C, a small amount of N_2 was detected additionally. The authors divided the decomposition process into three stages. The first stage is the well-known reaction of nitrate to nitrite ions (reaction (N)). It is followed by a first-order liquid-phase reaction that belongs to a complex mechanism which can be interpreted with peroxide or hyperoxide intermediates, e.g. equations 8–11. The third stage, characterized by the formation of sodium oxide, is increasingly important at higher temperatures.

$$NaNO_2 \rightleftharpoons 0.5\ Na_2O_2 + NO \quad (8)$$

$$Na_2O_2 \rightleftharpoons Na_2O + O \quad (9)$$

$$NaNO_2 + O \rightleftharpoons NaNO_3 \quad (10)$$

$$Na_2O_2 + O \rightleftharpoons NaO + O_2 \quad (11)$$

Olivares and Edwards [51] compared the decomposition of a ternary nitrate mixture (eutectic $LiNO_3$- $NaNO_3$-KNO_3) in 4 atm. The main decomposition gas product turned out to be *NO*. The TG-MS apparatus detected *NO* at 325, 425, 475 and 540 °C in argon, nitrogen, air and oxygen, respectively. The results indicate a stabilizing effect of oxygen in the atmosphere. The presence of oxygen reduces the amount of nitrite ions, which probably means that less reactant for subsequent decomposition reactions is available. Wei et al. [47,52] used a set-up that is composed of a quartz boat containing the salt sample in tubular corundum furnace, and a sophisticated gas analyzing system that absorbs NO_2 and *NO* separately, and quantifies the two gases by UV–vis absorption. For 100 g of solar salt and an air purge flow of 80 mL·min^{-1}, 350 mg·m^{-3} NO_x ($x = 1, 2$) and 1550 mg·m^{-3} NO_x were measured at 550 and 600 °C, respectively. The concentration of NO_2 was slightly lower than the concentration of *NO*. The formation of NO_x at 600 °C was explained to proceed via the reactions (12) and (13). NO_x formation at and below 550 °C was ascribed to reactions of nitrate salt with SiO_2 (from the quartz crucible).

$$4\ NaNO_3 \rightleftharpoons 2\ Na_2O + 4\ NO_2 + O_2 \quad (12)$$

$$2\ NaNO_3 \rightleftharpoons Na_2O + NO + NO_2 + O_2 \quad (13)$$

Oxides (M_2O) in molten nitrate matrix are reported to react to carbonates (M_2CO_3), if the molten salt is in contact with carbon dioxide gas, see equation (C) [21,28,39,53–55].

$$M_2O + CO_2 \rightarrow M_2CO_3 \quad (C)$$

To sum up the main literature findings concerning oxide ion formation kinetics, the following conclusions can be made:

- Decomposition of nitrates and nitrites to oxide ions in molten salt is only sparsely investigated. The experimental results are interpreted with many suggestions and assumptions.
- The regarded studies refer to various types and compositions of cations, and this difference may affect the decomposition mechanism. However, the cations are not directly involved in the nitrate or nitrite chemistry, and therefore findings can be generalized to a certain extent.
- Some studies [47,50–52] report experiments in a nitrate matrix (instead of a nitrite matrix) and are more comparable to molten Solar Salt in that regard.
- Several reaction equations were proposed, most of them with nitrite ions being the reactants, and with the production of nitrous gases, and also oxygen and nitrogen. First-order reaction kinetics with respect to the nitrite concentration seems to be the most probable mechanistic description, or at least can be applied reasonably [48–50]. That implies that the oxide formation follows on reaction (N).
- In the presence of carbon dioxide, oxide ions tend to react further to carbonate ions.
- Previous studies with the Solar Salt mixture utilize relatively big sample sizes of 100 g [47] and 1 kg [28]. Probably, the results are strongly influenced by mass transport effects.
- So far, the intrinsic kinetics of oxide formation in molten sodium nitrate or potassium nitrate, or mixtures of both, has not been evaluated.

1.3. Scope on the study

In this study, we present experiments on the kinetics of oxide and carbonate formation in Solar Salt (60 wt% $NaNO_3$, 40 wt% KNO_3) at 560–630 °C. Emphasis is put on the exclusion of mass transport limitations to measure the microkinetics. Salt composition changes are monitored over time. The nitrate and nitrite contents are examined with regard to chemical equilibrium. That way, the applied experimental method is validated, and thermodynamic equilibrium data up to 630 °C is gained. The oxide ion formation is approached in terms of the ion accumulation and the reaction rate. Following the studies of Protsenko, Lee and Hoshino [48–50], a rate law that is first-order with respect to the nitrite concentration is chosen. Fitting of the experiment results according to the rate law reveals the rate constants at each temperature. The rate constants are evaluated further according to the Arrhenius equation to obtain the temperature independent activation energy and pre-exponential factor. Investigation and evidence of a detailed reaction mechanism of the salt decomposition towards alkaline species and nitrous gases is not within the scope of this study. Reaction (O) will be taken as a placeholder for the true mechanism in the following. It implies the first-order reaction with respect to nitrite, and the coproduction of oxides and gaseous products.

$$MNO_2 \xrightarrow{k} 0.5\ M_2O + 0.5\ NO + 0.5\ NO_2 \quad (O)$$

2. Materials and methods

2.1. Materials

60 g of sodium nitrate (BASF, HQ untreated) and 40 g of potassium nitrate (Haldor Topsøe, technical grade) were weighed and blended. The mixture was heated for 5 h to 300 °C for homogenization. The molten salt was poured into an aluminum beaker for solidification, and then mortared. This material was used for all presented experiments.

2.2. Experimental

The experimental procedure comprises heating and thermal aging of the salt samples, and subsequent chemical analysis of the sample composition. The furnace set-up, and the step-by-step analysis procedure are sketched in Fig. 1. The temperature treatment of the salt sample is realized with a *Nabertherm HTCT 01/16* furnace. The insulated furnace chamber is heated with four SiC heating elements (see rods in Fig. 1), and the temperature is controlled with a *Nabertherm P330* controller. An external temperature sensor (thermocouple type K) verified a temperature accuracy of ±2 K. Two small openings (2 cm diameter, see ovals in Fig. 1) allow inflow and outflow of ambient air, which is driven by natural convection. The effectiveness of the air purge was verified by random control of the outflowing air with a NO_x sensor (*Dräger Pac 7000*), which confirmed low (≤2 ppm) NO_x concentrations. Two alumina crucibles (inner diameter 44 mm, height 70 mm) at the same time were arranged in the furnace chamber, one in the back and one in the front, close to the chamber hatch. For purification between the experiments, the crucibles were soaked in an aqueous solution of citric acid to dissolve all oxide and carbonate residues, purged with deionized water, and dried in a compartment drier at 130 °C. 1.5 g of salt were filled into each crucible. The two crucibles were inserted into the pre-heated furnace at 300 °C. Then, the system was heated with 10 K·min^{-1} to the desired temperature (560–630 °C), which was hold for 1–24 h. Finally, the temperature was reduced with 10 K·min^{-1} to 300 °C, and the crucibles were removed from the furnace chamber. This procedure avoids excessive temperature shocks and material breakage. Overall, 48 experiments at different temperatures and durations were performed (see also Table 1). The molten salt samples were poured into an aluminum beaker (see second step in Fig. 1) for solidification and stored in plastic vials until further analysis.

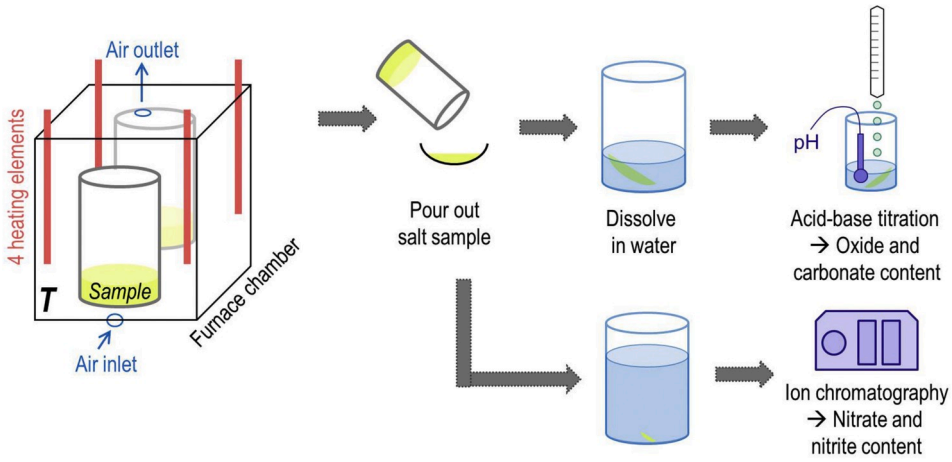

Fig. 1. Sketch of the experimental methods. The salt samples are heated in a furnace for thermal aging. Subsequently, the samples are poured into aluminum beakers, and split for two analytical methods to assess the salt compositions.

Table 1
List of experiments. Experiments written in bold are used for calculation of the equilibrium constants. Experiments written in italics are only used for method development, but are excluded further data evaluation.

Label	Temperature/ °C	Duration/h
OxKi_560	560	2, 4
OxKi_570	570	2, 3, 4, **5**
OxKi_580	580	2, 3, 4, **5**
OxKi_590	590	2, 3, **4**
OxKi_600	600	2, 3, **4**, *5, 6, 7, 8, 9, 10, 12, 14, 16, 18, 20, 24* (each x2)
OxKi_610	610	2, **3**
OxKi_620	620	2, **3**
OxKi_630	630	**2**

The molalities of nitrate and nitrite ions in the salt samples were analyzed by ion chromatography, which is illustrated by the lower path in Fig. 1. About 100 mg of salt were dissolved in 500 mL ultrapure water (*HiPerSolv, VWR,* Germany). The aqueous solution was measured in a *Metrohm model 930 Compact IC Flex* (*Metrohm,* Switzerland) IC apparatus. It is equipped with a *Metrosep A Supp* analytical column (5 × 250 mm), a *Metrosep RP2* guard column, and a suppressed conductivity detector, as also described in reference [28]. The recorded conductivity peaks are evaluated by means of calibration curves, and finally converted into nitrite contents of the salt samples.

The oxide and carbonate contents were analyzed by a titration method. When the salt samples dissolve in water, the oxide salts react with water to hydroxide ions (OH^-), and the carbonate salts dissolve to carbonate ions (CO_3^{2-}). Both cause an alkaline pH value of the aqueous solution. The titration method is based on acid-base reactions, more precisely the protonation of hydroxide and carbonate ions by an acidic compound, which leads to a decreasing pH value. The amount of added acid until characteristic changes in the pH value is used to determine the molalities of oxide and carbonate ions. For the analytical procedure (see upper path in Fig. 1), 10–500 mg of salt sample were dissolved in 150 mL ultrapure water. This aqueous salt solution was titrated with 0.01 M hydrochloric acid (*HCl*) under vigorous stirring. The titration system *Metrohm 905 Titrando* was used, equipped with a 20 mL dosing unit for dosing of the titrant. The pH value was measured by a *Metrohm* glass electrode. The software *Metrohm tiamo*^{TM} *2.5 light* was used for data recording and evaluation.

2.3. Data evaluation

Raw data in terms of molalities (b_{MNO_3}, b_{MNO_2}, $b_{M_2CO_3}$) from ion chromatography and titration analysis is transformed to molar ratios (x_{MNO_3}, x_{MNO_2}, x_{M_2O}) by equation (14), and to molar concentrations (c_{MNO_3}, c_{MNO_2}, c_{M_2O}) by equation (15). The calculated compositions describe a salt that contains oxides instead of carbonates (see discussion at the beginning of chapter 3). The data points in Figs. 2, 4 and 7(a) are the average values of 2 salt samples (average of 4 salt samples in the case of OxKi_600). All further data evaluation and calculations use these average values.

$$x_i = b_i \,/\, (b_{MNO_3} + b_{MNO_2} + b_{M_2O}) \tag{14}$$

$$\begin{aligned} c_i &= b_i \cdot \rho_{SoSa} / (1 - b_{M_2CO_3} \cdot M_{CO_2}) \\ i &= MNO_3,\ MNO_2,\ M_2O\ (M = Na_{0.64}K_{0.36}) \end{aligned} \tag{15}$$

The actual status of the reaction is expressed by the reaction quotient $Q(t)$, see equation (16). The reaction is thermodynamically favored to proceed towards the product side if $Q < K$, whereas it tends to react to the reactant side if $Q > K$. For the experiments in this work, only the forward reaction $Q < K$ is relevant.

$$Q(t) = x_{MNO_2}(t) \,\Big/\, x_{MNO_3}(t) \cdot (p_{O_2}/p_0)^{0.5} \tag{16}$$

The equilibrium constants K at 560–630 °C are calculated with equation (17). The applied nitrate and nitrite contents ($x_{MNO_3,eq}$ and $x_{MNO_2,eq}$) are gained by IC analysis of the experiments in equilibrium, see experiments written in bold in Table 1. A constant oxygen partial pressure $p_{O_2} = 0.2\ bar$ is assumed.

$$K = x_{MNO_2,eq} \,\Big/\, x_{MNO_3,eq} \cdot (p_{O_2}/p_0)^{0.5} \tag{17}$$

Reaction enthalpy ΔH and entropy ΔS are extracted from the van't Hoff plot of the equilibrium constants $K(T)$ (Fig. 6), according to the van't Hoff equation (18). The enthalpy is comprised in the slope of the linear fit ($-\ \Delta H/R$), and the entropy is included in the y-intercept ($\Delta S/R$).

$$\ln K(T) = -\Delta H / R \cdot T^{-1} + \Delta S / R \tag{18}$$

The temperature dependent rate constants $k(T)$ are plotted according to the Arrhenius equation (equation (19), Fig. 7(b)). The kinetics parameters, activation energy E_a and pre-exponential factor A, are calculated from the linear fit results (slope corresponds to $-\ E_a/R$, and y-intercept to $\ln A$).

$$\ln k(T) = \ln A - E_a / R \cdot T^{-1} \tag{19}$$

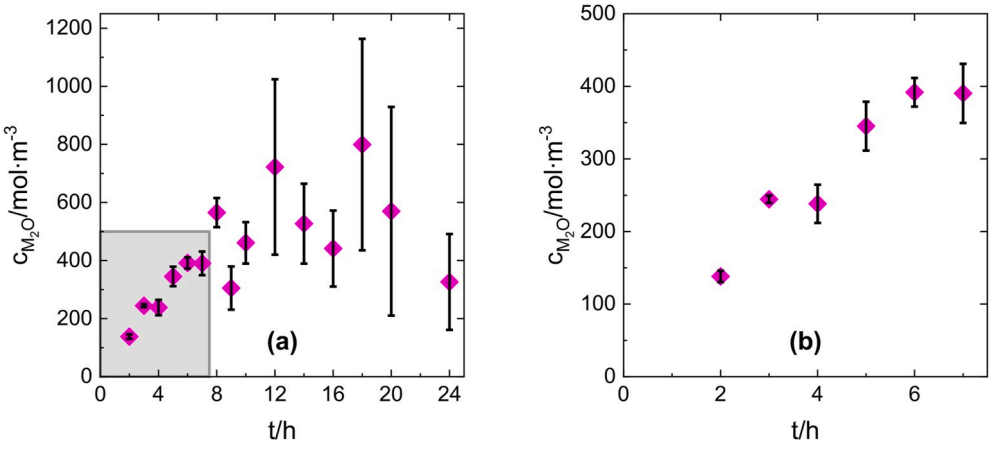

Fig. 2. Oxide production in the OxKi_600 experiments up to 24 h. The data points are the average oxide concentrations of the four samples. The error bars correspond to the standard deviation calculated via equation (20), and represent the experimental uncertainty. The grey area of (a) is enlarged in (b).

2.4. Error calculations

The uncertainty based on the experimental method is assessed by repetitions of the OxKi_600 experiments, see Table 1. The standard deviation of the anion concentrations $\Delta_{\%}c_i(t)$ is calculated for each time step according to equation (20). The average value over all time steps is formed (equation (21)), and adopted for the entire experiment series. The derived uncertainties $\Delta_{\%}c_i$ amount to 7%, 2% and 0.5% for c_{M_2O}, c_{MNO_2} and c_{MNO_3}, respectively. The oxygen partial pressure is assumed to have an uncertainty of 0.02 *bar*, and the temperature uncertainty is assumed to be within 2 *K*. The uncertainties of the salt density, molar masses and the universal gas constant are small and can be neglected. Propagation of uncertainties is calculated with the formula of quadratic error propagation. The errors of $\ln K(T)$ and $\ln k(T)$ are calculated by the root mean square error ($RMSE_C$) formula, equation (22).

$$\Delta_{\%}c_i(t) = 100\% \cdot \sqrt{\sum_m (c_{i,m}(t) - \overline{c_{i,m}(t)})^2 \Big/ 4} \Big/ \overline{c_{i,m}(t)} \tag{20}$$

$$\Delta_{\%}c_i = \overline{\Delta_{\%}c_i(t)} \tag{21}$$

$$RMSE_C = \sqrt{\frac{\sum (\ln C_{exp} - \ln C_{fit})^2}{N}} \tag{22}$$

$C : K,\ k$

2.5. Method development

Appropriate experiment durations and sample quantities had to be chosen for the thermal aging of the salt samples in the furnace chamber. The furnace method requires a heating and cooling time of about 1 h, see section 2.2. Due to inconstant temperatures, these periods are neglected in the reaction kinetics evaluation. Experiment durations of twice the heating and cooling time (≥2 h) are chosen in order to minimize the contribution of heating and cooling to the overall experiment results. For increasing experiment durations, increasing carbonate contents are expected. The solubility limit of carbonates in molten nitrate salts is reached at a certain threshold, resulting in precipitation of carbonate rich solid phases [39,55,56]. The coexistence of several phases causes inhomogeneities of the samples, and makes the composition analysis results sensitive to errors. This effect probably explains the increase of the error bars with increasing experiment duration in Fig. 2, which shows the oxide production of the OxKi_600 experiments over time. Intending high accuracy of the experimental results, the experiment duration is restricted to 5 h in this study, see numbers in black in Table 1. Besides, shorter experiment durations avoid problematic salt evaporation and creeping, which reduces the sample mass and could change the salt composition unintentionally.

The experimental method was also development with regard to the sample mass. Mass transport limitations must be excluded for measurement of intrinsic kinetics, which can be realized by small sample films with short diffusion paths of dissolved gases through the liquid phase. On the other hand, the samples should not be too small to provide enough material for chemical analysis, which requires about 1 g of material. Experiments at 600 °C (6 h) with 0.5, 1.0, 1.5 and 2 g of salt were made, and the oxide production was similar in all experiments. It was therefore concluded that mass transport limitations are negligible in the 1.5 g scale, because the experiments with smaller sample masses did not reveal faster reaction kinetics. A sample mass of 1.5 g of salt was chosen for all further experiments. Macroscopically, the salt was evenly distributed over the flat bottom of the alumina crucibles, except for the edges, where the salt film appeared slightly thicker. The inner and outer surface of the alumina crucibles seems to be wetted by salt because some crucibles stuck to the ground of the furnace chamber at the end of the experiments. This contributes to a higher surface of the salt film, and possibly further reduces mass transport limitations.

3. Results and discussion

Undecomposed Solar Salt before thermal treatment contains only nitrates (MNO_3), meaning nitrate anions (NO_3^-), and the sodium and potassium cations. Depending on the applied temperatures, the salt composition changes with time, which is shown in Fig. 4 for all eight experiment series. The underlying reaction steps are illustrated in Fig. 3. During decomposition, part of the nitrate ions reacts to nitrite ions (NO_2^-) via reaction (N) (first step in Fig. 3) [35–41], which explains the nitrite content $x_{NO_2^-}$ in Fig. 4. According to quantum mechanical calculations and experimental results, the nitrite ions are less stable than the nitrate ions. It is therefore very likely that nitrite ions decompose further to oxide ions (O^{2-}) via reaction (O) (second step in Fig. 3) [47–52]. Oxide ions in turn react with carbon dioxide to form carbonate ions (reaction (C), third step in Fig. 3). During heating in the furnace, the salt

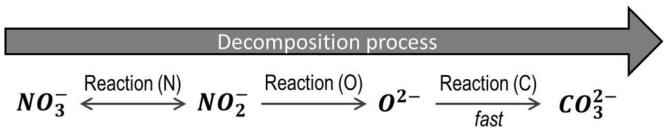

Fig. 3. Simplified schema of the decomposition process of molten nitrate salts under the experimental conditions of this study.

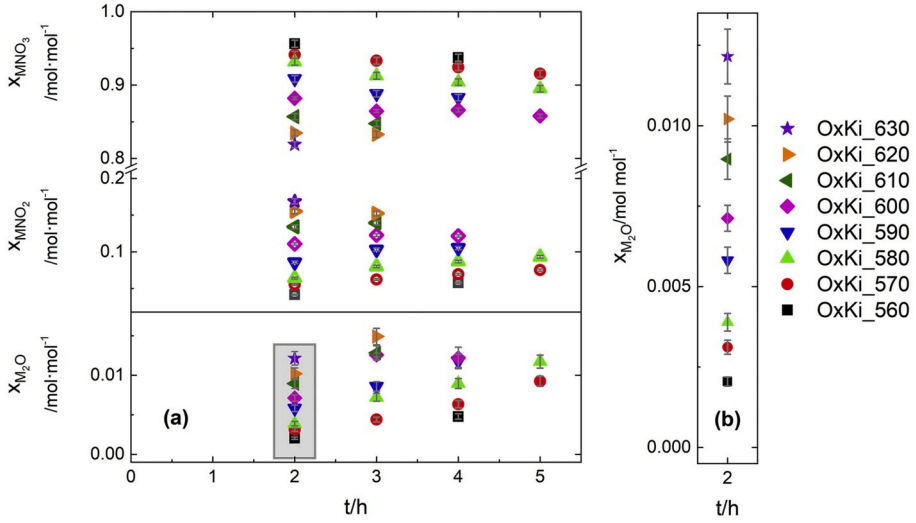

Fig. 4. (a): Experimental results in terms of molar ratios of nitrate (filled symbols, upper part), nitrite (unfilled symbols, upper part) and oxide (lower part). The oxide ratios after 2 h are shown in detail in (b).

samples are in contact with ambient air containing carbon dioxide. It is reported in the literature, that carbon dioxide dissolves in molten sodium and potassium nitrate characterized by Henry constants of 10^{-7} to 10^{-6} mol·cm^{-3}·atm^{-1} [57,58]. Also, reaction of oxide ions with carbon dioxide from the ambient air (CO_2 around 400 ppm) is stated in several publications [21,28,39,53–55]. According to those references, the ambient air seems to be the main source for reacting carbon dioxide. Besides, organic impurities of the salt material could be an additional minor source. Only carbonate ions are detected in all experiments instead of oxide ions. Therefore, reaction (C) is assumed to be fast compared to the oxide formation via reaction (O), and to be thermodynamically favored. Referring to Fig. 3, the third reaction step (reaction (C)) seems to be fast enough to directly convert all evolving oxide ions into carbonate ions. A general rule of reaction kinetics implies that the slowest reaction step in a sequence of reactions is rate determining [59,60]. Hence, it is justified to re-calculate salt compositions that assume the presence of oxide ions instead of carbonate ions. The results, obtained by equation (14), correspond to experiments with exclusion of carbon dioxide from the system, and consequently exclusion of reaction (C). A detailed discussion of the observations in Fig. 4, and data evaluation with regard to reaction equilibria and kinetics is given in the next sub-chapters.

3.1. Reaction (N): nitrite formation and chemical equilibrium

We assume that only nitrate is in the molten salt at time zero by neglecting the reactions during heating times. After 2 h, all samples contain a certain amount of nitrite, see Fig. 4(a). Evidently, nitrite is formed in the first 2 h in all experiments, which corresponds to the first step in the decomposition process of Fig. 3. The nitrate content is decreasing and nitrite content is increasing with temperature at any time. This observation can be explained in two ways that combine in the regarded case. First, nitrite formation kinetics increase with temperature. Second, chemical equilibrium of reaction (N) is shifted to the nitrite side at higher temperatures. This explanation is in accordance with literature [35–41]. Increasing equilibrium constants and consequently increasing nitrite contents are reported for increasing temperatures.

In principle, reaction (N) is able to obtain chemical equilibrium since all reactants and products are present in the system. Nitrate and nitrite ions are located in the molten salt, and oxygen exists in the gas phase as well as dissolved oxygen in the molten salt [61]. However, reaction (O) can form or remove nitrite ions, and in that way prevent the formation of a chemical equilibrium. Therefore, changes in the nitrate and nitrite content over time have to be considered carefully. In order to figure out if chemical equilibrium according to reaction (N) is established in the presented experiments, it is helpful to consider the reaction quotient Q (see equation (16) and Fig. 5). As long as Q is changing over time, the reactants and products of reaction (N) are not in chemical equilibrium. Q is slightly increasing between 2 and 3 h for the OxKi_560, OxKi_570, OxKi_580, OxKi_590, and OxKi_600 experiments. Whereas, Q appears to be more stable for the OxKi_610 and OxKi_620 experiments. We ascribe this difference to the increasing reaction kinetics of nitrite formation with increasing temperature. The nitrite formation is comparably slow and changes the nitrate-to-nitrite ratio over more than 2 h at temperatures ≤600 °C, whereas a steady state is reached in the first 2 h above 600 °C. The reaction quotients are not changing within the error of measurement between the second-to-last and the last measurement point of all experimental series except OxKi_560. At the end of the experiment series, kinetics of reaction (N) are obviously faster than those of reaction (O), and a steady reaction quotient of reaction (N) is maintained. Therefore, it is reasonable to talk about chemical equilibrium of reaction (N), and to use the last measurement points (unfilled symbols in Fig. 5) for evaluation of the equilibrium and the reaction thermodynamics.

The chemical equilibrium of reaction (N) (first step in Fig. 3) is assessed in terms of the equilibrium constant K. The temperature dependence of the equilibrium is analyzed in the van't Hoff plot in Fig. 6. Each of the seven symbols corresponds to the equilibrium

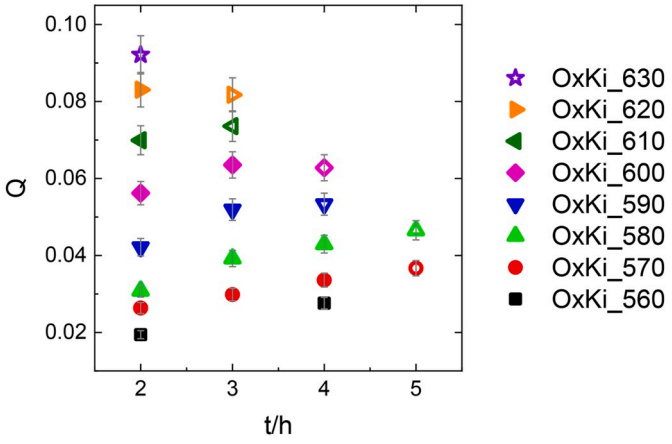

Fig. 5. Reaction quotient (equation (16)) of reaction (N) over time.

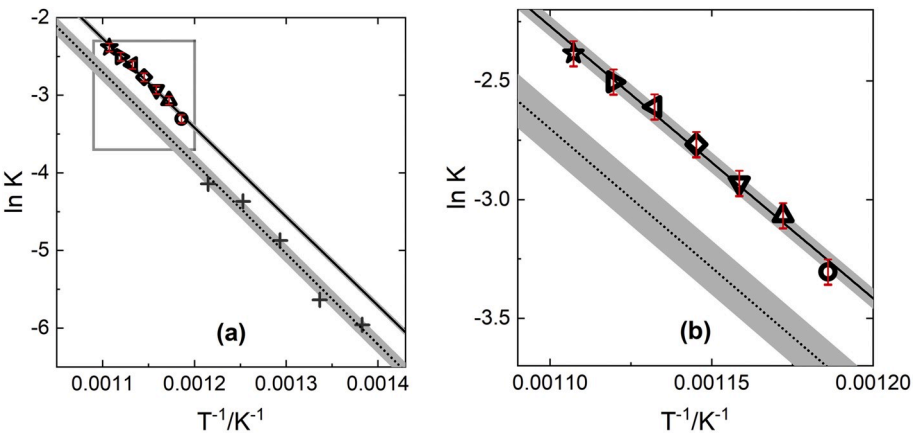

Fig. 6. Van't Hoff plots of the equilibrium constants of reaction (N). The unfilled symbols correspond to the equilibrium constants calculated in this study at 570–630 °C. The RMSE of this study amounts to 0.05, and is illustrated as grey tunnel behind the solid fit line. Equilibrium constants K at ≤550 °C (cross symbols), their linear fit (dotted line) and the uncertainty tunnel are taken from reference [41] and inserted in the diagrams for comparison. The framed area of (a) is enlarged in (b) for a better resolution of the temperature range 560–630 °C.

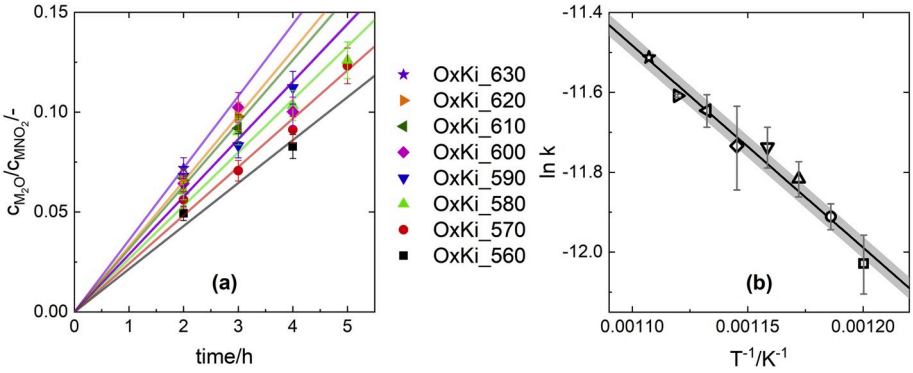

Fig. 7. Kinetics of the oxide formation in a range from 560 to 630 °C. (a): The quotient of the oxide and nitrite concentration versus time according to equation (24). (b) Arrhenius diagram of the kinetic rate constants. The symbol shape of each data point corresponds to the symbol shape in (a) at the respective temperature. The error bars represent the standard deviations of the linear fits in (a). The RMSE amounts to 0.03, and is illustrated as grey tunnel behind the solid fit line.

constant at the respective temperature. Linear fitting of the data points according to the van't Hoff equation (17) yields a reaction enthalpy ΔH of 95 ± 4 kJ·mol^{-1}, and a reaction entropy ΔS of 86 ± 5 J·mol^{-1}·K^{-1}.

The nitrite content, and consequently K as well as ln K increase with temperature and this is reflected in the diagrams of Fig. 6. The results can be compared to the equilibrium investigations at lower temperatures (450–550 °C) of a previous study [41] (cross symbols and dotted fit line in Fig. 6). The equilibrium constants of this study are higher than predicted by the previous results. More nitrite than expected was formed in the samples of this study. This can be ascribed to, first, different experimental methods. The previous study presented TGA experiments with platinum crucibles, and the different set-up might cause some systematic experimental error that is not included in the error calculations. Second, one could imagine a temperature dependent effect, e.g. side reactions that are only relevant in a certain temperature range, and affect the equilibrium. Besides, non-ideal behavior of the multicomponent phases (liquid phase and gas phase) should be contemplated. The second explanation is considered more likely because another literature study [38] also found higher equilibrium constants at higher temperatures (500–620 °C), just like this study. Given the different experimental configurations, it is reasonable to assume that temperature dependent effects are responsible for the systematic offset from predicted values above 550 °C. That means, the extrapolation of the equilibrium parameters gained up to 550 °C is restricted and involves large uncertainties. The authors recommend using thermodynamic reaction parameters that are gained in the temperature range of interest.

3.2. Reaction (O): oxide kinetics

Different literature studies have validated that nitrite ions can decompose to oxide ions according to reaction (O) [47–52]. This reaction is represented by the second step in the decomposition process of Solar Salt in Fig. 3. Experimental investigation and evaluation of the intrinsic kinetics of oxide formation are discussed in the following. During the experiments, product gases of reaction (O) such as *NO* and NO_2 are purged out of the system by natural convection. Consequently, the reaction does not reach chemical equilibrium. Instead, the reaction is pushed to the product side, and increasing levels of oxide ions are expected to be produced over time. Fig. 4(a) provides evidence that the oxide ratio increases with time at all temperatures. It was found that the increase is less pronounced at lower temperatures, e.g. the absolute increase of the oxide ratio of OxKi_570 (circle symbols) is smaller than the oxide increase of OxKi_620 (triangle symbols with right side pointing tips). Furthermore, the oxide ratio after 2 h continuously increases with temperature (see Fig. 4(b)). For instance, 0.002 mol·mol^{-1} is formed at 560 °C, and 0.012 mol·mol^{-1} is formed at 630 °C. The latter two observations are interpreted in terms of the reaction equation (O). First, higher temperatures entail higher nitrite concentrations, which are the reactants. Consequently, the reaction occurs more frequently because more reacting molecules are available in the salt volume. Second, reaction rate constants generally increase with temperature, meaning that the probability of reaction increases [59,60]. Both effects contribute to a higher oxide content, and to faster oxide formation when the temperature is raised.

The kinetic rate law in equation (23) is postulated for the oxide formation in Solar Salt. It is based on reaction equation (O), and on

references [49,50] saying that the oxide formation is first-order in the nitrite concentration. The experimental results are interpreted in terms of the rate law equation (23). The quotient of the oxide and the nitrite concentration is plotted versus time in Fig. 7(a). According to equation (24), which is a rearrangement of the rate law (23), the data in Fig. 7(a) can be fitted linearly, and the slope corresponds to the kinetic rate constant $k(T)$. Eventually, kinetic rate constants at eight temperatures can be extracted. The rate constants are plotted according to the Arrhenius equation (19) in Fig. 7(b). The linear fit parameters reveal an activation energy E_a of 42 ± 3 kJ·mol^{-1} for a pre-exponential factor A of 0.003 ± 0.001 s^{-1}.

$$r = dc_{M_2O}(t)/dt = k(T)\cdot c_{MNO_2}(t) \tag{23}$$

$$d(c_{M_2O}(t) / c_{MNO_2}(t)) / dt = k(T) \tag{24}$$

To the best of our knowledge, oxide formation kinetics in sodium nitrate or potassium nitrate, or mixtures of both, was not published so far. Previous studies investigated thermal decomposition of barium-, strontium-, and calcium nitrite [48], lithium nitrite [49] and sodium nitrate [50] with the oxide ion being one of the product ions. However, the kinetics evaluations of these studies merge all decomposition reactions, no matter what products are formed. Therefore, the presented rate constants in the range of 10^{-6} s^{-1} [49], and activation energies of 33–65 kJ·mol^{-1} [48] and of 243 kJ·mol^{-1} [50] are not comparable to the results of this study.

A model to predict the salt composition of Solar Salt with a focus on oxide formation can be built with the presented results. First, the chemical equilibrium of reaction (N) is calculated with equations (17) and (18), and with the thermodynamic results of chapter 3.1. Second, the reaction kinetics of reaction (O) are described by equations (19) and (23), and by the kinetics parameters presented in chapter 3.2. The salt composition calculated by this model for temperatures between 560 and 630 °C can be compared to the experimental results shown in Fig. 2(a). The oxide concentrations are predicted with relative deviations ($RD_{c_{M_2O}}$, see equation (25)) ranging from 0.9% (620 °C) to 26% (560 °C). The average deviation amounts to 9%. The reaction chemistry description can be considered accurate enough for future application in more complex mathematical models.

$$RD_{c_{M_2O}} = 100\%\cdot\sqrt{\frac{\sum\left(\left(c_{M_2O,exp} - c_{M_2O,mod}\right)/c_{M_2O,exp}\right)^2}{N}} \tag{25}$$

4. Conclusions

The intrinsic formation of oxide or carbonate ions in Solar Salt has not been investigated in the past in terms of reaction kinetics. However, it is a key to exhaust temperature limits of Solar Salt applications, and for lifetime predictions of the material. This study presents an appropriate method to measure oxide formation at 560–630 °C in the absence of mass transport limitations. It is concluded that the nitrite forming reaction, which delivers the reactant for further decomposition, reaches chemical equilibrium within the experiment times. The equilibrium parameters previously gained for a lower temperature range underestimate the nitrite content. Hence, reaction thermodynamics should be chosen carefully with respect to the considered temperatures. For the first time, the experiments enable evaluation of the oxide formation microkinetics in Solar Salt. The experimental data is fitted according to a reliable kinetic rate law, which allows extraction of the kinetic parameters. The oxide formation is successfully described in terms of a mathematical equation and the corresponding parameters. This equation can be combined with thermodynamics and kinetics of other reactions for a full assessment of Solar Salt chemistry. Furthermore, reaction kinetics of oxide formation gives valuable information for design of CSP components such as hot surfaces with molten salt flow (e.g. solar tower receiver, electric heater). The established reaction times in this work for oxide formation can be compared with molten salt hold-up times at elevated wall temperatures in such components. This can allow for further optimization (e.g. increase of wall temperatures) of such components.

Declaration of competing interest

The authors declare that they have no known competing financial interests or personal relationships that could have appeared to influence the work reported in this paper.

CRediT authorship contribution statement

Veronika Anna Sötz: Conceptualization, Methodology, Investigation, Writing - original draft, Visualization, Formal analysis. **Alexander Bonk:** Investigation, Writing - review & editing, Project administration. **Thomas Bauer:** Conceptualization, Supervision, Writing - review & editing, Funding acquisition.

Acknowledgements

This work was supported by the German Federal Ministry for Economic Affairs and Energy. We express our thanks to Andrea Hanke (DLR Stuttgart) for her support and expertise, especially during the experimental work.

Appendix A. Supplementary data

Supplementary data to this article can be found online at https://doi.org/10.1016/j.solmat.2020.110577.

References

[1] G.J. Janz, C.B. Allen, N.P. Bansal, R.M. Murphy, R.P.T. Tomkins, Physical Properties Data Compilations Relevant to Energy Storage. II. Molten Salts: Data on Single and Multi-Component Salt Systems, 1979.
[2] J.E. Pacheco, M.E. Ralph, J.M. Chavez, S.R. Dunkin, E.E. Rush, C.M. Ghanbari, M. W. Matthews, Results of Molten Salt Panel and Component Experiments for Solar Central Receivers: Cold Fill, Freeze/thaw, Thermal Cycling and Shock, and Instrumentation Tests, 1995.
[3] T. Bauer, N. Pfleger, N. Breidenbach, M. Eck, D. Laing, S. Kaesche, Material aspects of Solar Salt for sensible heat storage, Appl. Energy 111 (2013) 1114–1119.
[4] L. Miró, E. Oró, D. Boer, L.F. Cabeza, Embodied energy in thermal energy storage (TES) systems for high temperature applications, Appl. Energy 137 (2015) 793–799.
[5] K. Vignarooban, X. Xu, A. Arvay, K. Hsu, A.M. Kannan, Heat transfer fluids for concentrating solar power systems–a review, Appl. Energy 146 (2015) 383–396.
[6] V.M.B. Nunes, C.S. Queirós, M.J.V. Lourenço, F.J.V. Santos, C.A.N. De Castro, Molten salts as engineering fluids–a review: Part I. Molten alkali nitrates, Appl. Energy 183 (2016) 603–611.
[7] Y. Tian, C.Y. Zhao, A review of solar collectors and thermal energy storage in solar thermal applications, Appl. Energy 104 (2013) 538–553.
[8] C. Martin, N. Breidenbach, M. Eck, Screening and analysis of potential filler materials for molten salt thermocline storages, in: Proceedings of the ASME 2014 8th International Conference on Energy Sustainability, 2014. ES 2014.
[9] T. Bauer, N. Pfleger, D. Laing, W.-D. Steinmann, M. Eck, S. Kaesche, High-temperature molten salts for solar power application, in: Molten Salts Chemistry, Elsevier, 2013, pp. 415–438.
[10] W.-D. Steinmann, Thermo-mechanical concepts for bulk energy storage, Renew. Sustain. Energy Rev. 75 (2017) 205–219.
[11] M. Mehos, C. Turchi, J. Vidal, M. Wagner, Z. Ma, C. Ho, W. Kolb, C. Andraka, A. Kruizenga, Concentrating Solar Power Gen3 Demonstration Roadmap, 2017.
[12] K. Wang, Y.-L. He, H.-H. Zhu, Integration between supercritical CO2 Brayton cycles and molten salt solar power towers: a review and a comprehensive comparison of different cycle layouts, Appl. Energy 195 (2017) 819–836.
[13] T. Wang, D. Mantha, R.G. Reddy, Novel low melting point quaternary eutectic system for solar thermal energy storage, Appl. Energy 102 (2013) 1422–1429.
[14] C. Villada, A. Bonk, T. Bauer, F. Bolivar, High-temperature stability of nitrate/nitrite molten salt mixtures under different atmospheres, Appl. Energy 226 (2018) 107–115.
[15] A. Bonk, S. Sau, N. Uranga, M. Hernaiz, T. Bauer, Advanced heat transfer fluids for direct molten salt line-focusing CSP plants, Prog. Energy Combust. Sci. 67 (2018) 69–87.
[16] W. Ding, A. Bonk, T. Bauer, Molten chloride salts for next generation CSP plants: selection of promising chloride salts & study on corrosion of alloys in molten chloride salts, in: AIP Conference Proceedings, pp. 200014-200014.

[17] J.C. Gomez-Vidal, R. Tirawat, Corrosion of alloys in a chloride molten salt (NaCl-LiCl) for solar thermal technologies, Sol. Energy Mater. Sol. Cell. 157 (2016) 234–244.
[18] Y.-t. Wu, Y. Li, N. Ren, C.-f. Ma, Improving the thermal properties of NaNO3-KNO3 for concentrating solar power by adding additives, Sol. Energy Mater. Sol. Cell. 160 (2017) 263–268.
[19] B. Muñoz-Sánchez, J. Nieto-Maestre, E. Veca, R. Liberatore, S. Sau, H. Navarro, Y. Ding, N. Navarrete, J.E. Juliá, Á.G. Fernández, others, Rheology of Solar-Salt based nanofluids for concentrated solar power. Influence of the salt purity, nanoparticle concentration, temperature and rheometer geometry, Sol. Energy Mater. Sol. Cell. 176 (2018) 357–373.
[20] W. Ding, J. Gomez-Vidal, A. Bonk, T. Bauer, Molten chloride salts for next generation CSP plants: electrolytical salt purification for reducing corrosive impurity level, Sol. Energy Mater. Sol. Cell. 199 (2019) 8–15.
[21] K. Federsel, J. Wortmann, M. Ladenberger, High-temperature and corrosion behavior of nitrate nitrite molten salt mixtures regarding their application in concentrating solar power plants, Energy Procedia 69 (2015) 618–625.
[22] A. Bonk, D. Rückle, S. Kaesche, M. Braun, T. Bauer, Impact of Solar Salt aging on corrosion of martensitic and austenitic steel for concentrating solar power plants, Sol. Energy Mater. Sol. Cell. 203 (2019), 110162-110162.
[23] M. Gonzalez, U. Nithiyanantham, E. Carbó-Argibay, O. Bondarchuk, Y. Grosu, A. Faik, Graphitization as efficient inhibitor of the carbon steel corrosion by molten binary nitrate salt for thermal energy storage at concentrated solar power, Sol. Energy Mater. Sol. Cell. 203 (2019), 110172-110172.
[24] Á.G. Fernández, L.F. Cabeza, Molten salt corrosion mechanisms of nitrate based thermal energy storage materials for concentrated solar power plants: a review, Sol. Energy Mater. Sol. Cell. 194 (2019) 160–165.
[25] C. Prieto, J. Gallardo-González, F.J. Ruiz-Cabañas, C. Barreneche, M. Martínez, M. Segarra, A.I. Fernández, Study of corrosion by Dynamic Gravimetric Analysis (DGA) methodology. Influence of chloride content in solar salt, Sol. Energy Mater. Sol. Cell. 157 (2016) 526–532.
[26] A.S. Dorcheh, M.C. Galetz, Slurry aluminizing: a solution for molten nitrate salt corrosion in concentrated solar power plants, Sol. Energy Mater. Sol. Cell. 146 (2016) 8–15.
[27] A.G. Fernández, H. Galleguillos, E. Fuentealba, F.J. Pérez, Corrosion of stainless steels and low-Cr steel in molten Ca (NO3) 2–NaNO3–KNO3 eutectic salt for direct energy storage in CSP plants, Sol. Energy Mater. Sol. Cell. 141 (2015) 7–13.
[28] A. Bonk, C. Martin, M. Braun, T. Bauer, Material investigations on the thermal stability of solar salt and potential filler materials for molten salt storage, AIP Conference Proceedings 1850 (2017), 080008.
[29] F. Motte, Q. Falcoz, E. Veron, X. Py, Compatibility tests between Solar Salt and thermal storage ceramics from inorganic industrial wastes, Appl. Energy 155 (2015) 14–22.
[30] C. Martin, A. Bonk, M. Braun, C. Odenthal, T. Bauer, Investigation of the long-term stability of quartzite and basalt for a potential use as filler materials for a molten-salt based thermocline storage concept, Sol. Energy 171 (2018) 827–840.
[31] J. Gasia, L. Miró, L.F. Cabeza, Review on System and Materials Requirements for High Temperature Thermal Energy Storage. Part 1: General Requirements, Renewable and Sustainable Energy Reviews, 2017.
[32] F.G.F. Qin, X. Yang, Z. Ding, Y. Zuo, Y. Shao, R. Jiang, X. Yang, Thermocline stability criterions in single-tanks of molten salt thermal energy storage, Appl. Energy 97 (2012) 816–821.
[33] T. Esence, A. Bruch, S. Molina, B. Stutz, J.-F. Fourmigue, A review on experience feedback and numerical modeling of packed-bed thermal energy storage systems, Sol. Energy 153 (2017) 628–654.
[34] S.S.M. Tehrani, R.A. Taylor, K. Nithyanandam, A.S. Ghazani, Annual comparative performance and cost analysis of high temperature, sensible thermal energy storage systems integrated with a concentrated solar power plant, Sol. Energy 153 (2017) 153–172.
[35] R.F. Bartholomew, A study of the equilibrium KNO3(l)=KNO2(l)+1/2O2(g) over the temperature range 550-750°, J. Phys. Chem. 70 (1966) 3442–3446.
[36] E.S. Freeman, The kinetics of the thermal decomposition of sodium nitrate and of the reaction between sodium nitrite and oxygen, J. Phys. Chem. 60 (1956) 1487–1493.
[37] E.S. Freeman, The kinetics of the thermal decomposition of potassium nitrate and of the reaction between potassium nitrite and oxygen, J. Am. Chem. Soc. 79 (1957) 838–842.
[38] D.A. Nissen, D.E. Meeker, Nitrate/nitrite chemistry in NaN03-KN03 melts, Inorg. Chem. 22 (1983) 716–721.
[39] T.R. Tracey, C.E. Tyner, E.R. Weber, Conceptual Design of Advanced Central Receiver Power System, Martin Marietta Corporation, 1978 final report for contract EG77-C-03-1724.
[40] I. Barin, Thermochemical Data of Pure Substances, Wiley-VCH Verlag GmbH, 2008.
[41] V.A. Sötz, A. Bonk, J. Forstner, T. Bauer, Microkinetics of the reaction NO3-⇌ NO2- + 0.5 O2 in molten sodium nitrate and potassium nitrate salt, Thermochim. Acta 678 (2019), 178301.
[42] B.D. Bond, P.W.M. Jacobs, The thermal decomposition of sodium nitrate, J. Chem. Soc. Inorg. Phys. Theor. (1966) 1265–1268.
[43] F. Paniccia, P.G. Zambonin, Redox mechanisms in an ionic matrix. III. Kinetics of the reaction N02- + 1/2 O2 = NO3- in molten alkali nitrates, J. Phys. Chem. 77 (1973) 1810–1813.
[44] X. Wei, Q. Peng, J. Ding, X. Yang, J. Yang, B. Long, Theoretical study on thermal stability of molten salt for solar thermal power, Appl. Therm. Eng. 54 (2013) 140–144.
[45] K.B. Wiberg, Acidity of nitrous and nitric acids, Inorg. Chem. 27 (1988) 3694–3697.
[46] R.I. Olivares, The thermal stability of molten nitrite/nitrates salt for solar thermal energy storage in different atmospheres, Sol. Energy 86 (2012) 2576–2583.
[47] X. Wei, Y. Wang, Q. Peng, J. Yang, X. Yang, J. Ding, NOx emissions and NO2-formation in thermal energy storage process of binary molten nitrate salts, Energy 74 (2014) 215–221.
[48] P.I. Protsenko, E.A. Bordyushkova, Kinetics and mechanism of the thermal dissociation of the nitrites of calcium, strontium, and barium, Russ. J. Phys. Chem. 39 (1965) 1048–1051.
[49] A.K.K. Lee, E.F. Johnson, The stoichiometry and kinetics of the thermal decomposition of molten anhydrous lithium nitrite, Inorg. Chem. 11 (1972) 782–787.
[50] Y. Hoshino, T. Utsunomiya, O. Abe, The thermal decomposition of sodium nitrate and the effects of several oxides on the decomposition, Bull. Chem. Soc. Jpn. 54 (1981) 1385–1391.
[51] R.I. Olivares, W. Edwards, LiNO3–NaNO3–KNO3 salt for thermal energy storage: thermal stability evaluation in different atmospheres, Thermochim. Acta 560 (2013) 34–42.
[52] C. Yang, X. Wei, W. Wang, Z. Lin, J. Ding, Y. Wang, Q. Peng, J. Yang, NOx emissions and the component changes of ternary molten nitrate salts in thermal energy storage process, Appl. Energy 184 (2016) 346–352.
[53] A.G. Fernández, M.I. Lasanta, F.J. Pérez, Molten salt corrosion of stainless steels and low-Cr steel in CSP plants, Oxid. Metals 78 (2012) 329–348.
[54] S.H. White, U.M. Twardoch, Study of the Interactions of Molten Sodium Nitrate-Potassium Nitrate 50 Mol% Mixture with Water Vapor and Carbon Dioxide in Air. Final Report, June 2, 1980-June 30, 1981, 1981.
[55] R.W. Bradshaw, N.P. Siegel, Molten nitrate salt development for thermal energy storage in parabolic trough solar power systems, in: Energy Sustainability 2008, Jacksonville, Florida USA, 2008.
[56] J. Alexander, S.G. Hindin, Phase relations in heat transfer salt systems, Ind. Eng. Chem. 39 (1947) 1044–1049.
[57] E. Sada, S. Katoh, H. Yoshii, I. Takemoto, N. Shiomi, Solubility of carbon dioxide in molten alkali halides and nitrates and their binary mixtures, J. Chem. Eng. Data 26 (1981) 279–281.
[58] P.E. Field, W.J. Green, Interactions of gases in ionic liquids. I. Solubility of nonpolar gases in molten sodium nitrate, J. Phys. Chem. 75 (1971) 821–825.
[59] K.A. Connors, Chemical Kinetics: the Study of Reaction Rates in Solution, Wiley-VCH, 1990.
[60] M. Quack, S. Jans-Buerli, Molekulare Thermodynamik und Kinetik, Teil 1: Chemische Reaktionskinetik, Verlag der Fachvereine, Zuerich, 1986.
[61] E. Desimoni, F. Paniccia, P.G. Zambonin, Solubility and detection (down to 30 p.p. b.) of oxygen in molten alkali nitrates, J. Electroanal. Chem. Interfacial Electrochem. 38 (1972) 373–379.

Solar Energy 211 (2020) 453–462

Contents lists available at ScienceDirect

Solar Energy

journal homepage: www.elsevier.com/locate/solener

Defined purge gas composition stabilizes molten nitrate salt - Experimental prove and thermodynamic calculations

Veronika Anna Sötz [a,*], Alexander Bonk [b], Julian Steinbrecher [b], Thomas Bauer [a]

[a] Institute of Engineering Thermodynamics, German Aerospace Center (DLR), Linder Höhe, 51147 Köln, Germany
[b] Institute of Engineering Thermodynamics, German Aerospace Center (DLR), Pfaffenwaldring 38-40, 70569 Stuttgart, Germany

ARTICLE INFO

Keywords:
Thermal energy storage
Solar Salt
Salt decomposition
Oxide ion formation
Chemical equilibrium
Reaction thermodynamics

ABSTRACT

Thermal energy storage systems are integrated in concentrating solar power plants to improve the flexibility of the electricity generation. Commonly, the liquid storage material Solar Salt, a nitrate salt mixture, is applied to transport and store solar thermal energy. The lifetime and the temperature range of Solar Salt in the storage units are restricted by decomposition reactions of the material. Oxide ion formation is one of the fundamental issues. So far, it has not been proven if oxide ion formation can be prevented by addition of gaseous reaction products to the gas atmosphere. Also, a reliable reaction equation for the oxide ion formation is missing. In the presented experiments, molten salt at 600 and 620 °C is purged with a gas mixture of nitrogen, oxygen, and nitrous gases. Post-analysis of salt samples reveals stabilizing effects, depending on the purge gas compositions. Chemical equilibrium of the oxide ion forming reaction is demonstrated. It is proven that oxide ion formation can be controlled and suppressed. Reaction equations are evaluated and selected in order to quantify the reaction thermodynamics. The results contribute to recommendations for operating conditions and gas handling in storage systems of solar thermal power plants, which finally ensure reliable and constant material properties for extended lifetime and high temperatures.

1. Introduction

1.1. Technological background

The concentrating solar power (CSP) technology transforms the solar irradiation to solar thermal energy, which is finally used for electricity generation. Large-scale and commercial CSP plants exist in several countries. Prospectively, the technology is considered to gain importance due to the transition to renewable energies. An energy storage unit adds flexibility to CSP plants, making electricity generation adjustable to the electricity market. Also, a storage unit enables continuous electricity supply during the night or in cloudy weather. For the CSP technology, thermal energy storage with a nitrate salt mixture commonly known as Solar Salt is the state-of-the-art storage type with a significant market. Those storage units belong to the class of sensible heat storage, because the material is used exclusively in its liquid state at different temperature levels. (Mehos et al., 2017; Tian and Zhao, 2013)

Sensible heat storage with Solar Salt has many advantages. The material features excellent pumpability due to its low viscosity (Janz et al., 1979; Janz et al., 1972; Jin et al., 2016), which is not the case for alternatively considered solid storage materials. It is applicable at ambient pressure thanks to its low vapor pressure (Glazov et al., 2002). Compared to halide salts which are also discussed for sensible heat storage, it has low corrosivity (Bonk et al., 2018b; Ding et al., 2019; Gomes et al., 2019; Liu et al., 2019; Zhuang et al., 2019). Solar Salt is composed of sodium nitrate ($NaNO_3$) and potassium nitrate (KNO_3) which are inexpensive, e.g. compared to lithium containing salt mixtures (Durth et al., 2019; Villada et al., 2019). Their thermal stability exceeds the one of calcium nitrate mixtures which would also be a cost-efficient option (Gomez et al., 2013; Grosu et al., 2018). Hence, Solar Salt is considered a beneficial material for TES.

Over decades, the CSP community gained experience regarding parabolic trough CSP systems coupled with thermal storage systems at maximum temperatures of 400 °C (Tian and Zhao, 2013). Solar Salt has proven its thermal stability and durability up to this temperature limit. However, solar power tower CSP plants (instead of parabolic trough) have been built increasingly in the last few years, and are planned for the future. They feature considerably higher temperatures, more precisely an upper storage temperature of typically 565 °C, and local temperature peaks even above that temperature (McConohy and Kruizenga, 2014;

* Corresponding author.
E-mail address: Veronika.Soetz@dlr.de (V.A. Sötz).

https://doi.org/10.1016/j.solener.2020.09.041
Received 26 February 2020; Received in revised form 21 July 2020; Accepted 11 September 2020

Mehos et al., 2017; SolarPACES, 2017). Given the so far short operational life, there is a lack of experience in terms of material stability and durability for Solar Salt and connected components in the solar power tower CSP plants. For the future, further temperature increase is most desirable because it increases the storage capacity and the efficiency of the conversion heat to power (Turchi et al., 2018).

One major drawback is that decomposition reactions and corrosion rates increase with temperature, thereby affecting steel components in the molten salt loop (Bonk et al., 2018a, 2019; Federsel et al., 2015; Fei et al., 2019; Fernández et al., 2014; Fernández and Cabeza, 2019; McConohy and Kruizenga, 2014; Prieto et al., 2019). Briefly speaking, high temperatures are positive, because they improve the storage system performance, but are also negative, due to material stability issues. The goal is to solve this dilemma by maintaining the long-term thermochemical stability of the materials, even at elevated temperatures.

This study addresses the thermal stability of Solar Salt with a focus on one critical reaction product, which is the oxide ion. The following section (section 1.2) discusses the state of knowledge of the relevant liquid-gas reactions in nitrate salts. Afterwards the scope of the presented paper is set in more detail in section 1.3.

1.2. State of knowledge of nitrate salt chemistry

The decomposition process of Solar Salt can be subdivided into several steps. Some of them probably occur simultaneously or parallel. Initially, the undecomposed Solar Salt only contains nitrate salts (MNO_3, $M = Na, K$). The formation of nitrite ions (NO_2^-, anion in MNO_2) according to reaction (N) is widely accepted and well described in the literature (Bond and Jacobs, 1966; Freeman, 1956, 1957; Nissen and Meeker, 1983; Paniccia and Zambonin, 1976; Sötz et al., 2019; Tracey et al., 1978). If oxygen (O_2) is present in the system, the reaction can establish chemical equilibrium regarding nitrate and nitrite ions, and oxygen. The thermodynamics in terms of reaction enthalpy and entropy are published for a broad temperature range (260–593 °C) by Tracey et al. (Tracey et al., 1978), and for moderate temperatures (450–550 °C) by the authors of this article (Sötz et al., 2019).

$$2MNO_3 \rightleftharpoons 2MNO_2 + O_2 \quad \text{(N)}$$

The formation of oxide ions (O^{2-}, anion in M_2O or $M^{II}O$) is reported in several publications. Given the broad spectrum of studies and proposed reaction mechanisms, the existing literature is reviewed extensively. Protsenko (Protsenko and Bordyushkova, 1965) investigated the thermal decomposition of nitrite salts of bivalent cations (M^{II2+}) at 400–500 °C. Volumetric production of decomposition gases indicated reaction (1). It was concluded that the presence or absence of oxygen and nitrogen (N_2) in the atmosphere significantly affects the decomposition mechanism. Lee et al. (Lee and Johnson, 1972) analyzed the decomposition gases of lithium nitrite by mass spectrometry and interpreted the results and the stoichiometry of the measured gases in terms of reactions (2)–(4) and (N).

The book of Stern (Stern, 1972) reviews decomposition reactions of potassium and sodium nitrite and nitrate. For potassium nitrite, reaction (5) is considered to be the first step in a decomposition sequence, followed by reactions (4), (6) and (7). Above 800 °C, reaction (8) is considered to be strongly on the oxide ion (product) side. For potassium nitrate, oxide ion formation is explained by reaction (9) with equilibrium constants of $8.8{\cdot}10^{-27}$ and $3.9{\cdot}10^{-22}$ at 800 and 900 °C, respectively. For sodium nitrite the same decomposition steps as for potassium nitrite (reactions (5), (4), (6) and (7)) are suggested below 600 °C. At higher temperatures and in the presence of oxygen, nitrate will form according to reaction (N) until chemical equilibrium. Under inert atmosphere, decomposition can be expressed by reaction (8) which shows production of nitrogen and oxygen gas. For sodium nitrate, Stern mentions the complexity of the oxide ion forming decomposition reactions, and questions the sense of their thermodynamic considerations. Equilibrium constants of reaction (9) are given with $1.6{\cdot}10^{-18}$ and $1.3{\cdot}10^{-14}$ at 800 and 900 °C, respectively, reflecting the instability of sodium nitrate or nitrite compared to the corresponding potassium salt.

Hoshino et al. (Hoshino et al., 1981) detected oxygen, nitrogen monoxide (NO) and nitrogen gas in the purge gas flow of decomposing sodium nitrate using TG-MS. Reaction (10) is proposed based on the formation rates of NO and O_2 and their stoichiometric ratio. Abe et al. (Abe et al., 1983) measured decomposition gases of sodium nitrite depending on the temperature with gas chromatography. Below 600 °C, the main gaseous product is NO, whereas similar amounts of NO and O_2 are produced at higher temperatures. Also, trace amounts of nitrogen gas (N_2) are detected. The oxide ion formation is assumed to follow a mechanism with a peroxide (O_2^{2-}) intermediate. Reaction (2) is postulated for argon atmosphere, and for oxygen atmosphere the formation of nitrate according to reaction (N) is considered to be the main reaction. In a subsequent publication (Abe et al., 1984), Abe et al. identified the oxide ions to be the final decomposition product of sodium nitrite, because the measured weight loss is in agreement with equation (10). The formation of sodium nitrate is explained by reaction (2). In the order of their intensity, nitrogen monoxide, oxygen and nitrogen gas are detected. The publication supports the decomposition mechanism with peroxide intermediate which disproportionates into oxide ion and oxygen.

A sodium nitrate and potassium nitrate mixture was investigated via DSC/TG-MS by Olivares (Olivares, 2012). The thermal stability increases when nitrite ions are oxidized to nitrate ions, which indicates that the nitrite ion (instead of the nitrate ion) is decomposed. The oxide ion formation is postulated by reactions (5) and (8), and carbonate formation by reaction (11). Nitrogen monoxide and nitrogen dioxide (NO_2) were detected in all atmospheres, N_2 was detected in argon and oxygen atmosphere, and O_2 was detected in argon atmosphere. The ensuing publication (Olivares and Edwards, 2013) on a ternary nitrate mixture ($LiNO_3$-$NaNO_3$-KNO_3) revealed similar results with regard to the detected decomposition gases. The main gaseous decomposition gas was NO. The authors interpreted the results with regard to chemical equilibrium of reaction (N) and reaction (5) which produces NO and NO_2. Gas phase reactions were also considered. N_2 is assumed to be stable and does not react with other gases. NO, NO_2 and O_2 are involved in the gas-phase reaction (G).

Wright et al. (Wright et al., 2012) analyzed decomposition gases of equimolar sodium nitrate and potassium nitrate by a cathodeluminescence analyzer. The nitrogen species with highest concentration was NO. Nitrogen dioxide and nitrogen gas were detected in minor concentrations. In argon atmosphere, the concentration of nitrous gases (NO_x) was 40 times higher than in nitrogen and air atmosphere. Therefore, a stabilizing effect was attributed to air and nitrogen atmosphere in terms of reaction thermodynamics. The production of decomposition gases was explained by reactions (N), (4), (5), and (12). Reaction (8) was regarded as a generalized decomposition reaction for nitrite.

NO_x emissions from Solar Salt mixture were measured up to 600 °C by Wei et al. (Wei et al., 2014). More NO than NO_2 was detected. The NO_x production at $\geq$ 600 °C is explained with reactions (9) and (13) based on thermodynamic calculations of the free energy of reaction. Federsel et al. (Federsel et al., 2015) considered reactions (N), (5) and (11) as reasons for mass changes of a sodium and potassium nitrate and nitrite mixture.

$$4M^{II}(NO_2)_2 \rightleftharpoons 2M^{II}(NO_3)_2 + 2M^{II}O + 2NO + N_2 \quad (1)$$

$$3MNO_2 \rightleftharpoons M_2O + MNO_3 + 2NO \quad (2)$$

$$2MNO_2 \rightleftharpoons M_2O + N_2O + O_2 \quad (3)$$

$$2MNO_2 + 2NO \rightleftharpoons 2MNO_3 + N_2 \quad (4)$$

$$2MNO_2 \rightleftharpoons M_2O + NO_2 + NO \quad (5)$$

$$M_2O + 2NO_2 \rightleftharpoons MNO_2 + MNO_3 \quad (6)$$

$$MNO_2 + NO_2 \rightleftharpoons MNO_3 + NO \quad (7)$$

$$2MNO_2 \rightleftharpoons M_2O + N_2 + 1.5O_2 \quad (8)$$

$$2MNO_3 \rightleftharpoons M_2O + 2NO_2 + 0.5O_2 \quad (9)$$

$$MNO_2 \rightleftharpoons 0.5M_2O + NO + 0.25O_2 \quad (10)$$

$$M_2O + CO_2 \rightleftharpoons M_2CO_3 \quad (11)$$

$$NO + 0.5O_2 \rightleftharpoons NO_2 \quad (G)$$

$$2MNO_3 \rightleftharpoons M_2O + N_2O + 2O_2 \quad (12)$$

$$2MNO_3 \rightleftharpoons M_2O + NO + N_2O + 2O_2 \quad (13)$$

The gas phase reaction (G) always has to be considered when NO_2 and/or NO in the presence of O_2 is produced (Olivares and Edwards, 2013). The reaction equilibrium can be calculated with listed thermodynamic values of the three gases, as it is done e.g. in the reference (Olsson et al., 1999). Below 350 °C, nitrogen dioxide predominates, whereas nitrogen monoxide predominates above 500 °C. Similar concentrations of nitrogen monoxide and nitrogen dioxide coexist at 400–450 °C. The gas phase reaction kinetics of the oxidation of nitrogen monoxide by oxygen are reviewed by Tsukahara et al. (Tsukahara et al., 1999). Among many original research publications only the ones of Tipper et al. (Tipper and Williams, 1961), Ashmore et al. (Ashmore et al., 1962) and Olbregts et al. (Olbregts, 1985) are appropriate for the temperature range that is relevant in this paper (600–620 °C). The reaction kinetics in those three publications are consistent. They indicate oxidation times of nitrogen monoxide until chemical equilibrium around 300–1000 min at 300 °C, and around 30–250 min at 600 °C, each depending on the initial NO_x concentrations.

To sum up the literature on oxide ion formation in salt systems similar to the Solar Salt mixture, some key points are figured out:

- A large number of reaction equations is considered for the oxide ion formation in molten nitrate-nitrite salts (reactions (1)–(3), (5), (6), (8), (9), (10), (12) and (13)).
- Those reaction equations differ in the involved ionic compounds (MNO_3 and/or MNO_2) and gaseous species (NO, NO_2, N_2O (dinitrogen oxide), N_2 and O_2). NO and O_2 appear to be the most relevant reaction gases.
- Also, the reaction equations differ in the stoichiometry of the reaction products. For example, both reaction (5) and (10) produce oxide ions and nitrogen monoxide, but in different stoichiometric ratios.
- All referred studies report purged experiments. The reaction gases (or at least some of them) are removed from the system by a continuous purge gas flow. Consequently, the salt mixtures could not obtain chemical equilibrium, and it was not demonstrated that the proposed reaction equations are valid in terms of equilibrium reactions.
- The reversible reaction (N) of nitrate ions to nitrite ions is mentioned in most publications, and should always be considered.
- If NO is produced as a decomposition gas, it can react to NO_2, and vice versa. The chemical equilibrium of NO and NO_2 (reaction (G)) is strongly temperature dependent. Full chemical equilibrium in the gas phase may not be reached due to slow reaction kinetics.

Despite those findings in the literature, major questions are still unsolved. It remains uncertain if the amount of oxide ions can be restricted intentionally by atmospheric conditions. Clear evidence of a chemical equilibrium with oxide ions in the molten nitrate salt is not reported. Also, a reliable reaction equation with justified stoichiometry is not identified.

1.3. Scope of the study

The work presented in this paper aims to prove that oxide ion formation in Solar Salt is based on equilibrium reactions. Accordingly, the reaction is expected to cease at a certain product (oxide ion) concentration and gas phase composition. The experimental part of the study intends to demonstrate that the concentration of oxide ions can be controlled by adjusting partial pressures of the purge gases. For this purpose, a molten salt system is purged with a mixture of the presumed reaction gases. Increasing the partial pressures of the reaction gases is expected to lower the oxide content at chemical equilibrium.

In the second part, the reaction equations are considered in terms of thermodynamic equilibrium calculations. It is contemplated to systemize the numerous existing reaction equations, and to identify the key differences with regard to predicted equilibrium oxide ion contents. Finally, the thermodynamic calculations are compared with the experimental results to ascertain how the reaction equations can be linked to the experiments.

2. Materials and methods

2.1. Experimental

The eight experiments listed in Table 1 are performed in an autoclave test rig with approximately 100 g of Solar Salt mixture (60 wt% sodium nitrate, 40 wt% potassium nitrate, both Merck > 99% purity). The test rig is described in detail in the reference (Bonk et al., 2017). The salt is stirred, and heated to the desired temperature (600 or 620 °C, see Table 1). Salt samples are extracted over the course of the experiment. The gas phase is purged (100 mL·min^{-1}) with a mixture of 80 vol% nitrogen, 20 vol% oxygen, and varying concentrations of NO (see Table 1). Nitrogen with 1.25 times the target NO concentration is combined with oxygen gas. The gases come from Linde Gas (oxygen in all experiments, and NO in nitrogen for 620_500 and 620_200), and from basi Schöberl GmbH (NO in nitrogen for 600_50, 600_100, 600_200 and 600_500). The concentration of NO in nitrogen has an accuracy of 5% according to the analysis certificates. Oxygen and nitrogen gas has 5.0 grade.

Two analytical methods reveal the composition of the salt samples. First, about 125 mg of salt sample are dissolved in 500 mL ultrapure water (HiPerSolv, VWR, Germany), and analyzed by ion chromatography (IC) to measure the content of nitrate and nitrite ions. An IC apparatus of the type Metrohm 930 Compact IC Flex (Metrohm, Switzerland) equipped with a Metrosep A Supp analytical column (5 × 250 mm), and a suppressed conductivity detector are used. Second, approximately 0.8 g of salt sample is dissolved in ultrapure water (150 mL), and the oxide ion content is determined by acid-base titration. The titration is executed in a Metrohm Titrando 905 system with 0.01 mol·L^{-1} HCl titrant. The two methods are further described in the references (Bonk et al., 2020; Bonk et al., 2017; Sötz et al., 2019).

Table 1
List of experiments. Settings are specified with regard to temperature T, purge gas composition (NO_x in synthetic air, p_{NO_x}) and experiment duration.

Label	T/°C	p_{NO_x}/ppm	Duration/h
600_blank	600	0	1130
600_50	600	50	990
600_100	600	100	1010
600_200	600	200	910
600_500	600	500	930
620_blank	620	0	1300
620_200	620	200	1300
620_500	620	500	720

Raw data from IC and titration analysis in terms of weight fractions of nitrate, nitrite and oxide m_i (in *wt.*%, relative to the total mass) are transformed to molar fractions x_i (in $mol \cdot mol^{-1}$, relative to the total amount of ions) in Eq. (14). In the formula, M_i represents the molar mass of i, and d_i represents the van't Hoff factor of i (2 for nitrates and nitrites, and 3 for oxides). The uncertainties σ of $m_{NO_3^-}$ and $m_{NO_2^-}$ are calculated according to an error consideration with seven fold IC measurement repetition (NO_3^-: 0.142% for < 150 mg·L^{-1}, and 0.225% for > 150 mg·L^{-1}; NO_2^-: 0.330% for < 5 mg·L^{-1}, and 0.409% for > 5 mg·L^{-1}) (Bonk et al., 2018a). The error of x_i is calculated by quadratic error propagation based on Eq. (14), resulting in Eq. (15). For oxide ions, the error is assumed to be the limit of detection of the titration method that is $\pm 2.5 \cdot 10^{-5}$ for $x_{O^{2-}}$.

The reaction quotient of reaction (N) $Q_{(N)}(t)$ which describes the reaction progress is calculated according to Eq. (16), and its uncertainty via Eq. (17). Herein, p_{O_2} is the partial pressure of the oxygen, and p_0 is the reference pressure of 1 bar. The logarithmic equilibrium constant of reaction (N) $\ln K_{(N)}$ is the arithmetic mean of the logarithm of all $Q_{(N)}(t)$ values at chemical equilibrium $Q_{(N),eq}$, see Eq. (18). The corresponding standard deviation of $\ln K_{(N)}$ is calculated according to Eq. (19) with n being the number of values $\ln Q_{(N),i}$ that contribute to the average of Eq. (18).

$$x_i = \frac{m_i/M_i}{d_{MNO_3} \cdot m_{NO_3^-} \Big/ M_{NO_3^-} + d_{MNO_2} \cdot m_{NO_2^-} \Big/ M_{NO_2^-} + d_{M_2O} \cdot m_{O^{2-}} \Big/ M_{O^{2-}}} \tag{14}$$

$$\sigma_{x_i} = \sqrt{\left(\frac{(d_{i+1} \cdot m_{i+1}/M_{i+1} + d_{O^{2-}} \cdot m_{O^{2-}}/M_{O^{2-}})M_i}{(d_i m_i + (d_{i+1} \cdot m_{i+1}/M_{i+1} + d_{O^{2-}} \cdot m_{O^{2-}}/M_{O^{2-}})M_i)^2} \cdot \sigma_{m_i} \right)^2 + \left(-\frac{d_i \cdot m_i/M_i \cdot d_{i+1}}{M_{i+1} \cdot (d_i \cdot m_i/M_i + d_{i+1} \cdot m_{i+1}/M_{i+1} + d_{O^{2-}} \cdot m_{O^{2-}}/M_{O^{2-}})^2} \cdot \sigma_{m_{i+1}} \right)^2} \tag{15}$$

$$Q_{(N)}(t) = x_{NO_2^-}(t)\left(p_{O_2}/p_0\right)^{0.5} \Big/ x_{NO_3^-}(t) \tag{16}$$

$$\sigma_{Q_{(N)}(t)} = \sqrt{\left(\left(p_{O_2}/p_0\right)^{0.5} \Big/ x_{NO_3^-}(t) \cdot \sigma_{x_{NO_2^-}(t)} \right)^2 + \left(0.5 \cdot x_{NO_2^-}(t)\left(p_{O_2}/p_0\right)^{-0.5} \Big/ x_{NO_3^-}(t) \cdot \sigma_{p_{O_2}/p_0} \right)^2 + \left(- x_{NO_2^-}(t)\left(p_{O_2}/p_0\right)^{0.5} \Big/ x^2_{NO_3^-}(t) \cdot \sigma_{x_{NO_3^-}(t)} \right)^2} \tag{17}$$

$$\ln K_{(N)} = \overline{\ln Q_{(N),eq}} \tag{18}$$

$$\sigma_{\ln K_{(N)}} = \sqrt{\sum_i \left(\ln Q_{(N),eq,i} - \ln K_{(N)}\right)^2 \Big/ n} \tag{19}$$

2.2. Thermodynamic equilibrium calculations

Several reversible reactions are proposed for nitrate salt decomposition, see section 1.2. Based on the listed values (Barin, 2008; Stern, 1972) for the enthalpy (H_i) and entropy (S_i) of the reacting species i, the reaction enthalpy $\Delta_r H$, and the reaction entropy $\Delta_r S$ are calculated according to equations (20) and (21). The stoichiometric coefficient of the involved chemical compounds i are expressed by ν_i. The uncertainties of the reaction enthalpy and entropy, $\sigma_{\Delta_r H}$ and $\sigma_{\Delta_r S}$, are estimated to 5%. The Gibbs energy of the reaction $\Delta_r G$ is calculated in Eq. (22) (Barin, 2008; Wedler and Freund, 2012). The equilibrium constants K of the reactions are calculated via Eq. (23), and their errors follow the quadratic error propagation. The calculations in detail can be found in the supplementary data II.

$$\Delta_r H = \sum_i \nu_i H_i \tag{20}$$

$$\Delta_r S = \sum_i \nu_i S_i \tag{21}$$

$$\Delta_r G = \Delta_r H - T\Delta_r S \tag{22}$$

$$K = exp(-\Delta_r G/RT) \tag{23}$$

3. Results and discussion

3.1. Experimental investigation of Solar Salt stability

The salt composition changes over the course of the experiments defined in Table 1. The results are shown in terms of the nitrate and nitrite ion content in Fig. 1(a) and (b), and in terms of oxide ion content in Fig. 1(c).

Qualitatively, the formation of nitrite ions (see Fig. 1(b)) is fast in the beginning up to around 100 h in all experiments. Then, the nitrate and nitrite content stabilizes. This process is based on reaction (N), which proceeds towards the product (nitrite ion) side until chemical equilibrium is reached. The equilibrium is possible due to the presence of oxygen gas in the atmosphere (20 vol% in all experiments). The equilibrium nitrite content is higher for the 620 °C experiments, compared to the 600 °C experiments. This increase is consistent with the reaction thermodynamics of reaction (N), which favor the product side (higher nitrite content) at higher temperatures (Bond and Jacobs, 1966; Freeman, 1956, 1957; Nissen and Meeker, 1983; Paniccia and Zambonin, 1976; Sötz et al., 2019; Tracey et al., 1978). These observations agree with previous investigations of Solar Salt in synthetic air (without NO_x in the purge gas) (Bauer et al., 2012, 2013; Bonk et al., 2018a; Sötz et al., 2019).

The experimentally measured nitrate and nitrite contents are analyzed quantitatively by transforming them into the reaction quotient of reaction (N) $Q_{(N)}(t)$ (see Fig. 2 and Eq. (16)). If reaction (N) is ongoing, $Q_{(N)}(t)$ changes over time. Time constant $Q_{(N)}(t)$ reveals chemical equilibrium. The $Q_{(N)}(t)$ values of all experiments of Table 1 are shown in Fig. 2. $Q_{(N)}(t)$ is increasing at the beginning, which reflects macroscopic anion composition changes based on reaction (N). The ratio of nitrite ions to nitrate ions is changing over time in this first stadium. In the ensuing stadium, $Q_{(N)}$ stabilizes because chemical equilibrium has established, and the ratio of nitrite ions to nitrate ions is stable. The average of the stabilized $Q_{(N)}$ values is considered to be the equilibrium constant $K_{(N)}$ of each experiment (illustrated by horizontal lines in Fig. 2). To compare all $K_{(N)}$ values, their van't Hoff plot is presented in Fig. 3.

The nitrate-nitrite equilibria of this study are compared with previous results (Sötz et al., 2019) in Fig. 3. The equilibrium constants of this study (circle symbols) are similar, but above the prediction of the reference (dotted fit line) for the two considered temperatures 600 and

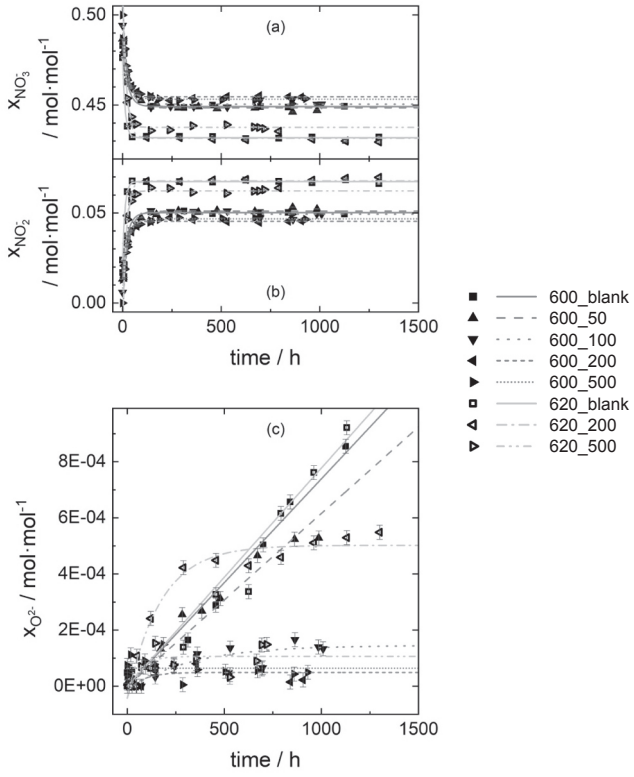

Fig. 1. Changes of the salt composition over time for all experiments (Table 1). The fits serve as guide to the eye. (a) Nitrate ion content. (b) Nitrite ion content. (c) A smaller scaling is chosen for the oxide ion content.

620 °C. Lower nitrite concentrations than actually measured in this study are expected according to the reference equilibrium description. The fit line of the reference study is based on experiments at ≤ 550 °C (+symbols in Fig. 3), which is below the temperatures of this study. Seemingly, extrapolating the equilibrium results to higher temperatures slightly reduces the accuracy of the equilibrium description. Due to the small deviations and in order to stay consistent with the previous publication, the thermodynamic reaction parameters of the reference (Sötz et al., 2019) are applied in all data evaluation and calculations in this study.

In the following, the oxide content (see Fig. 1(c)) and changes therein are discussed qualitatively. The numerous reactions from the literature (1)–(3), (5), (6), (8), (9), (10), (12) and (13) are summarized and simplified to reaction (O) in this section for reasons of clarity and comprehensibility. Reaction (O) is in agreement with the literature reactions, because it describes the formation of oxide ions based on the nitrite ion, which is certainly present in the molten Solar Salt. The reaction is accompanied by the evolution of nitrous gases, oxygen and/or nitrogen. The produced gases are summarized to 'N_2O_3' since literature does not reveal the exact composition of the emerging gases.

$$2MNO_2 \rightleftharpoons M_2O + \text{'}N_2O_3\text{'} \quad \text{(O)}$$

The reference experiments 600_blank and 620_blank both reveal continuous formation of oxide ions over 1130 h and 1300 h, respectively. In those experiments, the nitrous gases are constantly purged out of the system by a synthetic air gas flow. In other words, one part of the reaction products is constantly removed from the liquid–gas system. The reaction is driven to the product side which manifests in the steady formation of oxide ions. Consequently, the oxide ion content does not stabilize in the 600_blank and 620_blank experiments.

The oxide content stabilizes in the experiments 600_100, 600_200, 600_500, 620_200, 620_500. Compared to the respective blank experiments without NO_x in the purge gas (600_blank and 620_blank), each of those experiments shows a lower oxide content towards the end of the experiment time. The purge gas of the experiments 600_100, 600_200, 600_500, 620_200, 620_500 is composed of nitrogen, oxygen, and nitrogen monoxide. Certainly, nitrogen dioxide is formed by the fast reaction of nitrogen monoxide with oxygen (Eq. (G)) (Ashmore et al., 1962; Olbregts, 1985; Tipper and Williams, 1961; Tsukahara et al., 1999). Thus, two types of nitrous gases are always present in the gas phase, and probably dissolve to a certain concentration in the molten salt. The specific atmospheric conditions obviously stabilize the salt in terms of lower oxide ion contents. Therefore, it can be assumed that the product gases of the decomposition reaction (O) are mostly covered by the mixture of nitrogen, oxygen, nitrogen monoxide and nitrogen dioxide. It seems that the presence of those gases enables chemical equilibria of a large part of the decomposition process summarized in reaction (O), analogous to the stabilizing effect of O_2 on the nitrite forming reaction (N). A similar effect was recently published by the authors of this study for closed Solar Salt systems. Closing the liquid–gas system enables accumulation of reaction gases in the system, and

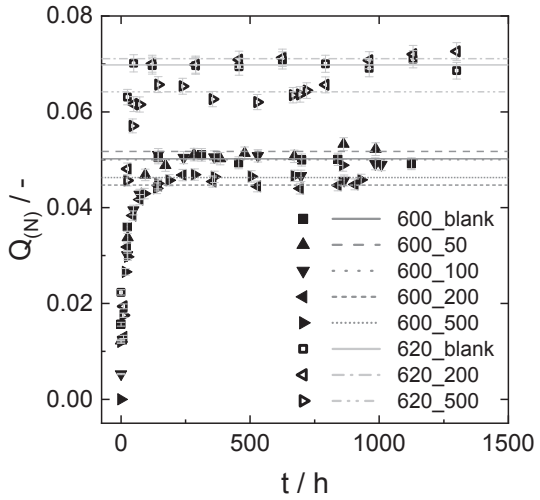

Fig. 2. Reaction quotient of reaction (N) $Q_{(N)}$ over time for all experiments. The horizontal lines represent the constant $Q_{(N)}$ value towards the end of each experiment. These values are considered as equilibrium constants $K_{(N)}$, and further analyzed in Fig. 3.

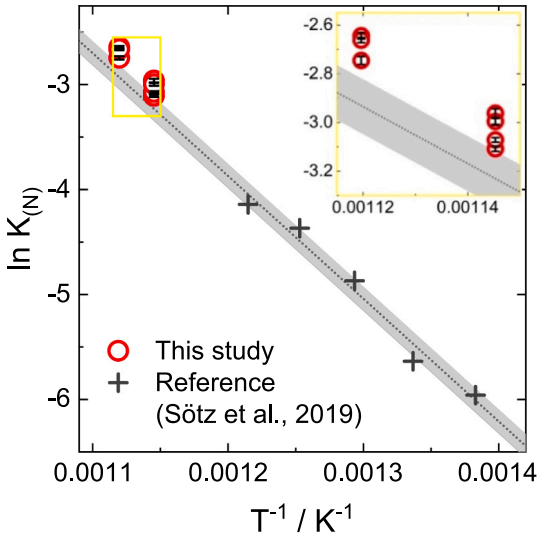

Fig. 3. Van't Hoff plot of the equilibrium constant of reaction (N) $K_{(N)}$ based on experiments at 600 and 620 °C. For comparison, the equilibrium results of a previous study (Sötz et al., 2019) are also shown in the diagram.

reduced the formation of decomposition products such as oxide ions (Bonk et al., 2020). To the best of our knowledge, the presented experiments are the first proof of reducing oxide ion formation in molten nitrate salt by a specific gas purge. This result is crucial for the molten salt energy storage technology, because oxide ions play a major role in metallic corrosion of structural materials, and their formation should be prevented.

Compared to the reference experiment 620_blank, the oxide content of 620_200 is lower after 750 h, which indicates a stabilizing effect of the 200 ppm NO_x atmosphere. Yet, the oxide content is slowly increasing between 750 and 1500 h. Perhaps, chemical equilibrium was not reached during the time of the experiment for kinetics or mass transport reasons. Otherwise, it is also possible, that the composition of the purge gas has to be further optimized to enable perfectly equilibrated oxide contents. Some of the previous publications mention the formation of N_2O during decomposition processes with oxide ion formation (Lee and Johnson, 1972; Wei et al., 2014; Wright et al., 2012). Perhaps, adding N_2O to the purge gas would be necessary to keep all reaction gases in the system, and to enable full chemical equilibrium. Overall, the participation of N_2O seems to be small, because chemical equilibrium was demonstrated in several experiments in this study, all without N_2O in the purge gas. Possibly, the influence of N_2O only becomes visible at high temperatures (≥620 °C) and low NO_x concentrations (≤200 ppm).

The accumulation of oxide ions in the experiment 600_50 is similar to that in the reference experiment 600_blank. The oxide content is constantly increasing, and the NO_x concentration of 50 ppm seems not to have a stabilizing effect within the experiment duration of 990 h. Due to the very low NO_x concentration, it is reasonable to expect a relatively high equilibrium oxide content, which only appears in long-term experiments. Stabilization of the molten salt should be possible with the applied purge gas, but could not be demonstrated in the duration of the experiment.

Some general trends are revealed by summarizing the equilibrium oxide contents of the experiments 600_100, 600_200, 600_500, 620_200, 620_500 in table 2. At a fixed temperature, a higher NO_x concentration results in a lower oxide content (e.g. $x_{O^{2-},eq}(600.100) > x_{O^{2-},eq}(600.200) \approx x_{O^{2-},eq}(600.500)$, and $x_{O^{2-},eq}(620.200) > x_{O^{2-},eq}(620.500)$). At a fixed NO_x level, an increase in temperature leads to a higher oxide content (e.g. $x_{O^{2-},eq}(600.200) < x_{O^{2-},eq}(620.200)$). In other words, low temperatures and high NO_x concentrations are most favorable for the purpose of best possible salt stabilization. Temperature-wise, this was already demonstrated in the past, but it is proven for this first time in this study as far as the NO_x concentrations are concerned.

3.2. Thermodynamic calculations of the oxide ion equilibrium

The introduction of this article provides an overview of the reaction equations (1), (2), (5), (6), (8), (9) and (10) that were proposed for the oxide ion formation in molten nitrate and nitrite salts. Nitrate and nitrite ions are involved as reactants or as products, or both. It can be stated that the stoichiometry of nitrate and/or nitrite ions in those reaction Eqs. ((1), (2), (5), (6), (8), (9) and (10)) is irrelevant for equilibrium considerations since the nitrate-nitrite equilibrium is clearly described by the thermodynamics of reaction (N) in Eq. (25) (see Fig. 4).

Furthermore, the stoichiometric ratio of the involved gases (namely N_2, O_2, NO, NO_2 and N_2O) differs. The contribution of N_2O is neglected in this study because N_2O is measured only in minor concentrations in the literature. The stoichiometry of NO, NO_2 and O_2 in the oxide ion forming reaction equations ((1), (2), (5), (6), (8), (9) or (10)) is irrelevant for equilibrium considerations because the equilibrium of those three gases is clearly described by the thermodynamics of the nitrous gases reaction (G) in Eq. (27) (see Fig. 4).

Hence, the remaining difference of all oxide ion forming reaction equations ((1), (2), (5), (6), (8), (9) and (10)) can be found in the stoichiometric number of nitrogen gas that is produced per oxide ion, expressed by the fraction $\nu_{N_2}/\nu_{O^{2-}}$. Several reaction equations can express the same $\nu_{N_2}/\nu_{O^{2-}}$. For example, nitrogen is not involved in both reaction (5) and (9), resulting in $\nu_{N_2}/\nu_{O^{2-}}$ equal to 0. However, the reactions differ in the reacting species (nitrite in reaction (5) and nitrate in reaction (9)), and in the stoichiometry and type of produced gases. Despite those differences, reaction (5) can be converted into reaction (9), when combining it with reactions (N) and (G). Reactions (N) and (G) are always relevant in molten nitrate salt systems according to literature (Bond and Jacobs, 1966; Freeman, 1956, 1957; Nissen and Meeker, 1983; Olivares and Edwards, 2013; Paniccia and Zambonin, 1976; Sötz et al., 2019; Tracey et al., 1978), see section 1.2. It is demonstrated in a mathematical way in the supplementary data I, that reactions (5) and (9) in combination with reactions (N) and (G) describe the same equilibrium composition. This finding can be generalized for all reactions with the same $\nu_{N_2}/\nu_{O^{2-}}$: the chemical equilibrium can be assigned to the stoichiometric ratio $\nu_{N_2}/\nu_{O^{2-}}$, irrespective of the stoichiometry of MNO_3, MNO_2, O_2, NO, NO_2, if reaction (N) and (G) are included in the thermodynamic calculation.

According to this understanding, the reaction equations (1), (2), (5), (6), (8), (9) or (10) are arranged in Table 3. Five reaction equations from the literature ((2), (5), (6), (9) and (10)) do not include nitrogen gas ($\nu_{N_2}/\nu_{O^{2-}}$ equal to 0). Reaction (1) postulates a stoichiometric ratio $\nu_{N_2}/\nu_{O^{2-}}$ of 0.5. In reaction (8), one nitrogen gas molecule is produced per oxide ion ($\nu_{N_2}/\nu_{O^{2-}}$ equal to 1). This ordering clearly reduces the number of literature reactions that have to be considered for equilibrium salt compositions. One representative reaction equation of each stoichiometric ratio (equation number written in bold in Table 3) is chosen for the following theoretical equilibrium calculations to assess the role of N_2 formation in the oxide ion reaction. The respective equations are merged with reactions (N) and (G). Keep in mind that the equilibrium results remain the same, irrespective of the particular chosen reaction equation of each block for a fixed stoichiometric ratio $\nu_{N_2}/\nu_{O^{2-}}$.

In this work, the following procedure (sketched in Fig. 4) was developed to calculate the salt composition and the gas phase composition at chemical equilibrium for a system with nitrate, nitrite and oxide ions, as well as N_2, O_2, NO and NO_2 gas. Three reactions are considered. Reaction (N) transforms nitrate to nitrite ions, and vice versa. Reaction (G) describes the reversible oxidation of NO with O_2 in the gas phase. The third reaction describes the formation of oxide ions, and it differs depending on the chosen ratio $\nu_{N_2}/\nu_{O^{2-}}$. Either reaction (5) or (24) or (8) is selected. The equilibrium constants K for each reaction are calculated with thermodynamic data (Barin, 2008; Sötz et al., 2019; Stern, 1972) via Eqs. (20)–(23), and connected to the law of mass action according to the reaction equation. This is shown in equations (25), (26) and (27) in Fig. 4, for the reactions (N), (5) and (G), respectively. Eq. (26) (based on reaction (5)) is only valid for $\nu_{N_2}/\nu_{O^{2-}}$ equal 0 and has to be exchanged for equations based on reaction (24) or (8) when a different ratio $\nu_{N_2}/\nu_{O^{2-}}$ is considered. The thermodynamic data of sodium salts (Barin, 2008; Stern, 1972) (instead of the Solar Salt mixture $Na_{0.64}K_{0.36}$) are used for calculation of $K_{(N)}$, $K_{(G)}$ and $K_{\text{REF\_Ref26280516\h*MERGEFORMAT(5)}}$, because the data for the Solar Salt mixture is not available. Previous studies have shown that Solar Salt can be approximated reasonably with thermodynamic data from pure sodium salts regarding thermal stability (Freeman, 1956; Nissen and Meeker, 1983; Sötz et al., 2019; Wei et al., 2014). Thermodynamic calculations require equal temperature of the liquid phase and the gas phase. The gas phase is described as a mixture of ideal gases. Furthermore, an ideal liquid mixture is assumed, and the

Table 2
Equilibrium oxide ion contents $x_{O^{2-}}$ of the experiments 600_100, 600_200, 600_500, 620_200, 620_500. The values are the average oxide ion contents of > 500 h in mol·mol^{-1}.

	100 ppm	200 ppm	500 ppm
600 °C	1.3E-4 ± 0.3E-4	3E-5 ± 2E-5	5.0E-5 ± 0.5E-5
620 °C		5.0E-4 ± 0.4E-4	1.0E-4 ± 0.5E-4

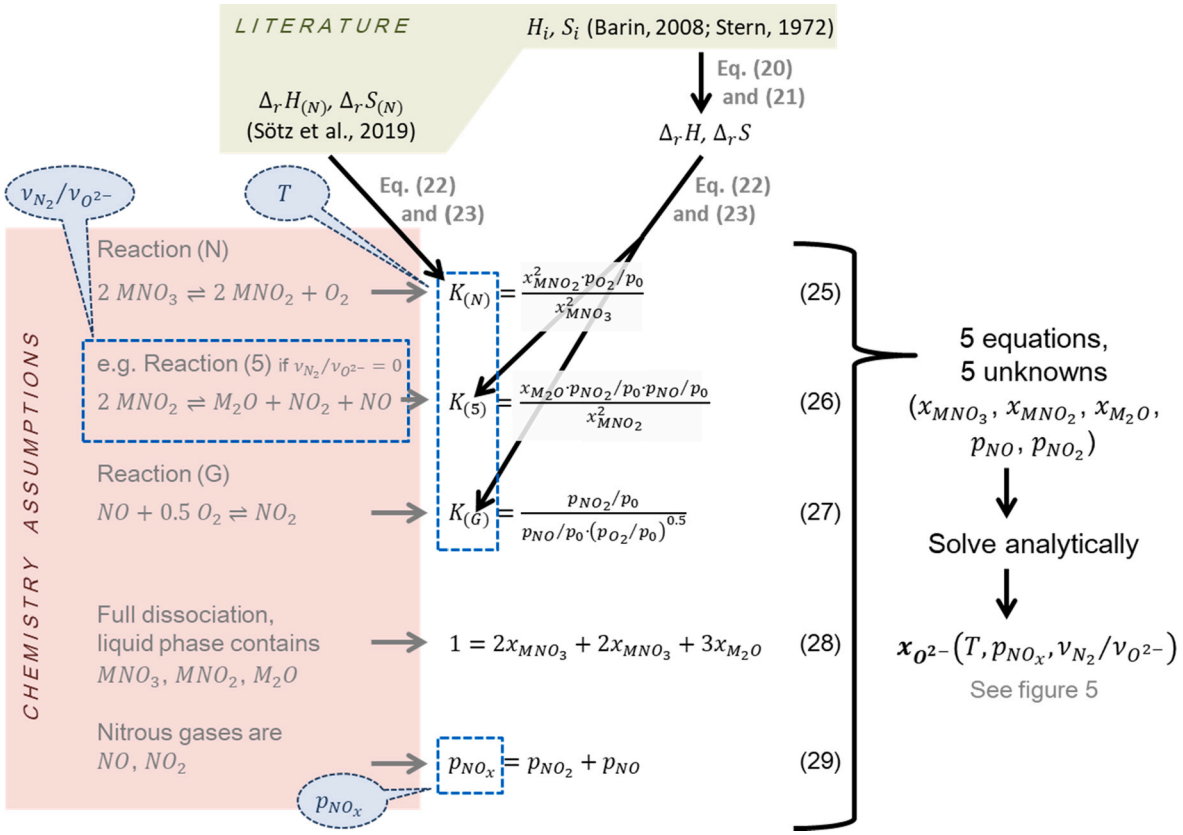

Fig. 4. Scheme of thermodynamic calculations. The detailed calculations can be found in the supplementary data III-V. The calculations are based on thermodynamic literature values (enthalpies H and entropies S in the upper shaded field), and on the chemistry description and assumptions (reactions and equations in the left shaded field). Combinations of both leads to a set of equations, and the unknown variables therein can be solved analytically. The results depend on the chosen parameters (temperature T, NO_x pressure p_{NO_x}, stoichiometric ratio N_2 to O^{2-} $\nu_{N_2}/\nu_{O^{2-}}$). The parameters are illustrated by the blue shaded bubbles, and defined in Table 4.

Table 3
Ordering of oxide forming reaction equations according to the stoichiometric ratio of nitrogen gas and oxide ions $\nu_{N_2}/\nu_{O^{2-}}$. Reaction (1) is adapted for monovalent cations resulting in reaction (24).

$\nu_{N_2}/\nu_{O^{2-}}$ =	Reaction equations from the literature, see also section 1.2	
0	$3MNO_2 \rightleftharpoons M_2O + MNO_3 + 2NO$	(2)
	$2MNO_2 \rightleftharpoons M_2O + NO_2 + NO$	**(5)**
	$M_2O + 2NO_2 \rightleftharpoons MNO_2 + MNO_3$	(6)
	$2MNO_3 \rightleftharpoons M_2O + 2NO_2 + 0.5O_2$	(9)
	$MNO_2 \rightleftharpoons 0.5M_2O + NO + 0.25O_2$	(10)
0.5	$4M^{II}(NO_2)_2 \rightleftharpoons 2M^{II}(NO_3)_2 + 2M^{II}O + 2NO + N_2$	(1)
	$2MNO_2 \rightleftharpoons M_2O + NO + O_2 + 0.5N_2$	(24)
1	$2MNO_2 \rightleftharpoons M_2O + N_2 + 1.5O_2$	**(8)**
	+	
	$2MNO_3 \rightleftharpoons 2MNO_2 + O_2$	(N)
	+	
	$NO + 0.5O_2 \rightleftharpoons NO_2$	(G)

ions are considered separately (meaning full dissociation of the salts) for calculation of the molar fractions x_i. This means for example, that unreacted Solar Salt (64 mol% $NaNO_3$, 36% mol% KNO_3) contains 50 mol% nitrate ions, 32 mol% sodium ions and 18 mol% potassium ions. Consequently, Eq. (28) in Fig. 4 describes the entire liquid phase which is assumed to consist of six salts: $NaNO_3$, KNO_3, $NaNO_2$, KNO_2, Na_2O and K_2O. Eq. (29) in Fig. 4 assumes from the exclusion of other nitrous gases besides NO and NO_2. Altogether, the system is described by a set of five equations (25)-(29) including five unknown variables ($x_{NO_3^-}$, $x_{NO_2^-}$, $x_{O^{2-}}$, p_{NO}, p_{NO_2}). The set of equations can be solved analytically, thereby revealing $x_{O^{2-}}$ and the entire equilibrium salt composition for the chosen parameters. The calculations in full length and interim results are recorded in the supplementary data III-V.

Table 4
Parameters for the thermodynamic calculations. Temperature T, NO_x partial pressure p_{NO_x}, and the stoichiometric ratio N_2 to O^{2-} $\nu_{N_2}/\nu_{O^{2-}}$ are varied in the calculations. The nitrogen partial pressure p_{N_2} and the oxygen partial pressure p_{O_2} are fixed. The uncertainties are estimated based on the experimental conditions of the experiments listed in Table 1.

Parameter	Values	Uncertainty
T	600 °C, 620 °C	±5 K
p_{NO_x}	50 ppm, 100 ppm, 200 ppm, 500 ppm (600 °C)	±5%
	200 ppm, 500 ppm (620 °C)	±5%
$\nu_{N_2}/\nu_{O^{2-}}$	0 → (Eq. (5))	
	0.5 → (Eq. (24))	
	1 → (Eq. (8))	
p_{O_2}	0.2 bar	±5%
p_{N_2}	0.8 bar	±5%

The parameters of the thermodynamic calculations are summarized in Table 4. They are chosen with regard to the experiments presented in section 3.1. Also, the uncertainties intend to reflect the experimental situation. For example, the temperature and pressure control each have an uncertainty of ± 5 K. The detailed error calculation is shown in the supplementary data III and IV.

The analytically calculated salt compositions in terms of equilibrium

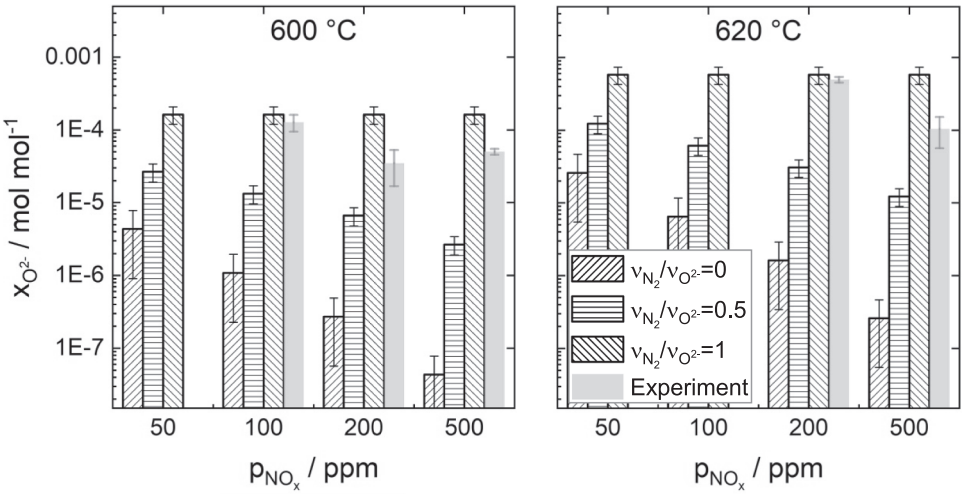

Fig. 5. Equilibrium oxide ion contents $x_{O^{2-}}$ in logarithmic scale according to thermodynamic calculations, and experimental results. The parameter settings are summarized in Table 4.

oxide ion contents are shown in Fig. 5. They are of particular interest because oxide ions are considered to aggravate corrosion issues in storage systems. The equilibrium oxide ion content varies with temperature (left versus right side of the diagram in Fig. 5), NO_x pressure (increases along the abscissas), and stoichiometric ratio N_2 formed per oxide ion $\nu_{N_2}/\nu_{O^{2-}}$ (differently striped columns). The effect of those parameters on the thermodynamically calculated results is discussed in the following paragraphs.

The oxide content increases with temperature because all considered oxide ion forming reactions are endothermic, and high temperatures therefore support the oxide ion formation.

The oxide content decreases with increasing NO_x pressure p_{NO_x} (except for $\nu_{N_2}/\nu_{O^{2-}}$ equal 1). All reactions in Table 3 with $\nu_{N_2}/\nu_{O^{2-}}$ unequal to 1 produce nitrous gases coupled with oxide ions. When the concentration of one product (NO_x) decreases, the concentration of another product (O^{2-}) must increase to maintain chemical equilibrium. This correlation is in agreement with the calculated results. For the case of $\nu_{N_2}/\nu_{O^{2-}}$ equal 1, the oxide content is independent of the NO_x pressure, because the corresponding reaction (8) does not include any nitrous gases. Consequently, the calculated equilibrium results are unaffected by changing NO_x pressures.

The oxide content increases with the stoichiometric ratio $\nu_{N_2}/\nu_{O^{2-}}$. Nitrogen gas N_2 is thermodynamically more stable than e.g. NO or NO_2 which could be produced alternatively to N_2. The formation of a stable reaction product (N_2 in this case) drives the reaction equilibrium to the product side, and thereby promotes the formation of oxide ions. Accordingly, more oxide ions are produced, when it is accompanied by the formation of more N_2 in terms of reaction stoichiometry.

3.3. Comparing experiments and calculations

The experimental results (grey columns) are compared to the calculations (striped columns) in Fig. 5. The measured oxide ion contents are in between the calculated results for $\nu_{N_2}/\nu_{O^{2-}} = 0.5$ and $\nu_{N_2}/\nu_{O^{2-}} = 1$. For the parameter combinations 600 °C and 100 ppm NO_x, and 620 °C and 200 ppm NO_x, the experiment and the $\nu_{N_2}/\nu_{O^{2-}} = 0.5$ column agree within the error bars. All calculations for $\nu_{N_2}/\nu_{O^{2-}} = 0$ (which exclude the formation of N_2) underestimate the corresponding experiments significantly.

The disagreement of experimental and calculated data for the ratio $\nu_{N_2}/\nu_{O^{2-}} = 0$ leads to the conclusion that the reaction equations without N_2 involvement are not appropriate to describe the Solar Salt chemistry of the experiments. Although those reaction equations are overwhelmingly reported in the literature, the accordingly predicted oxide contents are not confirmed with the presented experiments. It is considered more likely, that the oxide ion formation (or at least some reaction paths) is accompanied by nitrogen gas N_2 production. The $\nu_{N_2}/\nu_{O^{2-}} = 0.5$ reaction equation better describes the oxide ion formation processes in Solar Salt meaning that nitrogen gas N_2 apparently plays a role and should be included in the reaction equation. This finding is not necessarily inconsistent with all postulated $\nu_{N_2}/\nu_{O^{2-}} = 0$ reactions. However, it means that those reactions ($\nu_{N_2}/\nu_{O^{2-}} = 0$) are not fully sufficient to cover the underlying reaction mechanism, and they for example should be combined with other reactions.

The $\nu_{N_2}/\nu_{O^{2-}} = 1$ reaction predicts oxide contents close to the experimental values. It is crucial to state that this reaction without NO_x involvement cannot be the only basis for oxide ion formation in Solar Salt. Otherwise, the oxide content should stabilize at chemical equilibrium in experiments with synthetic air atmosphere (blank experiment without NO_x in the purge gas), which was never observed. Obviously, nitrogen and oxygen gas are not sufficient to provide equilibrium conditions for the oxide ion formation, which contradicts the $\nu_{N_2}/\nu_{O^{2-}} = 1$ reaction. Yet, it is possible, that this reaction contributes to the oxide ion formation, together with reaction equations that comprise NO and/or NO_2.

The discussion of the thermodynamic calculations and the experimental results suggests that oxide ion formation is probably based on several parallel reactions, and cannot be explained by one of the so far reported reaction equations. For chemical equilibrium predictions, reactions with $\nu_{N_2}/\nu_{O^{2-}} = 0.5$ seem to be more appropriate than $\nu_{N_2}/\nu_{O^{2-}} = 0$ or $\nu_{N_2}/\nu_{O^{2-}} 1 =$ reactions. It is conceivable that reactions with $\nu_{N_2}/\nu_{O^{2-}}$ between 0.5 and 1 are appropriate for equilibrium considerations. An example for $\nu_{N_2}/\nu_{O^{2-}} = 0.75$ is given in Eq. (30). This reaction attempts to sum up several reactions with different $\nu_{N_2}/\nu_{O^{2-}}$.

$$2MNO_2 \rightleftharpoons M_2O + 0.5NO + 1.25O_2 + 0.75N_2 \quad (30)$$

4. Summary and conclusions

A mixture of nitrate salts referred to as Solar Salt is commercially used to store solar thermal energy in concentrating solar power plants. For the future, increased operation and storage temperatures are desired to enhance the efficiency of the power plants. Thermal stability of Solar Salt is addressed both on an experimental level, and in terms of thermodynamic calculations in this study. The focus is on the requirements for, and the experimental prove of chemical reaction equilibria, as well as on the evaluation of numerous reaction equations that are available in the literature.

The presented experiments show the effect of NO_x in the purge gas on the chemical composition of the salt. The nitrite content is comparable to previous studies, which means that the reversible reaction from nitrate to nitrite, and its equilibrium, remains valid for the experiments of this study. This reaction seems to be widely unaffected by the NO_x gas. The oxide ion content stabilizes in the presence of NO_x gas in the synthetic air purge. The stabilizing effect was demonstrated experimentally for two relevant temperatures (600 and 620 °C) in laboratory tests for about 1000 h. Stepwise increase of the concentration of nitrous gases remarkably reduced the formation of oxide ions. At 600 °C, stabilization was shown for 100 ppm NO_x and higher. At 620 °C, 500 ppm are required to keep the oxide content at a low level, close to the detection limit. To the best of our knowledge, it is proven for the first time that the addition of nitrous gases (in particular nitrogen monoxide) to the purge gas is a successful approach to stabilize Solar Salt, and to maintain a low level of oxide ions. These results could allow specific gas operating conditions for Solar Salt applications, when a certain oxide level must not be exceeded to minimize steel corrosion. Furthermore, the results could open a technical solution to raise the operation temperature of Solar Salt e.g. in concentrating solar power plants beyond the state-of-the-art temperature (565 °C).

A large number of reaction equations is available in the scientific literature to explain the formation of oxide ions in molten Solar Salt, or in similar salt systems such as sodium nitrate. Those reactions are consulted for thermodynamic considerations in this paper. The equilibrium reactions are arranged systematically, and finally differ only in the stoichiometric number of the nitrogen gas, that is formed simultaneously with each oxide ion. For three stoichiometric numbers, the equilibrium salt compositions are calculated. The calculated oxide ion level at equilibrium increases with stoichiometric number of the nitrogen gas, because N_2 is thermodynamically stable and therefore pushes the reaction to the product side. Additionally, the oxide content increases with increasing temperature, and decreasing NO_x concentration in the purge gas, which is in agreement with the experimental results.

The experimental results are in between the calculations for stoichiometric numbers of 0.5 and 1. Most likely, the oxide ions are formed by a sophisticated and complex reaction mechanism that might be comprised of several parallel reaction paths. However, it should be possible to describe the chemical equilibrium with a formal reaction. Based on the presented results, a stoichiometric number between 0.5 and 1 seems to be appropriate for such a formal reaction. Using a stoichiometric number of 1 is not advisable because it does not reflect the effect of NO_x in the gas phase. Assuming a stoichiometric number of 0 distinctly underestimates the oxide ion content. Finally, oxygen, nitrogen and NO_x gas are identified to be required in the gas phase to enable chemical equilibrium of molten Solar Salt. These results are a substantial step towards a reliable description of the oxide ion forming chemical reactions in nitrate salts. For the first time, it provides a guideline for equilibrium calculations with oxide ions and the associated decomposition gases.

Declaration of Competing Interest

The authors declare that they have no known competing financial interests or personal relationships that could have appeared to influence the work reported in this paper.

Acknowledgement

This work was supported by the German Federal Ministry for Economic Affairs and Energy. The authors thank Markus Braun and Andrea Hanke for technical work and great expertise in experimental methods.

Appendix A. Supplementary material

Supplementary data to this article can be found online at https://doi.org/10.1016/j.solener.2020.09.041.

References

Abe, O., Utsunomiya, T., Hoshino, Y., 1983. The Reaction of Sodium Nitrite with Silica. Bull. Chem. Soc. Jpn. 56 (2), 428–433. https://doi.org/10.1246/bcsj.56.428.

Abe, O., Utsunomiya, T., Hoshino, Y., 1984. Acid-base and redox reactions in fused sodium nitrite. Thermochim. Acta 74 (1–3), 131–141. https://doi.org/10.1016/0040-6031(84)80013-1.

Ashmore, P.G., Burnett, M.G., Tyler, B.J., 1962. Reaction of nitric oxide and oxygen. Trans. Faraday Soc. 58, 685–691. https://doi.org/10.1039/TF9625800685.

Barin, I., 2008. Thermochemical Data of Pure Substances. Wiley-VCH Verlag GmbH.

Bauer, T., Laing, D., Tamme, R., 2012. Characterization of Sodium Nitrate as Phase Change Material. Int. J. Thermophys. 33, 91–104. https://doi.org/10.1007/s10765-011-1113-9.

Bauer, T., Pfleger, N., Breidenbach, N., Eck, M., Laing, D., Kaesche, S., 2013. Material aspects of Solar Salt for sensible heat storage. Appl. Energy 111, 1114–1119. https://doi.org/10.1016/j.apenergy.2013.04.072.

Bond, B.D., Jacobs, P.W.M., 1966. The thermal decomposition of sodium nitrate. J. Chem. Soc. A 1265–1268. https://doi.org/10.1039/j19660001265.

Bonk, A., Braun, M., Hanke, A., Forstner, J., Rückle, D., Kaesche, S., Sötz, V.A., Bauer, T., 2018a. Influence of different atmospheres on molten salt chemistry and its effect on steel corrosion. AIP Conf. Proc. 2033, 090003 https://doi.org/10.1063/1.5067097.

Bonk, A., Braun, M., Sötz, V.A., Bauer, T., 2020. Solar Salt – Pushing an old material for energy storage to a new limit. Appl. Energy 262, 114535. https://doi.org/10.1016/j.apenergy.2020.114535.

Bonk, A., Martin, C., Braun, M., Bauer, T., 2017. Material investigations on the thermal stability of solar salt and potential filler materials for molten salt storage. AIP Conf. Proc. 1850, 080008 https://doi.org/10.1063/1.4984429.

Bonk, A., Rückle, D., Kaesche, S., Braun, M., Bauer, T., 2019. Impact of Solar Salt aging on corrosion of martensitic and austenitic steel for concentrating solar power plants. Sol. Energy Mater. Sol. Cells 203, 110162. https://doi.org/10.1016/j.solmat.2019.110162.

Bonk, A., Sau, S., Uranga, N., Hernaiz, M., Bauer, T., 2018b. Advanced heat transfer fluids for direct molten salt line-focusing CSP plants. Prog. Energy Combust. Sci. 67, 69–87. https://doi.org/10.1016/j.pecs.2018.02.002.

Ding, W., Bonk, A., Bauer, T., 2019. Molten chloride salts for next generation CSP plants: Selection of promising chloride salts & study on corrosion of alloys in molten chloride salts. AIP Conference Proceedings 2126, 200014. https://doi.org/10.1063/1.5117729.

Durth, M.P.C., Rodriguez-Sanchez, A., Patino-Rodriguez, D., Cabeza, L.F., 2019. Effects of sodium nitrate concentration on thermophysical properties of solar salts and on the thermal energy storage cost. Sol. Energy 182, 57–63. https://doi.org/10.1016/j.solener.2019.02.038.

Federsel, K., Wortmann, J., Ladenberger, M., 2015. High-temperature and corrosion behavior of nitrate nitrite molten salt mixtures regarding their application in concentrating solar power plants. Energy Procedia 69, 618–625. https://doi.org/10.1016/j.egypro.2015.03.071.

Fei, Z., Zhang, Y., Ge, M., Wang, Y., Li, Y., Cheng, J., Wei, B., Hou, H., Liu, H., 2019. Probing thermal decomposition mechanism of molten nitrite/nitrates salt by time of flight mass spectrometry. Sol. Energy 183, 823–828. https://doi.org/10.1016/j.solener.2019.03.067.

Fernández, Á.G., Cabeza, L.F., 2019. Molten salt corrosion mechanisms of nitrate based thermal energy storage materials for concentrated solar power plants: A review. Sol. Energy Mater. Sol. Cells 194, 160–165. https://doi.org/10.1016/j.solmat.2019.02.012.

Fernández, A.G., Galleguillos, H., Pérez, F.J., 2014. Thermal influence in corrosion properties of Chilean solar nitrates. Sol. Energy 109, 125–134. https://doi.org/10.1016/j.solener.2014.07.027.

Freeman, E.S., 1956. The Kinetics of the Thermal Decomposition of Sodium Nitrate and of the Reaction between Sodium Nitrite and Oxygen. J. Phys. Chem. 60 (11), 1487–1493. https://doi.org/10.1021/j150545a005.

Freeman, E.S., 1957. The Kinetics of the Thermal Decomposition of Potassium Nitrate and of the Reaction between Potassium Nitrite and Oxygen. J. Am. Chem. Soc. 79 (4), 838–842. https://doi.org/10.1021/ja01561a015.

Glazov, V.I., Dukhanin, G.P., Losev, V.A., 2002. Saturated Vapor Pressure over the Melts of the NaNO2 NaNO3 System. Russ. J. Appl. Chem. 75 (6), 888–890. https://doi.org/10.1023/a:1020312024138.

Gomes, A., Navas, M., Uranga, N., Paiva, T., Figueira, I., Diamantino, T.C., 2019. High-temperature corrosion performance of austenitic stainless steels type AISI 316L and AISI 321H, in molten Solar Salt. Sol. Energy 177, 408–419. https://doi.org/10.1016/j.solener.2018.11.019.

Gomez, J.C., Calvet, N., Starace, A.K., Glatzmaier, G.C., 2013. Ca(NO3) 2—NaNO3—KNO3 Molten Salt Mixtures for Direct Thermal Energy Storage Systems in Parabolic Trough Plants. J. Sol. Energy Eng. 135, 021016 https://doi.org/10.1115/1.4023182.

Grosu, Y., Bondarchuk, O., Faik, A., 2018. The effect of humidity, impurities and initial state on the corrosion of carbon and stainless steels in molten HitecXL salt for CSP application. Sol. Energy Mater. Sol. Cells 174, 34–41. https://doi.org/10.1016/j.solmat.2017.08.026.

Hoshino, Y., Utsunomiya, T., Abe, O., 1981. The Thermal Decomposition of Sodium Nitrate and the Effects of Several Oxides on the Decomposition. Bull. Chem. Soc. Jpn. 54 (5), 1385–1391. https://doi.org/10.1246/bcsj.54.1385.

Janz, G.J., Allen, C.B., Bansal, N.P., Murphy, R.M., Tomkins, R.P.T., 1979. Physical properties data compilations relevant to energy storage. II. Molten salts: data on single and multi-component salt systems.

Janz, G.J., Krebs, U., Siegenthaler, H.F., Tomkins, R.P.T., 1972. Molten salts: volume 3, nitrates, nitrites, and mixtures, electrical conductance, density, viscosity, and surface tension data. J. Phys. Chem. Ref. Data 581–746.

Jin, Y., Cheng, J., An, X., Su, T., Zhang, P., Li, Z., 2016. Accurate viscosity measurement of nitrates/nitrites salts for concentrated solar power. Sol. Energy 137, 385–392. https://doi.org/10.1016/j.solener.2016.08.037.

Lee, A.K.K., Johnson, E.F., 1972. The Stoichiometry and Kinetics of the Thermal Decomposition of Molten Anhydrous Lithium Nitrite. Inorg. Chem. 11 (4), 782–787. https://doi.org/10.1021/ic50110a025.

Liu, T., Xu, X., Liu, W., Zhuang, X., 2019. Corrosion of alloys in high temperature molten-salt heat transfer fluids with air as the cover gas. Sol. Energy 191, 435–448. https://doi.org/10.1016/j.solener.2019.09.015.

McConohy, G., Kruizenga, A., 2014. Molten nitrate salts at 600 and 680 °C: Thermophysical property changes and corrosion of high-temperature nickel alloys. Sol. Energy 103, 242–252. https://doi.org/10.1016/j.solener.2014.01.028.

Mehos, M., Turchi, C., Vidal, J., Wagner, M., Ma, Z., Ho, C., Kolb, W., Andraka, C., Kruizenga, A., 2017. Concentrating solar power Gen3 demonstration roadmap. National Renewable Energy Lab. (NREL), Golden, CO (United States). doi: 10.2172/1338899.

Nissen, D.A., Meeker, D.E., 1983. Nitrate/Nitrite Chemistry in NaN03-KN03 Melts. Inorg. Chem. 22 (5), 716–721. https://doi.org/10.1021/ic00147a004.

Olbregts, J., 1985. Termolecular reaction of nitrogen monoxide and oxygen: A still unsolved problem. Int. J. Chem. Kinet. 17 (8), 835–848. https://doi.org/10.1002/kin.550170805.

Olivares, R.I., 2012. The thermal stability of molten nitrite/nitrates salt for solar thermal energy storage in different atmospheres. Sol. Energy 86 (9), 2576–2583. https://doi.org/10.1016/j.solener.2012.05.025.

Olivares, R.I., Edwards, W., 2013. LiNO3–NaNO3–KNO3 salt for thermal energy storage: Thermal stability evaluation in different atmospheres. Thermochim Acta 560, 34–42. https://doi.org/10.1016/j.tca.2013.02.029.

Olsson, L., Westerberg, B., Persson, H., Fridell, E., Skoglundh, M., Andersson, B., 1999. A kinetic study of oxygen adsorption/desorption and NO oxidation over Pt/Al2O3 catalysts. J. Phys. Chem. B 103 (47), 10433–10439. https://doi.org/10.1021/jp9918757.

Paniccia, F., Zambonin, G., 1976. Thermodynamics of the Systems NO3- = NO2- + 1/2 O2 and NO3- + 1/2 O22- = NO2- + O2- in Molten Alkali Nitrates. J. Chem. Soc., Faraday Trans. 1 (72), 1512–1518.

Prieto, C., Ruiz-Cabañas, F.J., Rodríguez-Sanchez, A., Abujas, C.R., Fernández, A.I., Martínez, M., Oró, E., Cabeza, L.F., 2019. Effect of the impurity magnesium nitrate in the thermal decomposition of the solar salt. Sol. Energy 192, 186–192. https://doi.org/10.1016/j.solener.2018.08.046.

Protsenko, P.I., Bordyushkova, E.A., 1965. Kinetics and mechanism of the thermal dissociation of the nitrites of calcium, strontium, and barium. Russ. J. Phys. Chem. 39 (8), 1048–1051.

SolarPACES, 2017. CSP Projects Around the World. https://www.solarpaces.org/csp-technologies/csp-projects-around-the-world/. Accessed 10.02.2020.

Sötz, V.A., Bonk, A., Forstner, J., Bauer, T., 2019. Microkinetics of the reaction NO3-⇌ NO2-+ 0.5 O2 in molten sodium nitrate and potassium nitrate salt. Thermochim Acta, 178301. https://doi.org/10.1016/j.tca.2019.178301.

Stern, K.H., 1972. High Temperature Properties and Decomposition of lnorganic Salts. Part 3. Nitrates and Nitrites. J. Phys. Chem. Ref. Data 1 (3), 747–771.

Tian, Y., Zhao, C.Y., 2013. A review of solar collectors and thermal energy storage in solar thermal applications. Appl. Energy 104, 538–553. https://doi.org/10.1016/j.apenergy.2012.11.051.

Tipper, C.F.H., Williams, R.K., 1961. The effect of sulphur dioxide on the combustion of some inorganic compounds. Part 2. —The nitric oxide+ sulphur dioxide+ oxygen system. Trans. Faraday Soc. 57, 79–86.

Tracey, T.R., Tyner, C.E., Weber, E.R., 1978. Conceptual Design of Advanced Central Receiver Power System. Martin Marietta Corporation, final report for contract EG77-C-03-1724.

Tsukahara, H., Ishida, T., Mayumi, M., 1999. Gas-Phase Oxidation of Nitric Oxide: Chemical Kinetics and Rate Constant. Biol. Chem. 3 (3), 191–198. https://doi.org/10.1006/niox.1999.0232.

Turchi, C., Vidal, J., Bauer, M., 2018. Molten salt power towers operating at 600–650 °C: Salt selection and cost benefits. Sol. Energy 164, 38–46. https://doi.org/10.1016/j.solener.2018.01.063.

Villada, C., Jaramillo, F., Castano, J.G., Echeverria, F., Bolivar, F., 2019. Design and development of nitrate-nitrite based molten salts for concentrating solar power applications. Sol. Energy 188, 291–299. https://doi.org/10.1016/j.solener.2019.06.010.

Wedler, G., Freund, H.-J., 2012. Lehrbuch der physikalischen Chemie. John Wiley & Sons.

Wei, X., Wang, Y., Peng, Q., Yang, J., Yang, X., Ding, J., 2014. NOx emissions and NO2-formation in thermal energy storage process of binary molten nitrate salts. Energy 74, 215–221. https://doi.org/10.1016/j.energy.2014.05.064.

Wright, S., Tran, T., Chen, C., Olivares, R.I., Sun, S., 2012. Thermal stability of potassium and sodium nitrate molten salt mixtures above 500 C, Ninth International Conference on Molten Slags, Fluxes and Salts (Molten12), Beijing.

Zhuang, X., Liu, W., Xu, X., 2019. Hot corrosion of different alloys in chloride and carbonate molten-salt mixtures under argon atmosphere. Sol. Energy 189, 254–267. https://doi.org/10.1016/j.solener.2019.07.065.